MECHANICAL MODELING OF SKELETAL MUSCLE FUNCTIONING

B.J.J.J. van der Linden

De promotiecommissie is gevormd door:

Voorzitter en secretaris:

Prof. dr D. Feil	Universiteit Twente

Promotoren:

Prof. dr ir H.J. Grootenboer	Universiteit Twente
Prof. dr P.A.J.B.M. Huijing	Universiteit Twente en Vrije Universiteit Amsterdam

Assistent-promotor:

Dr ir H.J.F.M. Koopman	Universiteit Twente

Leden:

Prof. P. Powell	Universiteit Twente
Prof. dr J. de Vries	Universiteit Twente en Revalidatiecentrum Het Roessingh Enschede
Prof. dr T.M.G.J. van Eijden	Academisch Centrum Tandheelkunde Amsterdam (ACTA)
Prof. dr ir T. Arts	Universiteit van Maastricht

Coverpage: Borelli (1680)

ISBN 90 - 36511496

MECHANICAL MODELING OF SKELETAL MUSCLE FUNCTIONING

PROEFSCHRIFT

ter verkrijging van
de graad van doctor aan de Universiteit Twente,
op gezag van de rector magnificus,
prof. dr F.A. van Vught,
volgens besluit van het College van Promoties
in het openbaar te verdedigen
op donderdag 28 mei 1998 te 13.15 uur

door
Bart Jochem Julius Joost van der Linden
geboren op 13 augustus 1966
te ‘s-Gravenhage.

Dit proefschrift is goedgekeurd door:

De promotoren:	Prof. dr ir H.J. Grootenboer
	Prof. dr P.A.J.B.M. Huijing
De assistent-promotor:	Dr ir H.J.F.M. Koopman

Contents

1 GENERAL INTRODUCTION 9

1.1. Skeletal muscle 11
1.1.1. Morphology and physiology 11
1.1.2. Mechanics of muscle 13

1.2. Modeling 14
1.2.1. Hill-type models 14
1.2.2. Huxley or Cross-bridge models 15
1.2.3. Morphological models 15
1.2.4. Morpho-Mechanical models 15

1.3. Scope of the thesis 16

1.4. Contents of this thesis 17

2 MODELING FUNCTIONAL EFFECTS OF MUSCLE GEOMETRY 19

2.1. Abstract 20

2.2. Introduction 21

2.3. Methods and Models 22
2.3.1. Model 1: parallel fibered model 23
2.3.2. Model 2: original planimetric model 23
2.3.3. Model 3: planimetric model with elastic aponeurosis 24
2.3.4. Model 4: C-C model 24
2.3.5. Model 5: C-E model 25

2.4. Results 27

2.5. Discussion 30

3 REVISED PLANIMETRIC MODEL OF UNIPENNATE SKELETAL MUSCLE: A MECHANICAL APPROACH 35

3.1. Abstract 36

3.2. Introduction 37

3.3. Methods 38

3.4. Results 42

3.5. Discussion 42

3.6. Appendix 44

4 A FINITE ELEMENT SKELETAL MUSCLE MODEL FOR SIMULATION OF ISOMETRIC AND CONCENTRIC CONTRACTIONS 47

4.1. Abstract 48

4.2. Introduction 49

4.3. Model and Methods 50

4.3.1. Muscle tissue 50
4.3.2. Tendinous tissue 55
4.3.3. FEM-muscle model 55

4.4. Results 57

4.4.1. Isometric conditions 57
4.4.2. Concentric conditions 60

4.5. Discussion 62

5 A REDUCING CROSS-BRIDGE MODEL EXPLAINS EXPERIMENTALLY OBSERVED CONTRACTION HISTORY EFFECTS 67

5.1. Abstract 68

5.2. Introduction 69

5.3. Methods 70

5.3.1. Huxley-model 70
5.3.2. The reducing cross-bridge model 72
5.3.3. Stiffness 74
5.3.4. Contractions modeled 75

5.4. Results 76

5.4.1. Reducing cross-bridge-model versus Huxley-model 76
5.4.2. Effects of shortening velocity 77
5.4.3. Effects of eccentric velocity 80
5.4.4. Stiffness 83
5.4.5. Sarcomeres in series 85

5.5. Discussion 85

5.5.1. Length dependence 86
5.5.2. Other model adjustments 86
5.5.3. Conclusions 87

6 ACUTE EFFECTS OF TENOTOMY, APONEUROTOMY AND MYOTOMY MODELED TO STUDY INTRAMUSCULAR FORCE TRANSMISSION IN SKELETAL MUSCLE 91

6.1. Abstract 92

6.2. Introduction 93

6.3. Method 94

6.3.1. FEM- skeletal muscle element 94
6.3.2. The EDL model 95
6.3.3. Tenotomy 98
6.3.4. Aponeurotomy 98
6.3.5. Myotomy 98
6.3.6. Shear stiffness 99
6.3.7. Role of the aponeurosis 99

6.4. Results 100

6.4.1. Model of intact EDL 100
6.4.2. Effects of tenotomy 102
6.4.3. Effects of aponeurotomy per se 105
6.4.4. Effects of myotomy 107
6.4.5. The role of shear stress and effects of decreased shear stiffness 110
6.4.6. The role of the disconnected aponeuroses after aponeurotomy 114

6.5. Discussion 115

6.5.1. Muscle integrity and role of aponeurosis 115
6.5.2. Force transmission and shear 118

7 GENERAL DISCUSSION 121

7.1. Introduction 123

7.2. Transmission of force 123

7.2.1. Sarcomere, the force generator 123
7.2.2. Sarcomere-sarcomere interaction in series 123
7.2.3. Myofascial force transmission 124
7.2.4. Motor-unit interactions 126
7.2.5. Myo-tendinous force transmission 127

7.3. Prediction of muscle performance 127

7.4. Reconsideration isolated muscle research 128

7.5. Recommendations 129

7.5.1. Muscle element 129
7.5.2. Aponeurosis element 129
7.5.3. Adaptation 130

References 133

Summary 143

Samenvatting **147**

Dankwoord **151**

Chapter 1

General Introduction

Human locomotion is a typical example of a complex movement of a body where efforts of the central nervous system (CNS) and the muscular-skeletal system are combined. The CNS coordinates movement by sending signals to the correct skeletal muscle at the correct moment. After receiving a signal, muscle initiates movement by exerting force to body segments. For locomotion the contribution of a large number of muscles of different size and shape is necessary. With a feedback system, consisting of numerous specialized sensors, the CNS evaluates the initiated movements. In healthy humans all these complex coordinated actions lead unconsciously to smooth movements. However, due to disease or accident an impairment of one or more of these systems affects the ability to move smoothly or to move at all. For the development of techniques to restore control and reduce disabilities, detailed knowledge is needed of the different systems. Specific tasks of the CNS can be taken over by a functional electrical stimulation (FES) system. Research of these systems focuses on the development of specialized electrodes and stimulation techniques in combination with stimulation strategies. For successful application of such a system, knowledge of muscle is essential. Another example in which insight in muscle performance is necessary, is the development and improvement of existing surgical interventions to reduce disabilities such as spasticity.

To increase the understanding of muscle functioning, questions have to be answered, such as: How much force can muscle produce under specific conditions, why are there so many different muscles. Individual muscle performance is on one hand defined by individual muscle characteristics and on the other hand on generalized muscle characteristics that are valid for all muscles. This thesis focuses on aspects such as geometry and material properties and not on size or location of a specific muscle in the body. Therefore are several different models used. Conclusions of the present thesis are applicable to the vast majority of muscle.

Examining muscle using models exclusively, one should not expect to reveal all essential muscle properties determinating for muscle performance. Model results have to be compared to experimental data. Therefore, simultaneous to the research project presented in this thesis, a project has been executed with the emphasis on experimental determination of muscle characteristics. The results of that project are reported in the thesis of Meijer (1998).

1.1. Skeletal muscle

For many centuries (Stensen, 1664; Borelli, 1680; Swammerdam, 1767) research is devoted to skeletal muscle, which is the motor behind initiation and counteraction of movement of body or body segments. In skeletal muscle research, many authors (e.g. Borelli, 1680, see fig. 1-1; Benninghoff and Rollhauser, 1952; Gans and Bock, 1965) addressed the importance of the geometrical arrangement of muscle fibers in a muscle belly for exertion of force. This arrangement of fibers in muscle makes a transformation of fiber characteristics necessary to obtain muscle characteristics. Muscles appear in many different shapes, i.e. architecture, which suggests that architecture is related to muscle function. Herewith is the focus introduced of this dissertation: the relation between muscle architecture and the amount of force exerted under a specific condition.

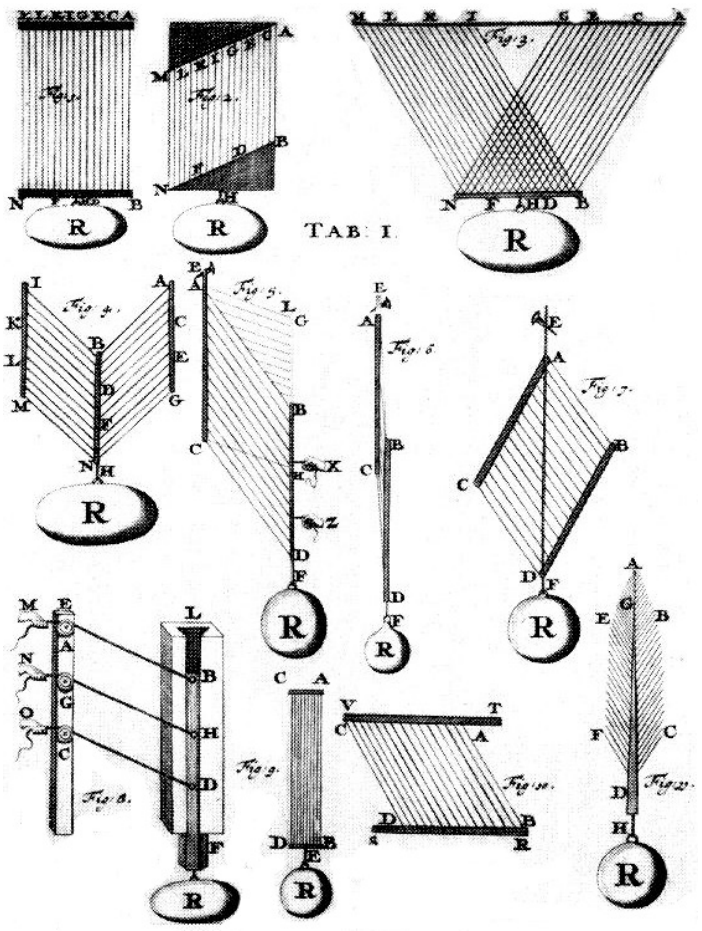

Figure 1-1 Muscle structures according to Borelli (1680), and the relation between force (R) and muscle architecture.

1.1.1. Morphology and physiology

The function of muscle is to contract. During a contraction is force produced and exerted at origin and insertion of the muscle. If a muscle produces force without initiating a movement, i.e. muscle length is constant, this is called an isometric contraction. Contractions in which muscle shortens or lengthens are indicated as concentric and eccentric contractions, respectively.

Muscles exert force when activated by stimuli from a nerve or artificially by an electrode (FES). These stimuli start a chain reaction of chemical processes that initiates, a connection to be made between the actin filament and opposite myosin filament. Such a connection is addressed as a cross-bridge. The myo-filaments, actin and myosin, form together the smallest functional unit of a muscle, the sarcomere (fig. 1-2). In a muscle fiber a large number of sarcomeres are arranged in series. The alignment of sarcomeres in series observed in parallel arranged fibers attributes to the name of striated muscle. Movement is initiated when the myo-filaments slide

past one another. A large number of muscle fibers arranged in parallel form a muscle belly. Through aponeuroses (tendon-sheets) and tendons, the muscle fibers are attached to the bone structure at origin and insertion. Therefore, aponeuroses and tendons are assumed to be in series arranged with the fibers. An aponeurosis is made of tendinous tissue at which fibers are attached at an angle. At one end an aponeurosis turns into a tendon.

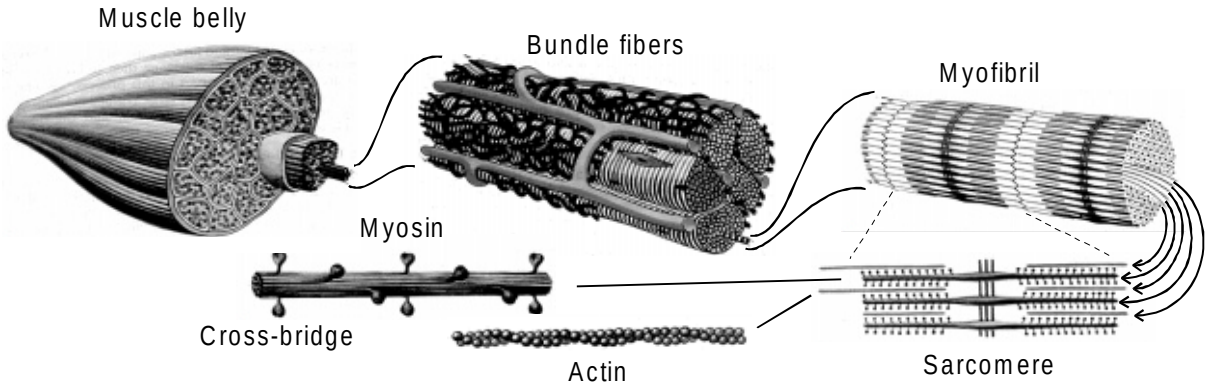

Figure 1-2 Muscle anatomy adapted from Gray's anatomy (Warwic and Willems, 1973)

The arrangement of the fibers with respect to the line of pull in muscle defines muscle architecture. A schematic representation of a classification in architectural characteristics is given in figure 1-3. The most common muscle architectures are the parallel fibered and the pennate muscles. In parallel fibered muscle is assumed that, fibers are arranged along the line of pull of the muscle and have lengths similar to the muscle length. In contrast with pennate muscle in which fibers are relatively short compared to the muscle length and have an angle of operation with respect to the muscle line of pull. That so many different muscle architectures

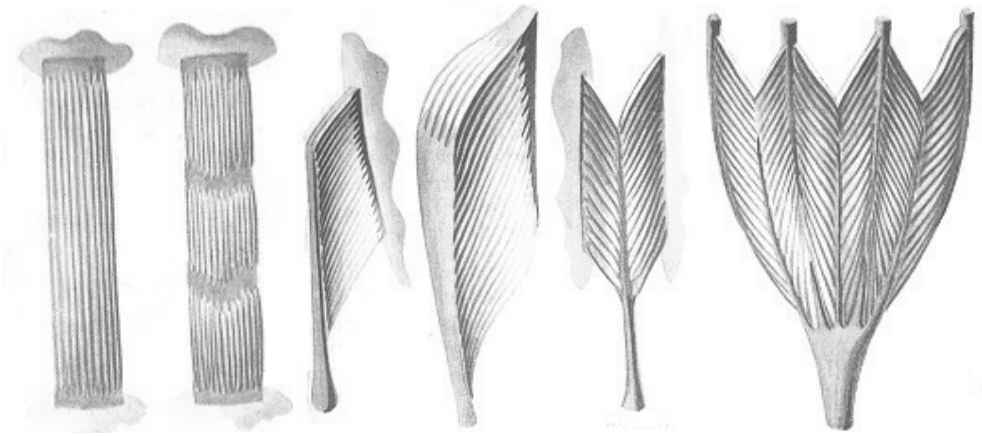

Figure 1-3 Variety of muscle architectures, with from left to right: two parallel fibered, two uni-pennate and bi-pennate and multi-pennate muscle, adapted from Gray's anatomy (Warwic and Willems, 1973).

exist, suggests a relation with the amount of force a muscle can exert under a specific condition.

1.1.2. Mechanics of muscle

Several aspects of muscle physiology and morphology have important consequences for the mechanics of muscle tissue. Many of these consequences are addressed in detail in the present thesis. The properties that define the amount of force exerted can be distinguished in material and structural properties.

1.1.2.1. Material properties

Muscle is made of soft tissues, which allows for large deformations. It has, like other soft biologic tissues, non-linear passive properties (Fung, 1981). Furthermore, since experiments performed by Swammerdam in the 17th century, as is reported in the 18th century (Swammerdam, 1767) is it known that the muscle volume is constant during contractions. In contrast with other soft tissues, muscle has the ability to exert force when activated. First of all, the level of activation determines the amount of force exerted. However, the level of activation depends on non-mechanical properties such as firing rate of nerves, reaction rate of chemical processes and other activation dynamics. The present thesis only deals with maximally activated muscle. Second, of great importance for the amount of force exerted, is muscle length, expressed in the force-length curve. According to the sliding filament theory (Huxley, 1957) sarcomere force depends on the amount of overlap of the myo-filaments. A characteristic point in this curve is the length at which maximal force is exerted, addressed as optimum length of sarcomere, fiber or muscle. For lengths smaller than optimum length, the force exerted is reduced. The lowest length at which any force is exerted is called active slack length. Over optimum length, active force decreases with length. In addition, passive force contributes also to the total force for lengths over passive slack length; i.e. the smallest length any force is exerted under passive conditions. An isometric force-length curve is constructed for data from numerous isometric contractions at different lengths. The active force is obtained from the subtraction of the total and the passive force, to a custom in general myology. Third, during dynamic contractions force depends on velocity of movement, expressed in the force-velocity relationship. If the force-length and force-velocity characteristics are assumed to be independent (Hill, 1938), it is possible to construct a three-dimensional surface (fig. 1-4). This surface is sufficient for most purposes of

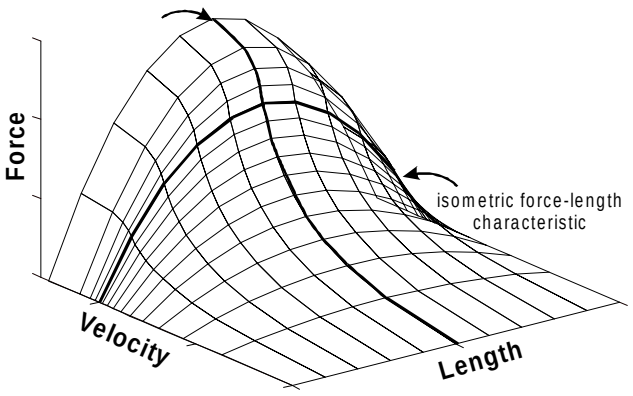

Figure 1-4 The variables of muscle function: force, velocity and length (Hill, 1938). The thick curves indicate the isometric force-length curve and force-velocity curve at optimal length.

investigating the amount of force exerted. However, many authors reported that the force level depends on properties that change in time during sustained contractions (e.g., Abbott and Aubert, 1952, Edman *et al.*, 1978, Sugi and Tsuchiya, 1988, Meijer et al, 1997). These changes in force are addressed as the effects of contraction history, such as: fatigue, a force deficit after shortening and force enhancement after lengthening.

A muscle-tendon complex consists besides muscle tissue of tendinous tissue. Aponeuroses (tendon sheets) and tendons in general have non-linear elastic properties. Due to the fact that force produced by fibers is transmitted to muscle origin and insertion through the aponeuroses and tendons the tendinous structures are assumed to be arranged in series with fibers.

1.1.2.2. Structural properties

That sarcomeres are arranged in series with each other in a fiber suggests that force generated by these sarcomeres is equal. The fact that not all sarcomeres in series are identical, results in interactions that can lead to mechanical instable behavior at lengths over fiber optimum length (e.g., Julian and Morgan, 1979a,b; Morgan and Proske, 1984; Sugi and Tsuchiya, 1988). In addition, the number of sarcomeres in series determines the active length range of a muscle fiber. The amount of fibers arranged in parallel, the physical cross sectional area (PCSA) is a measure for the maximal active muscle force. The alignment of fibers in muscle is an indication that muscle has anisotropic properties. In pennate muscle, the fibers are arranged at an angle with the line of pull of the muscle. Due to this angle, functional characteristics of muscle are obtained from the transformation of fiber characteristics. Therefore, muscle architecture is an important structural property as well.

1.2. Modeling

The attractiveness of modeling is that many research questions can be tested, i.e. the heuristic purpose of a model (Huijing, 1995), and the number of animal or human experimental subjects can be limited. The great virtue of models is the heuristic purpose, besides predicting specific aspects of complex function. Another big advantage of a model is the freedom of the researcher to make the model as simple or as complex as his questions require or as detailed as the outcome require. This thesis deals with several sub-goals and therefore different types of models are used to reach these specific goals of heuristic nature. Since the 17th century (Borelli, 1680, see fig. 1-1), models are frequently used to study or describe muscle function. A distinction is developed historically in addressing several types of models. These types are distinguished by the level muscle structures are described.

1.2.1. Hill-type models

An extensively used model was proposed by Hill (1938). This model is based on experimental observations and consists of a contractile element that is in series arranged with a spring. The contractile element represents the contraction machinery with the force-length-velocity surface (fig. 1-4). The spring represents the contribution of tendon and aponeuroses. A third element

representing passive muscle properties is arranged in parallel and some aspects of activation dynamics were incorporated in this model (e.g., Hatze, 1981) to increase the capabilities of predicting force of different muscle. Hill-type model describes the interactions of the contractile machinery and the series elastic structures.

1.2.2. Huxley or Cross-bridge models

A model of different nature is proposed by Huxley (1957) based on cross-bridges dynamics. With this model experimentally determined force-velocity characteristic is described. Furthermore, predictions of the energy metabolism have been improved. That this model describes the dynamics of cross-bridges in time makes this model suitable for study of variations of force in time. Extensions (e.g., Hill *et al.*, 1975; Eisenberg *et al.*, 1980; Ma and Zahalak, 1990) and approximations (Zahalak, 1981) of this model allow the study of force transients, energy utilization and excitation dynamics in more detail.

1.2.3. Morphological models

Based on the knowledge that muscle the amount of force exerted under a specific condition is strongly related to morphology, models have been developed that combine geometrical aspects, such as fiber and aponeurosis length, fiber and aponeurosis angle. Modeling of pennate muscle started with accounting for fiber orientation with respect to the line of pull. Other geometrical characteristics are introduced in muscle modeling to account for relative lengths and pennation angles. The demand of constant muscle volume is incorporated in the model with the introduction of a planimetric model (Huijing and Woittiez, 1984) and a three-dimensional version of it (Woittiez *et al.*, 1984). These models focus on the prediction of muscle geometry as well as isometric force-length curve. The relation between the demand of constant volume and internal muscle pressure inspired researchers (e.g., van Leeuwen and Spoor 1992, 1993; Otten, 1988) to develop models for uni- and bi-pennate muscle that allow the prediction of mechanically stable muscle geometries. These model results show that muscles should have curved fibers and aponeuroses to be mechanical stable. They also stated that a mechanical approach to muscle is essential for understanding of the mechanism that is responsible for the amount of muscle force exerted.

1.2.4. Morpho-Mechanical models

Mechanical models that are based on the finite elements method (FEM) are intrinsically stable. Such models are developed for cardiac muscle (e.g. Huyghe, 1984; Hunter et al, 1988; Horowitz *et al.*, 1988; McCulloch *et al.*, 1992) and recently for soft tissue to study blood perfusion by Vankan *et al.* (1996 and 1997). This method is able to handle the combination of all specific structural and material properties of skeletal muscle mentioned in the preceding sections. FEM-models are the first models that account for several passive properties of muscle tissue as a continuum. In addition, this method allows studying the mechanism of force exertion by muscle in more detail than existing models without modeling every structure, as is indicated in the results of cardiac muscle modeling.

1.3. Scope of the thesis

As is referred to in the preceding sections this thesis focuses on the relation between morphology and force of a muscle-tendon complex under various conditions. In this model study, a distinction is made in material and structural properties, such as fibers, passive muscle tissue, i.e. extracellular matrix, aponeurosis and tendons. The amount of muscle force and muscle geometry are studied under isometric, concentric and eccentric conditions. Muscles are assumed to be mechanical force generators, therefore mechanically relevant properties are incorporated in the models.

Several research questions are dealt with in this thesis:

- How simple can models be to predict force of uni-pennate muscle?
- Why has a muscle a specific morphology and what is the consequence of this morphology for the muscle force?
- What is the contribution of individual structures and properties to muscle force exerted?
- How can experimentally observed force changes during sustained contractions be described?
- How is force, generated in the sarcomeres, transmitted to origin and insertion of muscle?
- What are the effects of surgical interventions on muscle?

In order to reduce the complexity, muscle is modeled in two dimensions. The plane, in which muscles are studied, contains most characteristic properties and structures, to obtain a representative model. In this thesis, it becomes apparent that this approach is justified. A great deal of this study is applied to the gastrocnemius medialis (GM) muscle of the rat. This muscle is chosen as a starting point for the study of muscle architecture, for its large angle of pennation, and for the easy access to experimental data gathered by Meijer (1998).

1.4. Contents of this thesis

The present thesis consists of chapters separately offered for publication, which can be studied independently of each other. The goal of this thesis is addressed with three different types of models. In chapter 2 and 3 morphological models are used. A cross-bridge model is presented in chapter 5. In chapter 4 and 6 are the capacities explored of a morpho-mechanical model based on the finite element method.

In chapter 2, a simple planimetric model of rat GM is used to study the effects of pennation on the force-length characteristics of muscle and on linearized muscle geometry under isometric conditions. Furthermore, the effect of an elastic aponeurosis on these characteristics is addressed. The demand of constant muscle volume is challenged with this two-dimensional and a simple three-dimensional extension of this model. Chapter 3 deals with the functional transformation from fiber characteristics to muscle characteristics based on mechanical equilibrium of the geometry of whole muscle, in contrast with equilibrium of the aponeurosis as assumed in chapter 2.

In chapter 4, a newly developed two-dimensional finite element model of skeletal muscle tissue is presented. The role of several muscle structural and material properties is studied with a model of rat GM under isometric and concentric conditions. Furthermore is focused on interactions of the structures such as fibers and aponeurosis.

In chapter 5, a cross-bridge model describes several phenomena experimentally observed that lead to a change in force during sustained contractions, i.e. the effects of contraction history. This model utilized with one simple alteration in the cross-bridge kinetics to describe the effects experimentally observed.

The approach of chapter 4 is continued in chapter 6, which is focused on force transmission in muscle and the role of aponeuroses. Furthermore, the effects of surgical operations applied to a muscle-tendon complex are studied with a finite elements muscle model. The results indicate that this model can be of relevance in clinical applications.

Finally, chapter 7 is used for a general discussion of results presented in this thesis. Reflections are given on the consequences for the understanding of muscle functioning. Finally, some recommendations are given for future research.

Chapter 2
Modeling Functional Effects of Muscle Geometry

2.1. Abstract

Muscle architecture is an important aspect of muscle functioning. Hence, geometry and material properties of muscle have great influence on the force-length characteristic of muscle. We compared experimental results for the gastrocnemius medialis muscle (GM) of the rat to model results of simple geometric models such as a planimetric model and three dimensional versions of this model. The capabilities of such models to adequately calculate muscle geometry and force-length characteristics were investigated. The planimetric model with elastic aponeurosis predicted GM muscle geometry well: maximal differences are 6%, 1%, 4% and 6% for fiber length, aponeurosis length, fiber angle and aponeurosis angle respectively. A slanted cylinder model with circular fiber cross section did not predict muscle geometry as well as the planimetric model, whereas the geometry results of a second slanted cylinder model was identical to the planimetric model. It is concluded that the planimetric model is capable of adequately calculating the muscle geometry over the muscle length range studied. However, for modeling of force-length characteristics more complex models are needed, as none of the models yielded results sufficiently close to experimental data. Modeled force-length characteristics showed an over-estimation of muscle optimum length by 2 mm with respect to experimental data and in addition force at the ascending limb of the length force curve was underestimated. The models presented neglect important aspects such as non-linear geometry of muscle, certain passive material properties and mechanical interactions of fibers. These aspects may be responsible for shortcomings in modeling.

It is argued that, considering the inability to adequately model muscle length-force characteristics for an isolated maximally activated (*in situ*) muscle, it is to be expected that prediction will fail for muscle properties in conditions of complex movement with many interacting factors. Therefore modeling goals should be limited to the heuristic domain rather than expect to be able to predict or even approach medical or biological reality. However the increased understanding about muscular mechanisms obtained from heuristic use of such simple models may very well be used in creating progress in for example clinical applications.

(van der Linden *et al.*, 1998a, J Electromyography Kinesiology, in press)

2.2. Introduction

Already in the 17th century (e.g. Stensen, 1667; Borelli, 1681) scientific research was aimed at skeletal muscle. More recently, a specific part of this research is dedicated to the strong relation between architecture and functional capabilities. This relation is still not fully understood even though muscle modelling has added to understanding.

A muscle can be considered as a volume with a specific geometry. Already in the seventeenth century Swammerdam (1737) observed that muscle volume is constant during contraction and length changes. One aspect of muscle geometry is the cross sectional area of the fibers which is an estimate for the amount of force that can be exerted maximally. Other aspects of muscular geometry are length and orientation angles of fibers, tendon, tendon-sheets. In case the fibers are not parallel to the line of action of the muscle, the muscle is considered pennate. The effects of pennation are among the most influential characteristics of muscle morphology on muscle functioning (e.g. Brand *et al.*, 1986; Huijing and Woittiez, 1984 & 1985; Otten, 1988; Scott and Winter, 1991; Spector *et al.*, 1980; van Leeuwen and Spoor, 1992 & 1996; Winters and Stark, 1987). If number of sarcomeres in series is equal, for a given muscle volume muscles with a lower degree of pennation will exert a lower maximal force but have a wider active length range when compared to muscle with a high degree of pennation (e.g. Huijing and Woittiez, 1984 & 1985; Huijing 1989; Scott and Winter, 1991). Therefore, the functional consequences of pennation such as maximal muscle force and the maximal length range of motion are expressed in the length-force characteristic. Due to growth (Heslinga and Huijing, 1990; Willems and Huijing, 1992), and as a consequence of immobilization (Heslinga and Huijing, 1993), architecture is altered.

Since the presentation of the planimetric (Huijing and Woittiez, 1984) and related models, many models with increasing complexity have been developed to study effects of muscle geometry on muscle functioning, (see review articles of Winters and Stark, 1987 and Zajac, 1989). A complex linearized three-dimensional version of the planimetric model (Woittiez *et al.*, 1984) allowed prediction of muscle geometry and length-force characteristics. Van Leeuwen and Spoor (1992) developed a model based on mechanical equilibrium in muscle. The balance between internal pressure and external forces causes the aponeurosis and the fibers to curve in their model. Such curvature is also predicted by Otten (1988). He proposed a three-dimensional model based on the mechanical equilibrium in a discrete number of points in the aponeurosis. Between these points he assumed springs representing the passive elasticity of the aponeurosis. Fibers act independently and exert force in the same points. Equilibrium in all points allowed him to calculate geometry and the internal pressure distribution of different types of muscles. These models have in common that they need a large numerical effort and are more focused on details of geometry and muscle pressure than on length-force and force-velocity characteristics. The question rises whether these complex models are needed to study the relation between muscle geometry and function. How well do the relative simple, two-dimensional models perform?

The goal of this study is to evaluate five of these simple models for their capabilities of adequately modeling muscle geometry and length-force characteristics of the gastrocnemius medialus (GM) of the rat. The models are based on the planimetric model (Huijing and Woittiez, 1984 & 1985) but are extended to incorporate different experimental observations. All models have a linearized geometry and do not attempt to take into account curvature of structures. This implies that mechanical equilibrium is not guaranteed in all points.

2.3. Methods and Models

The models presented in this paper are applied for the medial gastrocnemius muscle (GM) of the rat. Figure 2-1A shows a schematic representation of this muscle and figure 1B shows the linearized two-dimensional version based on the marker positions. This unipennate muscle is suitable for studying the effects of architecture because of the large angle of pennation and the enormous amount of experimental data available.

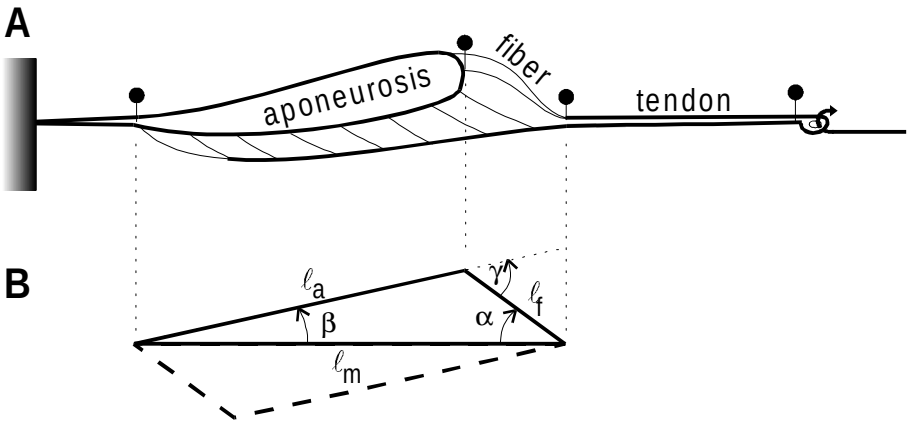

Figure 2-1 A. A schematic representation of rat gastrocnemius medialis (GM) muscle. Markers are positioned on strategic positions. **B.** The lower panel shows a two-dimensional linearized representation of rat GM based on the marker positions. Such geometry is the foundation of the planimetric model (Huijing and Woittiez, 1984 & 1985) with muscle length (ℓ_m), fiber length (ℓ_f) and aponeurosis length (ℓ_a), the fiber angle (α), aponeurosis angle (β) and what is referred to as the angle of pennation ($\gamma=\alpha+\beta$) (Model 2 and 3).

The model muscle is assumed to have the following properties:

- Muscle geometry is linearized, therefore curvature and bulging of fibers and aponeurosis are neglected.
- Homogeneous muscle geometry is assumed and the fibers are modeled according the length and orientation of the most distal fiber, i.e. all fibers have identical length and properties.
- Isometric contractions at different muscle length are performed in order to construct the length-force characteristics of the muscle.
- Muscle volume remains constant during contraction (Swammerdam, 1737). This is implemented for three-dimensional models to be used here. For the two-dimensional models

it is assumed that the muscle area (figure 2-1B) remains constant, which is in agreement with experimental observations (Zuurbier and Huijing, 1993).

- The fiber length-force curve is constructed on the basis of sarcomere length-force characteristics and a fixed number of identical sarcomeres in series. Therefore, effects of sarcomere length heterogeneity are not considered (Julian and Morgan, 1979a,b).
- Force-velocity characteristics are not considered.
- The muscle is fully recruited and activated maximally.
- The effects of fatigue and potentiation on muscle force are not considered.
- The aponeurosis is not constant in length for each contraction. Zuurbier and Huijing (1994) showed that the aponeurosis is very elastic. Therefore, the aponeurosis length depends on force exerted on it. Bending forces are not considered, because the models presented in this paper are not able to describe curved aponeuroses.
- The active muscle force (F_{ma}) depends on the active fiber force (F_{fa}) according to eq. 1, in which the angular effects of pennate muscle (Otten, 1988) are taken into account:

$$F_{ma} = F_{fa} \cdot \frac{cos(\alpha + \beta)}{cos(\beta)} \tag{1}$$

These assumptions are common to five models presented in this paper:

2.3.1. Model 1: parallel fibered model

A basic model in which no pennation properties are included. In this model the fibers act parallel to the muscle line of action, i.e. a parallel fibered muscle model. This model represents the properties of the fibers of the muscle and is included for purposes of comparison with the other models to show effects of pennation.

2.3.2. Model 2: original planimetric model

This model represents the original planimetric model firstly presented by Huijing and Woittiez (1984 and 1985). The model is based on the linearized mid-longitudinal cross-sectional area of the rat GM (fig. 1B), i.e. a model within one plane. The aponeurosis is assumed to be in extensible. In this two-dimensional model the area of the muscle is kept constant. The muscle area (A_m) in the planimetric model is represented by the length of the cross sectional area (ℓ_{Afa}) multiplied by the fiber length:

$$A_m = \ell_f \cdot \ell_{Afa} = \ell_f \cdot \ell_a \cdot sin(\alpha + \beta) \tag{2}$$

The angles α and β represent the angles between the muscle line of pull and the fibers and aponeurosis, respectively (fig. 2-1B). The reference of the model is based on the geometry of the muscle at optimum length (ℓ_{mao}). The model area and the aponeurosis length are defined at that length. In the studied muscle length range the muscle geometry and force are calculated from the fiber length (ℓ_f), the aponeurosis length (ℓ_a) and the muscle area (see Appendix).

2.3.3. Model 3: planimetric model with elastic aponeurosis

This model is the same as the previous one but an iterative procedure is used to calculate the aponeurosis and fiber length. The aponeurosis elongation is related to the fiber force. It is assumed that the force exerted by all fibers is taken up by the entire aponeurosis. Furthermore, the aponeurosis is assumed to have a quadratic length-force relationship (Eq. 3):

$$F_{aa}(\ell_{aa}) = F_{fa}(\ell_{fa}) \cdot cos(\alpha + \beta) = c \cdot (\ell_{aa} - \ell_{aas})^2 \quad (3)$$

Where ℓ_{aas} is the aponeurosis active slack length (ℓ_{aa}: active aponeurosis length, ℓ_{fa}: active fiber length), defined as the aponeurosis length at which the active muscle exerts no force and the constant c is chosen such that the best fit at ℓ_{mao} is obtained (Table 2-1).

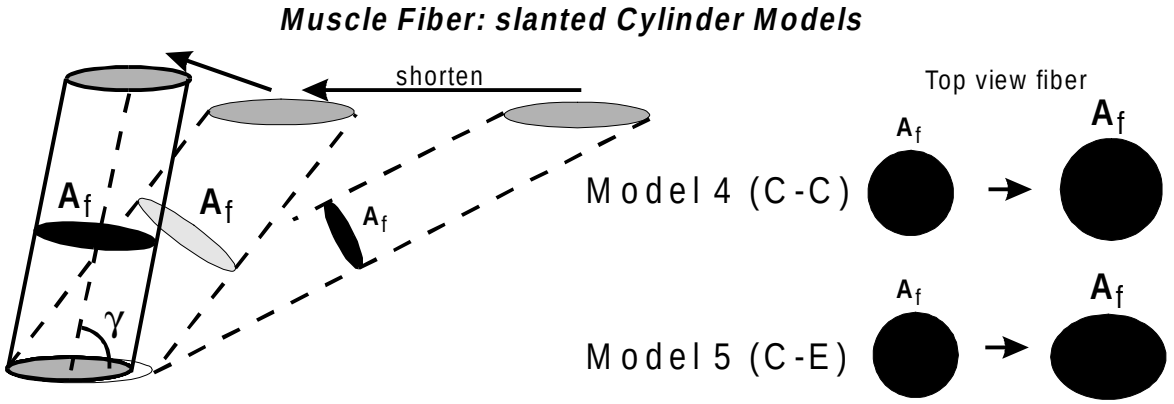

Figure 2-2 Representation of slanted cylinder models. During shortening of the fibers of the slanted cylinder models, the pennation angle (γ) has to increase due to constancy of muscle volume. As a consequence of elastic properties of the aponeurosis the angle of pennation has to increase even more. The bottom panel shows differences between the two slanted cylinder models used in this study. Model 4 (C-C) keeps fiber cross-sectional area (A_f) circular during shortening. For model 5 (C-E) the movement of volume is restricted to those directions for which increased fiber diameter can be accommodated by angular effects. Therefore fiber cross-sectional area becomes elliptic during shortening.

2.3.4. Model 4: C-C model

The slanted cylinder model (Willems and Huijing, 1994; Zuurbier and Huijing, 1992), (fig. 2-2) is a simple three-dimensional extension of the planimetric model. Where the fibers are represented by a slanted cylinder. The circular cylinder ends are assumed to remain parallel to each other and represent the aponeurosis. The slant angle varies as a combined result of fiber shortening and aponeurosis length changes calculated in an iterative procedure. This model includes an elastic aponeurosis, which length is proportional to the force exerted on the aponeurosis, as described in equation 3. This model allows the fibers to re-distribute volume equally in both the fiber diameter within longitudinal plane of the muscle as well as the one perpendicular to the plane (i.e. the cross-section remains circular).

2.3.5. Model 5: C-E model

The elliptic version of the slanted cylinder model initially (at ℓ_{mao}) has an identical geometry as model 4. But the active fiber cross-sectional area (A_{fa}) becomes elliptic (C-E) as fibers shorten (fig 2-2, right panel). Fiber diameter is only allowed to increase in the plane in which angular effects can accommodate such increases of diameter (i.e. longitudinal plane of the muscle). The perpendicular fiber diameter is assumed to remain constant.

Sarcomere length-force characteristics

Two types of sarcomere length-force curves are applied in the model described. One is based on contractions involving servo control, keeping sarcomere length constant (Gordon *et al.*, 1966). This sarcomere length-force relationship is assumed to consist of two parts (fig. 2-3A). Between sarcomere active slack length (ℓ_{sas}) and sarcomere active optimum length (ℓ_{sao}) the force is a quadratic function of length. Between ℓ_{sao} and the sarcomere active maximal length (ℓ_{sam}) a linear function is assumed. The characteristic length (ℓ_{sas}, ℓ_{sao}, ℓ_{sam}) are determined from filament length parameters (ℓ_z, ℓ_{thin}, ℓ_{thick}, ℓ_{bare}, Table 2-1) shown in figure 3B using the following equations:

Maximal active sarcomere length: $$\ell_{sam} = \ell_z + \ell_{thick} + 2 \cdot \ell_{thin} \quad (4)$$

Optimum sarcomere length: $$\ell_{sao} = \ell_z + \ell_{bare} + 2 \cdot \ell_{thin} \quad (5)$$

Approximation of active sarcomere slack length: $$\ell_{sas} \approx 0.9 \cdot \ell_{thin} \quad (6)$$

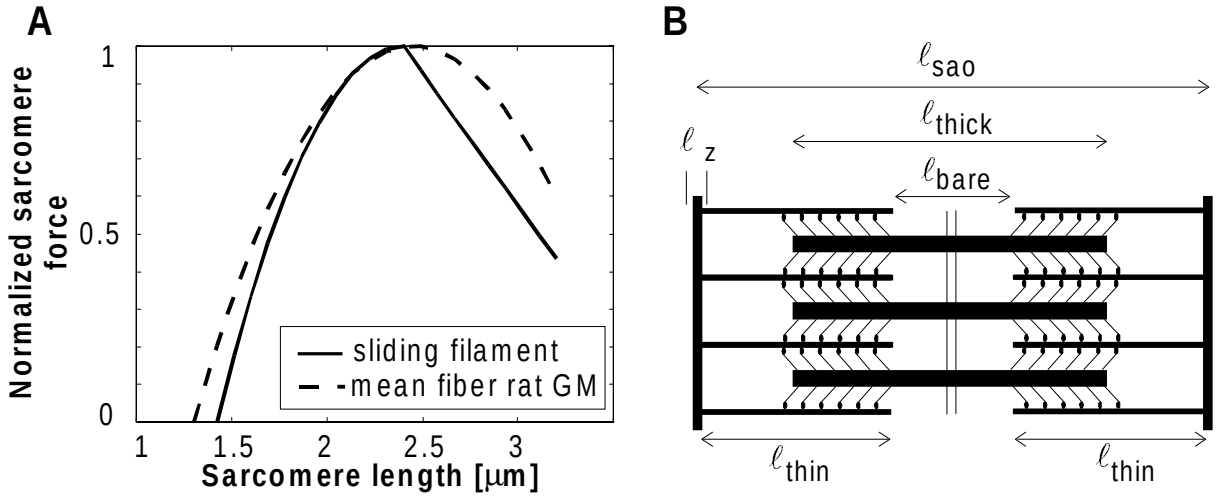

Figure 2-3 A. Sarcomere length normalized force characteristics of rat GM. The solid line indicates characteristics according to the sliding-filament theory (based on servo-controlled sarcomere length). The dashed line indicates mean sarcomere length force properties on the basis of experimental data from fixed end contractions on small bundles of fibers (Zuurbier *et al.*, 1995). **B.** A schematic representation of sarcomeres at sarcomere optimum length (ℓ_{sao}). Indicated are lengths of respectively: thick filament (ℓ_{thick}), thin filament (ℓ_{thin}), cross bridge bare zone (ℓ_{bare}) and the z-band (ℓ_z) (parameters see Table 2-1).

The second sarcomere length-force relationship incorporates effects of a non-uniform behavior of sarcomeres in series in muscle fiber (e.g. Edman *et al.*, 1978; Julian and Morgan, 1979a&b). This means that a muscle fiber does consist of a number of sarcomeres is series with lengths that are not identical. Using fixed end contractions for small bundle of fibers, Zuurbier *et al.* (1995) experimentally determined a mean sarcomere length-force curve, which is expressed as 4th order polynomial function shown in figure 2-3A (coefficients see Table 2-1). It incorporates some effects of in series homogeneities of sarcomere length. This is in contrast with the first sarcomere length-force relationship where the sarcomere length is servo-controlled, and therefore constant of length.

Table 2-1 Parameters of models 1 through 5, based on mean experimental data (n=6) of Zuurbier and Huijing (1992). In the last two columns are the coefficients indicated of the 4th order polynomial function representing the mean sarcomere force-length characteristic of rat GM (Zuurbier *et al.*, 1995)

Myo-filament data		Mean rat GM data		F-l (Zuurbier *et al.*, 1995)	
ℓ_z	0.1 μm	ℓ_{mao}	32.1 mm	p_0	-371.46351
ℓ_{bare}	0.16 μm	ℓ_{fao}	11.7 mm	p_1	407.83972
ℓ_{thin}	1.04 μm	ℓ_{aao}	21.2 mm	p_2	-93.47863
ℓ_{thick}	1.54 μm	F_{mao}	11.9 N	p_3	1.77145
#sarc	5765	ℓ_{aas}	19.8 mm	p_4	0.14914
		c	0.38 N/mm^2		

2.4. Results

Model results are compared to mean experimental (n=6) results for length-force characteristics and linearized geometrical data of rat GM (Zuurbier and Huijing, 1992), the model parameters are presented in Table 2-1.

Figure 2-4 shows length-force characteristics and geometry of the fiber model (model 1) and the planimetric model (model 2). Sliding filament theory based sarcomere length force curves were used here for model 1 and 2. For model 2 fiber length agrees well with experimental data (fig. 2-4, top panel), except at very small muscle lengths where fiber length is under-estimated by the model (by up to 1 mm at muscle active slack length (ℓ_{mas})). In contrast muscle force is not modeled well at all by model 2: Muscle force is largely underestimated at the ascending limb of the length force curve (fig. 2-4, bottom panel). Furthermore, muscle optimum length (ℓ_{mao}) is over-estimated by approximately 2 mm. For fixed end contractions mean length range of sarcomeres from rat GM is enlarged (fig. 2-3). Therefore, it is expected that using such a curve yield a better estimation of the length-force characteristics than using the sarcomere relationship based on the sliding-filament theory. However, the improvement of length range predicted is still minor compared to differences that exist with experimental data (results not shown).

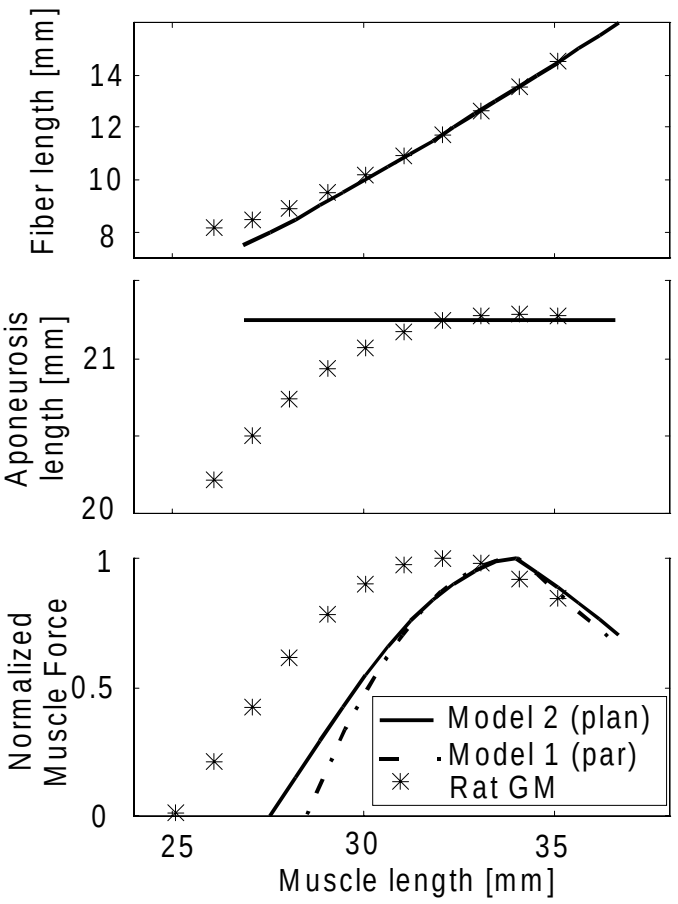

Figure 2-4 Results of the planimetric model with non-elastic aponeurosis (model 2, plan) compared to the parallel fibered model (model 1, par) and mean data of rat GM. Sliding-filament theory sarcomere length-force characteristics are used. Fiber length, aponeurosis length and muscle force are shown as a function of muscle length.

The effect of pennation is visible when results of model 1 and 2 are compared (fig. 2-4, bottom panel). The length range (from ℓ_{mas} to ℓ_{mao}) of force exertion is larger for pennate muscle (model 2) than for its fibers (model 1).

Results of model 3 (incorporating an elastic aponeurosis and using mean sarcomere length force characteristics) are presented in figure 2-5. Comparison to results of models 1 and 2 shows that effects of pennation increase substantially by introducing an elastic aponeurosis. Modeling of fiber length is improved (fig. 2-5, top panel) due to better prediction of aponeurosis length using a quadratic length-force relationship (eq. 3) (fig. 2-5, middle panel). However, the relation of muscle length to force is not modelled correctly at all lengths: modeled ℓ_{mao} still over-estimates the experimental value (i.e. no improvement compared to model 2), but, in contrast, modeled ℓ_{mas} is decreased and approximates experimental slack length ($\ell_{mas} \approx 25$ mm). This yields an underestimation of force for length under ℓ_{mao}, and an overestimation of muscle force for length over ℓ_{mao}.

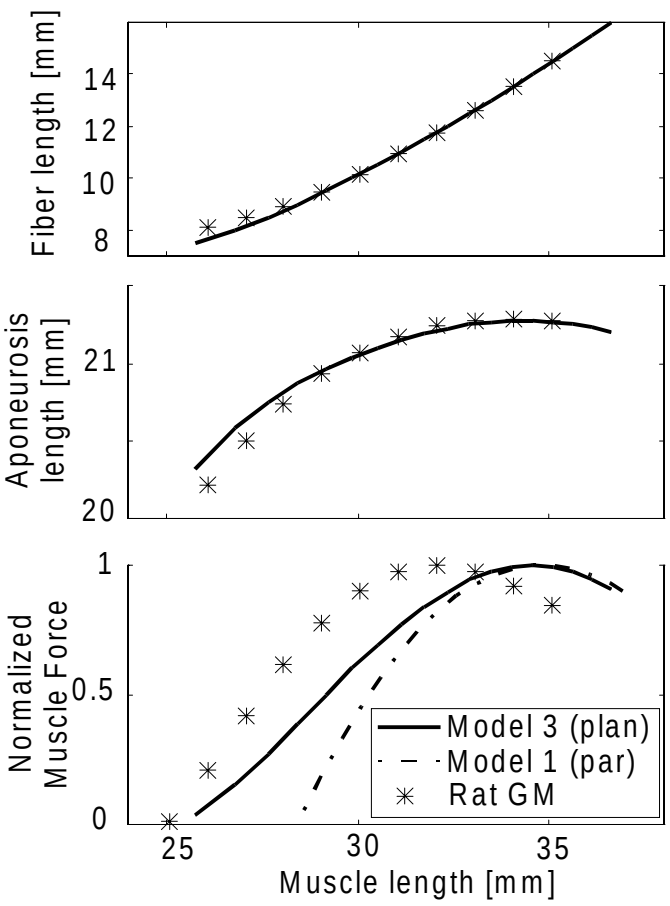

Figure 2-5 Results of the planimetric model with elastic aponeurosis (model 3, plan) compared to the parallel fibered model (model 1, par) and mean data of rat GM. Mean sarcomere length-force characteristics are used. Fiber length, aponeurosis length and muscle force are shown as a function of muscle length.

Results of the models 3 through 5 are compared to experimental data on aspects of muscle geometry first (fig. 2-6). These models have an aponeurosis with elastic properties and use the mean sarcomere length-force curve. Fiber and aponeurosis lengths (fig. 2-6A and B) are predicted well by all models. For model 3 and 5, the maximal differences are 6% and 1% of fiber length, aponeurosis length respectively. Furthermore, modelled fiber angle (α) shows a good agreement with experimental data, for model 3 and 5 the maximal difference is 4% of the fiber angle. A notable exception of model 4 (i.e. C-C) (fig. 2-6C). Near ℓ_{mas}, model 4 underestimates fiber angle by about 10 degrees (i.e. 25%). For aponeurosis angle (β), models 3 and 5 show a reasonable agreement with experimental data: at ℓ_{mas} the difference is approximately 1 degree (6%, fig. 2-6D). However for model 4, β is calculated to be almost constant over the active muscle length range studied.

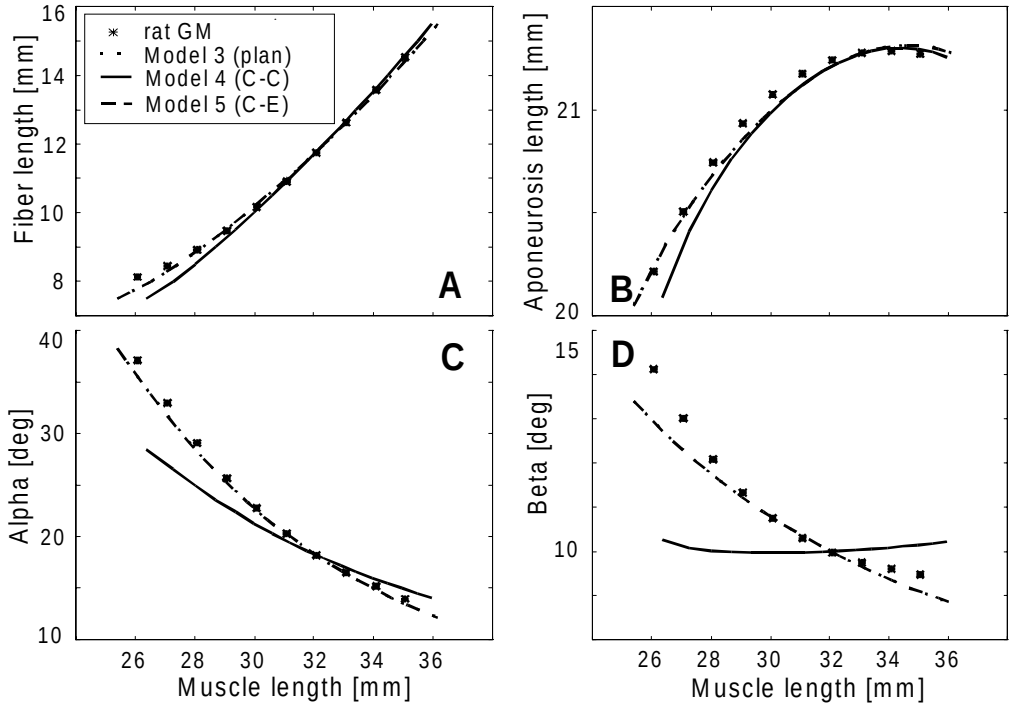

Figure 2-6 Comparisons of geometric results of models 3 through 5 and rat GM data. The models are the planimetric model with elastic aponeurosis, C-C model and C-E model. The fiber length (A), aponeurosis length (B), fiber angle (C) and aponeurosis angle (D) are plotted as a function of muscle length.

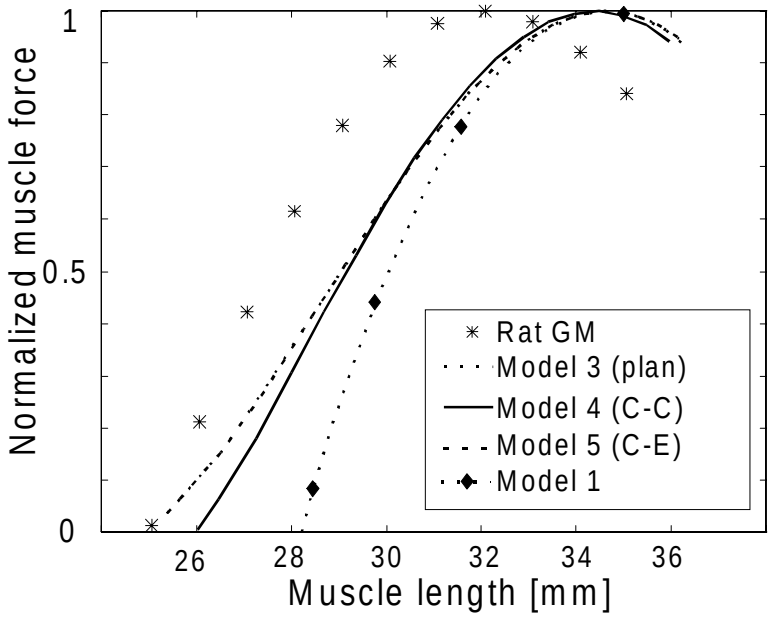

Figure 2-7 Muscle length force characteristics calculated by the models 3 through 5 compared to mean rat GM data. The models are the planimetric model with elastic aponeurosis, C-C model and the C-E model. Note that the curves of model 3 and 5 are superimposed.

On the basis of these results, it is expected that model 4 is not able to calculate muscle length-force characteristics approaching those found experimentally. This was found to be the case (fig. 2-7). However it should be noted that results for model 3 and 5 are identical and also differ substantially from experimental muscle length-force characteristics of rat GM.

2.5. Discussion

Improvement of the planimetric model by making the aponeurosis elastic, resulted in better prediction of muscle active slack length. The effects of an elastic aponeurosis induced additional changes in muscle geometry with muscle shortening and due to the changed angular effects the muscle force is altered. It is concluded that two-dimensional geometrical linearized models are able to predict (linearized) geometry of rat GM well when an elastic aponeurosis is included in the model. Additional assumptions such as fibers with circular cross-sectional areas (changing diameters equally in all directions with length change, model 4) does lead to much increased error of prediction of muscle geometry. This suggest that equal volume excursion in all directions of the fiber cross-section is not a correct assumption. Model 3 and 5 predict the linearized muscle geometry well and are therefore useful to study the effects of pennation on geometry.

The persisting errors in the modeled force-length characteristics compared to experimental data for rat GM, result in over-estimating the active length range (between optimum and active slack lengths) with 30% because over-estimating ℓ_{mao} is by 2.5 mm. The functional consequence is an under-estimation of the muscle force at ℓ_{mao} of about 15%.

In addition, simple models (such as model 3) may fulfill their heuristic purposes because they lead to the question which additional factors may be active causing length force characteristics not to be modeled well. A number of factors will be considered below:

1. Van der Linden *et al.* (1995) showed that even from an initially homogeneous muscle a distribution in fiber length and possibly sarcomere length will develop at activation of the muscle. Consequently, at muscle optimum length total fiber force decreases and therefore, the series elastic components are elongated less, which will result in a shift of ℓ_{mao} to smaller length. Fiber length distributions can not be predicted by the models presented in this paper. Huijing (1995) indicated that individual differences in the amount of mean sarcomere length distributions in skeletal muscle has to be dealt with. Figure 8 presents model results for model 3 based on an individual data of a rat GM. The difference between the model predictions and the experimental data is much smaller (fig. 2-8) than the results of models based on mean GM data (model 3 to 5) (fig. 2-7). This suggests that individual differences of muscles regarding fiber length distributions may explain some of the differences for models that can not handle fiber length distributions or mean fiber sarcomere length distributions.
2. For experimental muscles the linearized geometry of rat GM is asymmetrical with respect to the line of pull. This results in a primary distribution fiber lengths: the proximal fiber is about 10% shorter compared to the distal fiber (Zuurbier and Huijing, 1993). The fiber

angle (α) is not the same for all muscle fibers, nor are distal and proximal aponeurosis angles (β) similar. As the muscle shortens, muscle geometry changes in such a way that more area is encountered above the line of pull, whereas the area below the line of pull is decreased (Zuurbier and Huijing, 1993). This change of muscle geometry may well account for observed differences in length force curve between experimental and model results.

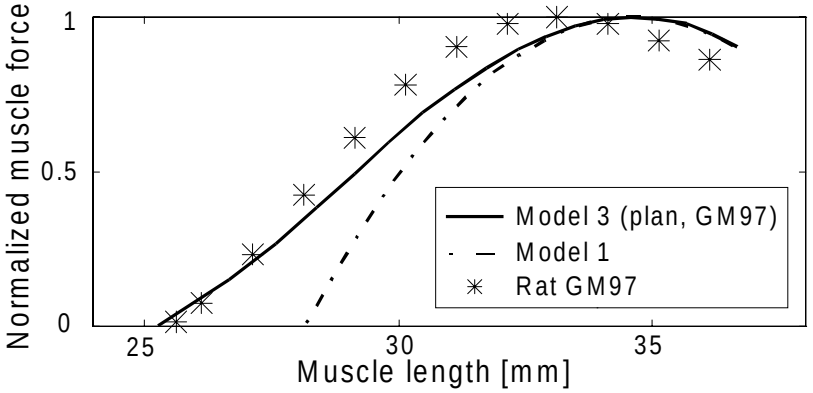

Figure 2-8 Example of length force characteristics of an individual rat GM. In this case model results of the planimetric model with elastic aponeurosis (model 3) comes much closer to experimental results than for mean data. This is taken as an indication that individual variation should be taken into account.

3. Although the assumption that muscle area is constant, it is not necessarily mimicking preservation of muscle volume, the three-dimensional models (model 4 and 5) of the present study did not show improved results compared to the planimetric model (model 3). Therefore it is concluded that the mechanisms of conservation of volume assumed (fig. 2-2: C-C or C-E) do not describe the real mechanism.

4. A property that is not included in the models presented is some aspects of passive stiffness of muscle tissue. Strumpf *et al.* (1993) showed in experiments on dog diaphragm that the contribution of stiffness perpendicular to the fibers as well as shear are not negligible. The models presented account for the elastic property of the aponeurosis, but also muscle tissue itself has substantial resistance against deformation in fiber direction, perpendicular to the fibers as well as against shear.

These considerations lead to the conclusion that in case a prediction of length-force characteristics of maximally activated muscle is needed, more of the above mentioned properties should be incorporated in the models. In fact, a model based on the Finite Element Method (FEM) has capabilities to do so (e.g., Huyghe, 1986; van der Linden *et al.*, 1995; Margulies *et al.*, 1994). Such a model is based on mechanical equilibrium of a continuum, with the possibilities to adapt geometry and mechanical properties of this continuum to required features of muscles. The FEM model allows study of muscle morphology and its functional effects in more detail. Effects and the interactions of these properties can be studied certainly

for heuristic purposes (Huijing, 1995). It may also allow identification of important factors that need to be incorporated in simpler models of muscles of different architecture if a more adequate modeling of muscle length force characteristics of maximally activated muscle are required.

When the results of this study are compared to results of other models, such as mentioned in the introduction the following can be concluded. In case the interest of study is only the prediction of linearized muscle geometry under static conditions, model 3 will give satisfactory results. But when non linearized geometries are required, more complex models are needed (e.g. Otten, 1988; van Leeuwen and Spoor, 1992 & 1996). This will be at the cost of an increased complexity and a less direct insight in the mechanism involved. Although, models of van Leeuwen and Spoor (1992 & 1996) and Otten (1988) showed heuristic value regarding internal muscle pressure as well as details of muscle morphology, the performance of these models in calculating muscle force over the entire active muscle length range was not evaluated. To some extent these models are able to handle fiber length distributions but they also neglect passive properties as indicated above.

From the above it is clear that even simple models can help to increase our understanding of muscle functioning. It is also clear that if we are not able to predict muscle length-force characteristics for an isolated maximally activated (*in situ*) muscle it is to be expected that prediction will fail in conditions of complex movement with many interacting factors. Therefore also for those purposes it is advisable to use the simplest models possible, but limit our goals to the heuristic domain rather than expect to be able to predict or even approach medical or biological complex reality. However the increased understanding about muscular mechanisms obtained from heuristic use of such simple models may very well be used in creating progress in for example clinical applications.

2.6. Appendix

The geometrical relationship of models 2 to 5 are based on a constant mid-longitudinal muscle area (A_m). The linearized muscle geometry (fig. 2-1) consists of two equal triangles. The area of an irregular triangle can be calculated, based on the length of the three sides with the equation of Heron:

$$A = \sqrt{s(s-a)(s-b)(s-c)}$$

with: $s = \frac{a+b+c}{2}$

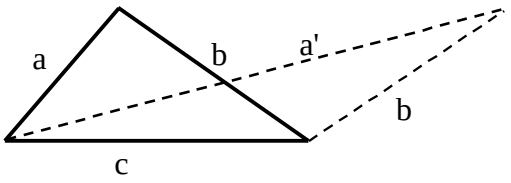

To calculate the length of a third side if two lengths and the area are known, the equation of Heron is inverted and yields determining the roots (a^2) of the polynomial function:

$$a^4 - \left(2 \cdot b^2 + 2 \cdot c^2\right) \cdot a^2 - 2 \cdot b^2 \cdot c^2 + b^4 + c^4 + 16 \cdot A^2 = 0$$

$$a^2 = b^2 + c^2 \pm 2 \cdot \sqrt{b^2 \cdot c^2 - 4 \cdot A^2}$$

From the two different roots (a^2 and a'^2) the length of the third side (a) is easy to choose in case of correct muscle geometry.

Chapter 3

Revised Planimetric Model of Unipennate Skeletal Muscle: A Mechanical Approach

3.1. Abstract

Objective. Planimetric models which are simple, in the sense that small numerical effort is needed, are used to study functional consequences of skeletal muscle architecture. This paper argues with the approach to derive force of a unipennate muscle based on only equilibrium of the aponeurosis (tendon-sheet). In such an approach intramuscular pressure gradients are neglected and no suitable aponeurosis force can be determined.

Method. The approach presented in this paper is based on mechanical equilibrium of whole muscle. A volume-related force is introduced to keep muscle volume constant. Mechanical equilibrium of whole muscle yields a different relation between fiber and muscle force as well as length changes as a consequence of pennation, compared to relations derived when only equilibrium of aponeurosis is considered.

Results. The newly derived relation improved prediction of the rat gastrocnemius medialis muscle force-length characteristics.

Conclusion. It is concluded that prediction of muscle geometry as well as prediction of force-length characteristics is very good with a simple model such as a planimetric model. This conclusion suggests that the influence of properties neglected in such a simple model are either small or are internally compensated for in the net effects.

Relevance

The revised planimetric model of uni-pennate skeletal muscle is a numerically simple model, which allows studying the effects of pennation on muscle functioning. Furthermore, the model enables to perform better predictions of length-force characteristics as well as linearized muscle geometry. Therefore, effects of growth and clinical intervention (e.g. immobilization), surgical operations (e.g. tenotomy, aponeurotomy) on muscle functioning can be modeled to acute effects.

(van der Linden *et al.*, 1998b, Clinical Biomechanics, in press)

3.2. Introduction

The relation between skeletal muscle morphology and function has been studied in a large number of experimental and model studies (e.g. Gans and Bock, 1965; Ettema and Huijing, 1989; Zajac, 1989). In this paper we focus on the planimetric model first presented by Huijing and Woittiez (1984). This model is a numerically simple one, which allows the functional consequences of skeletal muscle architecture to be studied. Variations of this model, in two dimensions as well as three dimensions (e.g. Woittiez *et al.*, 1984; van der Linden *et al.*, 1998a; chapter 2) have been proposed to improve predictions of the muscle force-length relations and of muscle geometry. The additional features of these models are an elastic aponeurosis and for the three dimensional versions conserving volume instead of area of the two dimensional representations. Otten (1988) derived relationships between muscle force and total fiber force for pennate muscle for planimetric models, which are commonly applied. Using these relations, the planimetric model is able to predict linearized geometry of the mid-longitudinal plane of the rat gastrocnemius medialis muscle (GM) well (chapter 2; van der Linden *et al.*, 1998a). However, the muscle force-length curve is not predicted well.

In this paper we approach the effects of pennation in skeletal muscle by considering mechanical equilibrium of a whole muscle, in contrast with Otten's approach (1988) which considered the equilibrium of the aponeurosis only. By doing so, the aponeurosis force can not be determined and intramuscular pressure gradients are neglected which results in an eccentrically placed pressure force vector on the aponeurosis. In the same paper Otten (1988) showed, with his tendon-sheet model, the existence of such pressure gradients.

The goal of the present work is to derive relationship describing force-length characteristics as well as fiber and muscle length changes under the condition of mechanical equilibrium of unipennate skeletal muscle in two dimensions. Consequently, the planimetric model is revised without increase in complexity and numerical efforts needed.

3.3. Methods

The planimetric model is a two-dimensional linearized representation of the mid-longitudinal plane of the unipennate rat gastrocnemius medialis (GM) muscle (figure 3-1), where α and β are the fiber and aponeurosis angle respectively with respect to the line of action of muscle. The fibers as well as the aponeurosis are assumed to be rigid against bending.

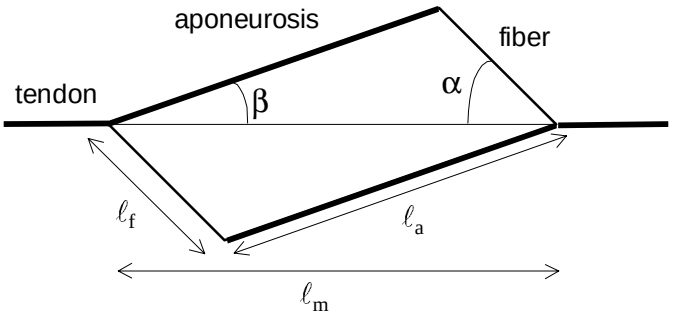

Figure 3-1 Planimetric model of unipennate muscle according to Huijing and Woittiez (1984). Fiber variables (fiber length and angle with the muscle line of pull) are represented by ℓ_f and α respectively, ℓ_a represents aponeurosis length and β aponeurosis angle with the muscle line of pull. Muscle (belly) length is represented by ℓ_m.

The forces acting on the aponeurosis of the muscle, are presented in figure 3-2 according to Otten (1988, cf. his figure 9), where F_f, F_p and F_m are fiber, pressure and muscle force respectively. The pressure force acts perpendicular on the aponeurosis to conserve the muscle volume. In this approach Otten assumed the aponeurosis not to stretch, the fibers to be straight and the pressure force to act in the middle of the aponeurosis.

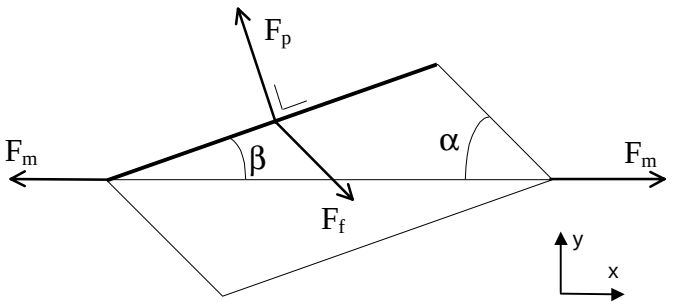

Figure 3-2 Forces acting on the aponeurosis in unipennate muscle according to Otten (1988, cf. his figure 9). F_p represents the force related to intramuscular pressure, F_f is total fiber force and F_m force exerted by the muscle.

Force equilibrium of the aponeurosis yields a relation between the fiber and muscle force (eq. 2).

$$F_p = F_f \cdot \frac{\sin(\alpha)}{\cos(\beta)} \tag{1}$$

$$F_m = F_f \cdot \frac{\cos(\alpha+\beta)}{\cos(\beta)} \tag{2}$$

A consequence of this approach is that force exerted on the aponeurosis can not be determined. Furthermore, this model yields no equilibrium for the moments of force unless the pressure force is located eccentrically on the aponeurosis. This could for example be the case as a result of a pressure gradient over the length of the aponeurosis as is shown by Otten himself (1988) with other models as well as by other researchers (e.g. van Leeuwen and Spoor, 1993; Huijing, 1996). However, the intramuscular pressure acts also in the direction perpendicular to the fibers, consequently bulging of fibers is observed *in vivo*. This pressure

force component is neglected when only equilibrium of the aponeurosis is considered. Therefore an alternative description which includes these characteristics is indicated.

The new approach is based on mechanical equilibrium in the corner points of the parallelogram (fig. 3-3). In the planimetric model the constancy of muscle volume is preserved by assuming the area to be constant, which is in agreement with experimental observations of Zuurbier and Huijing (1992). A volume-related force (F_v) is assumed to act in the two corner points (B), which has the same function as F_p in Otten's approach: preserving muscle volume. This volume related force can be considered as a combination of the intramuscular pressure force acting on the aponeurosis as well as on the most proximal and distal fibers. This approach yields mechanical equilibrium of force and moment of force under all conditions.

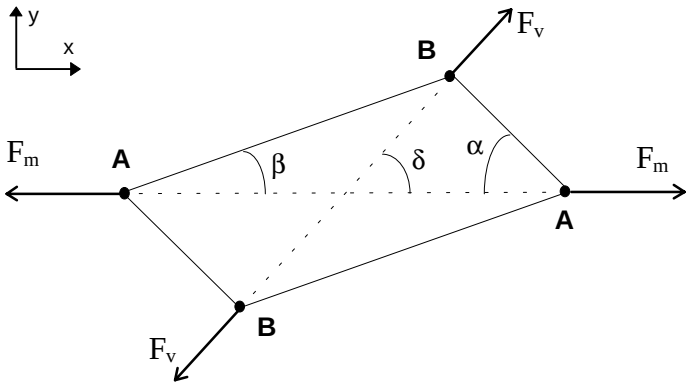

Figure 3-3 Mechanical equilibrium of the planimetric model. F_m is force exerted by the muscle. The force (F_v) is caused as a consequence of the constancy of muscle volume and acts at an angle δ with respect to the muscle line of pull.

In the planimetric model, the aponeurosis and fibers are assumed to be straight in order to avoid the model from becoming numerically complex and therefore the study of intramuscular pressure distributions and gradients is not applicable in such an approach.

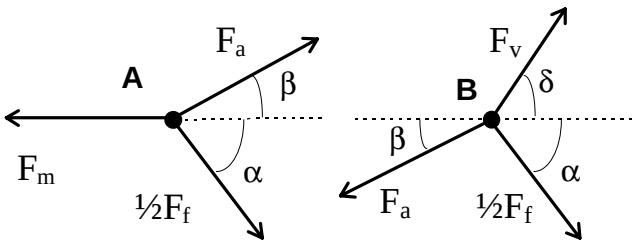

Figure 3-4 A: Mechanical equilibrium at corner A of the parallelogram. Equilibrium is reached by muscle force F_m, aponeurosis force F_a and half of the total fiber force F_f. The fiber angle with the aponeurosis equals α + β. **B**: Mechanical equilibrium at corner B of the parallelogram. Equilibrium is reached by volume related force F_v, acting at angle δ with the line of pull, aponeurosis force F_a, acting at angle β, and half of the total fiber force F_f, acting at angle α with the muscle line of pull.

As a consequence of assuming identical properties for the fibers, the total fiber force acts in the middle of the aponeurosis. Therefore half of this force acts at each end point (A and B, fig. 3-3) of the aponeurosis. When mechanical equilibrium is considered in point A (fig. 3-4 A) a

different relation between fiber and muscle force is obtained (eq. 4) compared to the one derived by Otten (eq. 2).

$$F_a = \tfrac{1}{2} F_f \cdot \frac{\sin(\alpha)}{\sin(\beta)} \tag{3}$$

$$F_m = \tfrac{1}{2} F_f \cdot \frac{\sin(\alpha+\beta)}{\sin(\beta)} \tag{4}$$

In reality the aponeurosis force (F_a) depends on the local fiber force, and will be distributed along the aponeurosis. In the present study the interest lays in the lengthening of the entire aponeurosis, hence the aponeurosis force described by (3) is sufficient to calculate the aponeurosis strain under elastic conditions. Based on equilibrium in point B (fig.3-4 B) the volume related force can be derived (eq. 5):

$$F_v = F_f \cdot \frac{\sin(\alpha)}{\sin(\delta)} \quad or \quad F_v = \tfrac{1}{2} F_f \cdot \frac{\sin(\alpha-\beta)}{\sin(\beta)\cdot\cos(\delta)} \tag{5}$$

The volume force is a summation of all forces that are related to preservation of muscle volume. Muscle geometry depends on the constancy of area and is not influenced by this force. Hence in this paper, no more attention will be paid to volume related force.

In addition to the effect of pennation on muscle force, the relation between the length change of fibers and length change of muscle is also affected as a result of angular effects. This relation is based on the geometrical constraint that the area of model must be constant over the entire length range of the muscle. This is not compatible with the assumption (Otten, 1998) that work of the muscle must be equal to the work delivered by the fibers, due to the fact that the contribution of the pressure or volume related force may not be neglected. The geometrical dependence of muscle length on fiber length is obtained from the derivative of the function that yields the area of muscle (A_{mus}), see the appendix.

$$\frac{d\,\ell_m}{d\,\ell_f} = \frac{\ell_m}{\ell_f} \cdot \left(\frac{\tan(\alpha+\beta) - \tan(\alpha)}{\tan(\alpha) + \tan(\beta)} \right) \tag{6}$$

The first quotient (ℓ_m/ℓ_f) as well as the second quotient between brackets in equation (6) are larger than 1, therefore, the length change of muscle is larger than that of fibers. This equation is based on the geometrical constraint of constant model area, therefore independent of force exerted. Equation 6 is applicable in case an elastic as well as a non-elastic aponeurosis is considered. It should be noted that for large $d\ell_f$ the error in the predicted $d\ell_m$ increases as a result of the fact that the angles α and β are not constant.

The amount of work delivered by muscle and fibers can be calculated. The difference between fiber work and muscle work is a measure of the work the volume related force delivers or absorbs. For an extensive study of these features, the model should include dynamic properties, which are not considered in the present study.

Simulations of isometric force-length properties have been performed with the planimetric model (chapter 2; van der Linden *et al.*, 1998a). For a given fiber length, the geometry is calculated under the condition that the area of the model is equal to the initial area (at muscle optimum length: ℓ_{mao}, see Table 3-1). Furthermore, the aponeurosis is assumed to be elastic, which property is described by a quadratic force-length relationship (eq. 7).

$$F_{aa}(\ell_{aa}) = \tfrac{1}{2} F_{fa}(\ell_{fa}) \cdot \frac{\sin(\alpha)}{\sin(\beta)} = c \cdot (\ell_{aa} - \ell_{aas})^2 \qquad (7)$$

The active aponeurosis force ($F_{aa,}$ eq. 3) at active aponeurosis length (ℓ_{aa}) is based on active fiber force at active fiber length (ℓ_{fa}) and depends on a constant ($c \approx 0.16$ N/mm^2) and the aponeurosis slack length (ℓ_{aas}). The parameters c and ℓ_{aas} are based on trial-and-error approximation of the experimental ℓ_a–ℓ_m relationship (Table 3-1). An iterative process is used to determine the aponeurosis length for the fiber force at a given fiber length, as described previously by van der Linden *et al.* (1998a; chapter 2). Based on the geometry determined, muscle force is calculated according to equation (4) as well as (2) for purposes of comparison. In order to assess the validity of the model simulations are performed of isometric contractions and compared to experimentally determined mean force-length data and muscle geometry of rat GM (Meijer *et al.*, 1997). Experimental data is obtain from an isolated rat GM which is activated maximally at constant length. Force was measured by a force-transducer and muscle geometry is registered by digitizing of photographic images made of the muscle-tendon complex during the sustained contraction. For thorough description of experimental procedures see Meijer *et al.* (1997).

Table 3-1 Mean experimental data (n=7) of rat GM (Meijer *et al.*, 1997)

Mean rat GM data	
ℓ_{mao}	31.7 mm
ℓ_{fao}	12.5 mm
ℓ_{aao}	20.0 mm
F_{mao}	11.3 N
ℓ_{aas}	18 mm
c	0.16 N/mm^2

3.4. Results

The geometrical relations of the planimetric model as presented by van der Linden *et al.* (1998; chapter 2) are unaltered. Consequently the prediction of muscle geometry is identical.

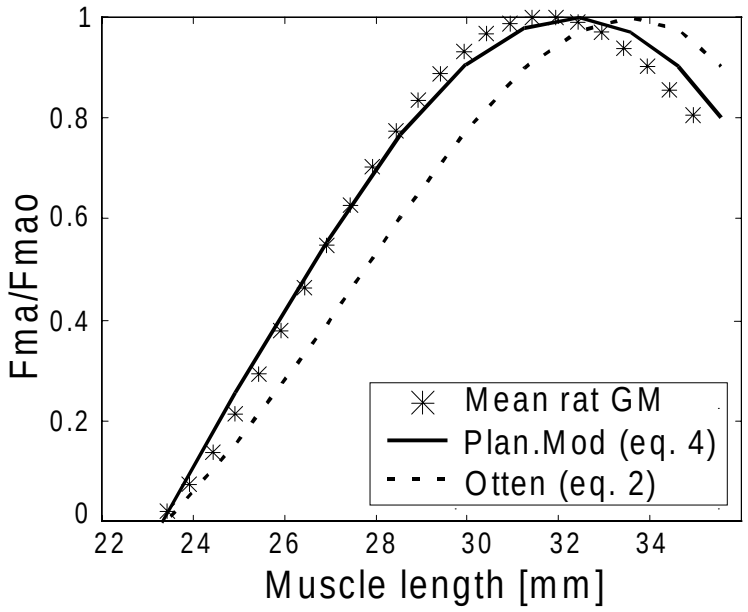

Figure 3-5 Comparison of experimental and modeled length force characteristics of rat medial gastrocnemius muscle. Experimental rat GM is obtained from Meijer *et al.* (1997). The normalized muscle force-length relationship predicted by the revised planimetric model (incorporating eq. 4) is compared to the original prediction based on equation (2) derived by Otten (1988).

However, prediction of muscle force is altered. Figure 3-5 shows a comparison between experimental data of rat GM, the planimetric model using equation 2 (van der Linden *et al.*, 1998; chapter 2; Otten, 1988) and using equation 4 of the revised planimetric model. The prediction of muscle optimum length is improved, the difference between the rat GM and the revised planimetric model is about 0.5 mm. The experimental rat GM force-length data is predicted very well for the muscle length range studied.

3.5. Discussion

The improved planimetric model is capable of predicting muscle geometry as well as muscle force rather well over the active muscle length range studied. The issue of this paper emphasizes the importance of a mechanical approach in finding relations between force and geometry in pennate muscle. The model presented is fairly simple and proves to be very useful in providing insights into the functioning of pennate muscle as well as in the prediction of muscle characteristics under static conditions. In clinical setting the model presented allows prediction of muscle force after muscle geometry adaptation as a result of growth (Heslinga

and Huijing, 1990), immobilization (Heslinga and Huijing, 1992) or surgical operations such as tendon lengthening (e.g. Friden and Lieber, 1994; Brunner, 1995) or aponeurotomy (Brunner *et al.*, 1997) where a gradual or instantaneous change of muscle geometry is observed.

The model presented assumed fibers and aponeurosis to be straight, although the contrary is found in experimental observations (Zuurbier and Huijing, 1992) and in model studies [e.g. van Leeuwen and Spoor, 1992, 1993 as well as three-dimensional tendon-sheet model of Otten, 1988). In the present model, equilibrium is considered for the whole muscle geometry, which is in contrast with models of van Leeuwen and Spoor and some models of Otten where geometry is derived locally, based on equilibrium of local intramuscular pressure and fiber and aponeurosis curvatures. This may explain why these models predict the force-length relationship in-adequately.

An intriguing question is now, how it is possible that our simple planimetric model is capable of predicting muscle functional characteristics so well, considering the number as well as the nature of the assumptions made:

1. The model is a two-dimensional linear simplification of a complex three-dimensional structure.
2. The primary fiber length distribution (Zuurbier and Huijing, 1993; Huijing, 1995, 1996, 1998) is neglected by assuming the mid-longitudinal area to be shaped like a parallelogram and fiber properties to be identical.
3. The muscle is modeled according to linearized presentation of the most distal fiber representing the behavior of all other fibers, whereas experimental (Huijing, 1995) as well as model studies (chapter 4; van der Linden *et al.*, 1998c) showed highly non homogeneous fiber behavior suggesting different contributions for all fibers.

These neglected properties suggest that either the effects of individual fiber differences are small or the effects compensate for each other in their contribution to muscle characteristics. More research is needed to reveal the contributions as well as the interactions of properties such as primary and secondary fiber length distributions and to take into account the fact that muscles are complex three-dimensional structures.

3.6. Appendix

To determine the relation between the muscle length change and the fiber length change the derivative of the muscle area (A_{mus}) is calculated. The area of the planimetric model is defined in the following ways:

$$A_{mus} = \begin{cases} \ell_m \cdot \ell_f \cdot \sin(\alpha) \\ \ell_m \cdot \ell_a \cdot \sin(\beta) \\ \ell_a \cdot \ell_f \cdot \sin(\alpha+\beta) \end{cases} \tag{8}$$

Calculating the derivative, under the assumption that aponeurosis length and muscle area are constant, three equations are obtained:

$$\begin{aligned} \frac{d\ell_m}{\ell_m} + \frac{d\ell_f}{\ell_f} + \frac{d\alpha}{\tan(\alpha)} &= 0 \\ \frac{d\ell_m}{\ell_m} + \frac{d\beta}{\tan(\beta)} &= 0 \\ \frac{d\ell_f}{\ell_f} + \frac{d(\alpha+\beta)}{\tan(\alpha+\beta)} &= 0 \end{aligned} \tag{9}$$

Solving these three equations yields the relation between the length change of the fibers and the length change of the muscle, under the assumption of small length changes in such a way that: $d\alpha + d\beta = d(\alpha+\beta)$.

$$\frac{d\ell_m}{d\ell_f} = \frac{\ell_m}{\ell_f} \cdot \left(\frac{\tan(\alpha+\beta) - \tan(\alpha)}{\tan(\alpha) + \tan(\beta)} \right) \tag{10}$$

An alternative description is:

$$\frac{d\ell_m}{d\ell_f} = \frac{\ell_m}{\ell_f} \cdot \left(\frac{\cos(\alpha)\cdot\cos(\beta)}{\cos(\alpha+\beta)} - \frac{\sin(\alpha)\cdot\cos(\beta)}{\sin(\alpha+\beta)} \right) \tag{11}$$

Chapter 4

A Finite Element Skeletal Muscle Model for Simulation of Isometric and Concentric Contractions

4.1. Abstract

To study the effects of muscle tissue properties and their interactions on mechanical muscle functioning we developed a mechanical muscle model based on the Finite Element Method (FEM). The strength of this method is the capability to combine non-linear material properties of fibers as well as incompressibility and anisotropic behavior of muscle within solutions of mechanically stable muscle geometries for various lengths and loads. The FEM model was applied to the medial gastrocnemius muscle (GM) of the rat. Simulations of static and dynamic muscle contractions are performed. Some modeling results were compared to experimental data for rat GM.

The model indicates the functional importance of combining properties such as passive stiffness (in fiber longitudinal direction, perpendicular to it and shear) as well as incompressibility. The fact that the model allows fibers and aponeurosis to curve, introduces secondary fiber length distributions in active muscle, even if the muscle tissue was initially modeled homogeneous. Under isokinetic conditions the fibers develop a different shortening velocity. The observed differences in length and velocity depend on the position of a fiber in the muscle belly and are based on two independent passive properties, stiffness perpendicular to the fibers and shear stiffness. It is concluded that these properties are of significant influence on whole muscle functioning.

(van der Linden *et al.*, 1998c, Comp Meth Biomech Biomed Eng, submitted)

4.2. Introduction

Muscle morphology appears to be strongly related to muscle functioning (e.g., Benninghoff and Rollhäuser, 1952; Gans and Bock, 1965). The relationship between skeletal muscle fiber and muscle properties is not fully understood. In pennate muscle a large number of fibers, arranged in parallel with respect to each other and attached at an angle ($\alpha+\beta$) to tendon sheets (aponeuroses), form a skeletal muscle belly (fig. 4-1). The muscle belly is connected to the skeleton by tendons. The muscle tissue has contractile capabilities and its mechanical properties are dominated by anisotropic behavior (e.g. Fung, 1981) and constant muscle volume (Swammerdam, 1767) as well as non-linear material properties (e.g. Fung, 1981; Strumpf *et al.*, 1993; Yin *et al.*, 1987). Interactions of fibers and tendinous components have important consequences for muscle function. The relations between fiber and muscle characteristics, such as length-force and force-velocity characteristics (Hill, 1938) are essential for understanding muscle function.

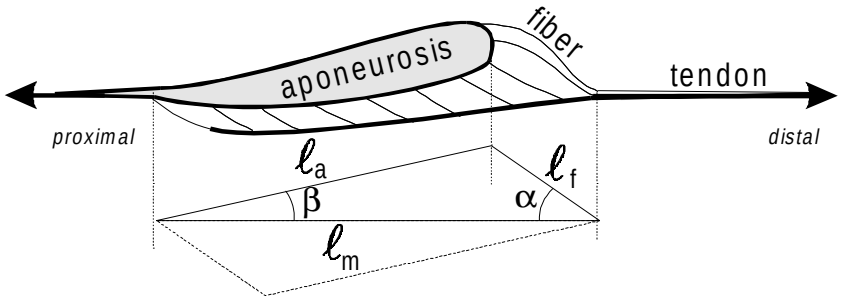

Figure 4-1 A schematic representation of the muscle-tendon complex of rat GM. The fiber (ℓ_f) and aponeurosis length (ℓ_a) ratios and angles are according to Meijer *et al.* (1997). The bottom part of the figure is an illustration of the linearized muscle geometry based on tendon and aponeurosis ends.

In the last decades substantial experimental and modeling work has been devoted to these relations. These studies showed important functional consequences of muscle properties such as: pennation (e.g. Spector *et al.*, 1980; Huijing and Woittiez, 1984; Savelberg *et al.*, 1995; van der Linden *et al.*, 1998), contribution of series elastic elements such as tendons and aponeurosis (e.g. Ettema and Huijing, 1990; Zuurbier and Huijing, 1992), incompressibility (e.g. Woittiez *et al.*, 1984; Otten, 1988; Huijing, 1995), curvature of fibers and aponeurosis (e.g. Otten, 1988; van Leeuwen and Spoor, 1992, 1993) and fiber length distributions (e.g. Zuurbier and Huijing 1993; Huijing, 1995, 1996, 1998). In addition, experimental observations showed complex passive stiffness of skeletal muscle tissue such as anisotropic behavior (e.g. Strumpf *et al.*, 1993; Margulies *et al.*, 1994) and lateral fiber interactions (Street, 1983). From cardiac muscle modeling (e.g. Huyghe, 1984; Huyghe *et al.*, 1992; Horowitz *et al.*, 1988a, b; Hunter *et al.*, 1988; McCulloch *et al.* 1992) using the Finite Element Method (FEM) (Zienkiewicz and Taylor, 1991, 1994) it is known that passive tissue in muscle has

considerable influence on muscle functioning (Horowitz *et al.*, 1988a). These findings show the importance of considering skeletal muscle as a mechanical continuum. FEM has been successfully applied to cardiac muscle, therefore FEM is promising in skeletal muscle modeling.

This paper presents a mechanical formulation of a two-dimensional FEM model to study skeletal muscle functioning. The model is applied to a generalized skeletal muscle-tendon complex. In a muscle-tendon complex, a distinction is made in muscular and tendinous tissue, which represent the muscle belly and tendon and aponeurosis (tendon sheet). The properties of muscle tissue do not fit in an element from the standard element library of commercial available FEM software packages. Therefore, a muscle element is designed (in FORTRAN) and linked to a finite element method software program (ANSYS 5.3[1]). In this paper we focus on uni-pennate medial gastrocnemius muscle (GM) of the rat, and model results are compared with experimental data of the rat GM. The model, composed of a finite number of muscle and tendon elements is used to verify muscle functioning under isometric and concentric conditions. Furthermore, the model is used to gain insight into muscle tissue mechanics, i.e. the heuristic purpose of the model (Huijing, 1995) is explored. In such a way, the mechanical contribution of the passive collagen network to muscle functioning is studied as well as the functioning of individual fibers in the muscle belly.

4.3. Model and Methods

In this paper FEM is used as a tool, the basics of the method is treated in the standard textbooks (e.g. Zienkiewicz and Taylor, 1991, 1994; see also for terminology in Fung, 1981). The properties of muscle considered, are of geometrical and material nature. The material properties are expressed in stress-strain relations. In the present work the theory is formulated for a two-dimensional model of skeletal muscle.

4.3.1. Muscle tissue

In the present paper muscle tissue is considered of homogeneous muscle properties, therefore, we ignore differences in slow and fast twitch fiber types. In muscle we anatomically distinguish a collagen network of connective tissue and excitable muscle fibers surrounded by fiber cell membrane (e.g. Fung, 1981). In the present model the collagen network is assumed to be two-dimensional, in which we distinguish a muscle fiber related direction and a direction perpendicular to the fiber, the cross-fiber direction. The total muscle stress is assumed to be a result of stretching passive tissue and stresses generated by the activated muscle fibers. The total stress in muscle tissue is defined as the sum of the passive stress and the active stress. Muscle, connective and endomysial tissues are represented in FEM muscle model by a muscle element. One muscle element represents a small bundle of muscle fibers arranged in parallel with identical mechanical properties.

[1]ANSYS © revision 5.3 (1996) is a FEM program of Swanson Analysis Systems Inc. (SASI) under an ANSYS License Agreement.

4.3.1.1. Passive stress

Passive stress is a result of deformation of the connective tissue network as well as intracellular elements. When we compose a passive stress-strain relation of muscle tissue, the following aspects are taken into consideration:

- Non-linear stress-strain relations for three deformation types: strain (x, y-direction) and shear (xy-direction), where y-direction is defined in the muscle fiber direction.
- Material anisotropic behavior i.e. different stress for equal strain in different directions.
- In order to incorporate the incompressibility of muscle, the area of muscle elements is kept constant. The constancy of the mid-longitudinal area of whole GM muscle is confirmed by experimental observations (Zuurbier and Huijing, 1992). Moreover, a modeling study (van der Linden *et al.*, 1998a, chapter 2) based on a planimetric model where a circular cross-sectional area of the muscle belly is assumed over the whole length range, showed no good prediction of the force-length relationship, in contrast to a good prediction when the initial circular cross-sectional area is allowed to become elliptical in such a way that the mid-longitudinal area remains constant over the length range.

Viscous properties are neglected, because in the first place the muscle is considered under static, i.e. isometric conditions, and in the second place are considered isokinetic conditions i.e. quasi-static. Moreover, in the present study we are not interested in transient effects in which viscous properties are expected to play a role of importance. The material is considered to be hyperelastic, i.e. deformations are extremely large and strains are recoverable. The material is defined by a unique relation between stress and strain. This property and the fact that there is no energy dissipation in a closed cycle of application and removal of stress (i.e. the muscle is pre-conditioned) (e.g. Fung, 1981), ensure the strain energy density function W to be a function of strain. The stress can be calculated by differentiation of W with respect to the strain tensor. The definitions for stress and strain used, are the second Piola-Kirchhoff stress and Green-Lagrange strain (Zienkiewicz and Taylor, 1991). The strain energy density function (W) in this study is composed of two parts.

$$W = W_1 + W_2 \tag{1}$$

The first part (W_1) maintains the non-linear stress-strain relations and the passive anisotropic material properties. The second part (W_2) has been added to fulfill the incompressibility condition of the muscle tissue.

The anisotropic and non-linear passive behavior is translated into three components, which are related to the direction of the muscle fibers. According to Huyghe (1986), we chose, for W exponential functions in the respective directions.

$$W_1 = W^x + W^y + W^{xy} \tag{2}$$

With: $W^i(\varepsilon_i) = k \cdot \left(e^{a_i \cdot \varepsilon_i} - a_i \cdot \varepsilon_i\right) \quad for: i = x, y \text{ or } xy$

and: $W^{xy}(\varepsilon_{xy}<0) = -W^{xy}(|\varepsilon_{xy}|)$

Where ε_i is the strain in a direction i. The y-direction is defined to be the muscle fiber longitudinal direction and xy is the shear component. The parameters a_i and k are constants and will be discussed in the paragraph (4.3.3) about the implementation of the model (see also Table 4-1). A graphical representation of these passive stress-strain properties is shown in figure 4-2.

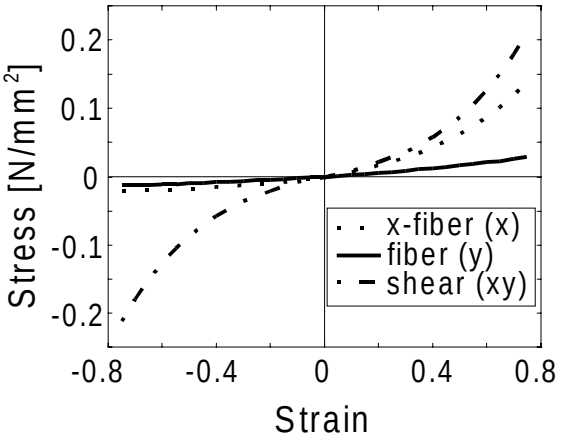

Figure 4-2 Passive stress-strain relationship with components in cross-fiber (x), along fibers (y) direction and shear (xy) at passive fiber slack length ($\approx \ell_{mao}$-1.5 mm) all strains and all stresses are zero.

The second part of the strain energy density function (W_2) contains a penalty function for the incompressibility condition of muscle tissue. FEM is a numerical method which approximates the mechanical equilibrium of a continuum and the demand of constant area is approximated by applying a penalty function. This procedure is chosen instead of assuming a Poisson's ratio of 0.5, which leads to numerical problems. The change in surface area of an infinitesimal small area is defined by the strain invariant I_3. Muscle fibers can be considered as cells filled with fluid. The intracellular fluid is assumed to have the ability to migrate freely within the cell. The solid elastic structures, such as filaments, are restricted in their moving space. Therefore, we used a penalty function to serve the demand of incompressibility conditions consisting of two parts. This penalty function is applied to local muscle element areas, which are related to the Gauss integration points (Zienkiewicz and Taylor, 1991). In every integration point with its local area I_3 is calculated, with I_3 representing the determinant of the right Cauchy-Green strain tensor. When the local muscle element areas are conserved by keeping all I_3 equal to one, the element is modeled as a solid. When the mean value of all I_3 is calculated (I_3^{avg}) and kept equal to one, the element is modeled as a fluid:

$$W_2 = \rho \cdot (I_3 - 1)^2 + \lambda \cdot (I_3^{avg} - 1)^2 \qquad (3)$$

with weighting factors ρ and λ (Table 1), representing the amount of penalty given when the local (solid, ρ) and the global (fluid, λ) area-parts deviate from the initial area respectively. W_2 will be zero if the area is constant. A combination of ρ and λ allows us to restrict migration of fluid but allows large deformations of the muscle elements. From a number of penalty functions, with exponential or higher order terms, equation 3 is chosen for the best results preserving the muscle element area and numerical efforts needed.

Table 4-1
Definition of constants used by the FEM model of the rat GM. In the last column is referred to equation numbers in the text.

Const	Value	Unit	Description (equation)
a_1	2.5	-	passive x-fiber stiffness (2)
a_2	1	-	passive fiber stiffness (2)
a_3	3	-	passive shear stiffness (2)
b_1	30	-	active stress-strain (5)
b_2	-5	-	active stress-strain (5)
b_3	1	N/mm^2	active stress-strain (5)
c_0	0.29	-	stress-strain velocity (6)
c_1	0.20	-	stress-strain velocity (6)
c_2	1.50	-	stress-strain velocity (6)
c_3	2.50	-	stress-strain velocity (6)
NS_t	250	mm^2	tendon normal stiffness
BS_t	1.5	mm^4	tendon bending stiffness
NS_{ap}	250 -20	mm^2	distributed (A → B) aponeurosis normal stiffness
BS_{ap}	1.5 - 0.5	mm^4	distributed (A → B) aponeurosis bending stiffness
ρ	1	N/mm^2	weight factor solid part incompressibility (3)
λ	5	N/mm^2	weight factor fluid part incompressibility (3)
k	0.01	N/mm^2	Initial passive stiffness (2)

4.3.1.2. Active stress

Active stress is exerted by the fibers in a muscle element when activated. The active stress in skeletal muscle depends on a number of factors. It is assumed that active fiber stress (S_{fiber}, the local Cauchy-stress in fiber direction) depends on three independent relations (Hatze, 1981):

$$S_{fiber} = q(t) \cdot S(\tilde{\varepsilon}) \cdot S(v) \qquad (4)$$

Where q(t) represents the activation function, $S(\tilde{\varepsilon})$ the length-force relation and S(v) the force-velocity relation. The following factors have been taken into consideration:

- For reasons of simplification only maximally activated muscle is chosen to study and to be able to compare with experimental results, therefore effects of sub-maximal activation and alterations in activation dynamics, such as fatigue, potentiation or Ca^{2+} sensitivity for activation are ignored. This is defined by the muscle activation function q(t), which is set to unity.

- According to the sliding-filament theory of Huxley (1957) the active stress depends on filament overlap and therefore, since all sarcomeres are assumed to be identical, the active stress depends on fiber strain. To account for length dependence of muscle fiber force, we fitted the experimentally determined length-force curve of rat GM fiber bundle (Zuurbier *et al.*, 1995) with an exponential function, $S(\tilde{\varepsilon})$ (fig. 4-3A). The function for active stress is chosen to be continuously positive. Fiber strain ($\tilde{\varepsilon}$) is defined as the proportional length change (Cauchy-strain) with respect to the fiber optimum length, i.e. when a fiber is at its optimum length the fiber strain is zero and the stress is one when the muscle is activated.

$$S(\tilde{\varepsilon}) = \begin{cases} b_3 \cdot e^{b_1 \cdot \tilde{\varepsilon}^4} & for \tilde{\varepsilon} \le 0 \\ b_3 \cdot e^{b_2 \cdot \tilde{\varepsilon}^3} & for \tilde{\varepsilon} > 0 \end{cases} \quad (5)$$

Where b_i are constants (Table 4-1).

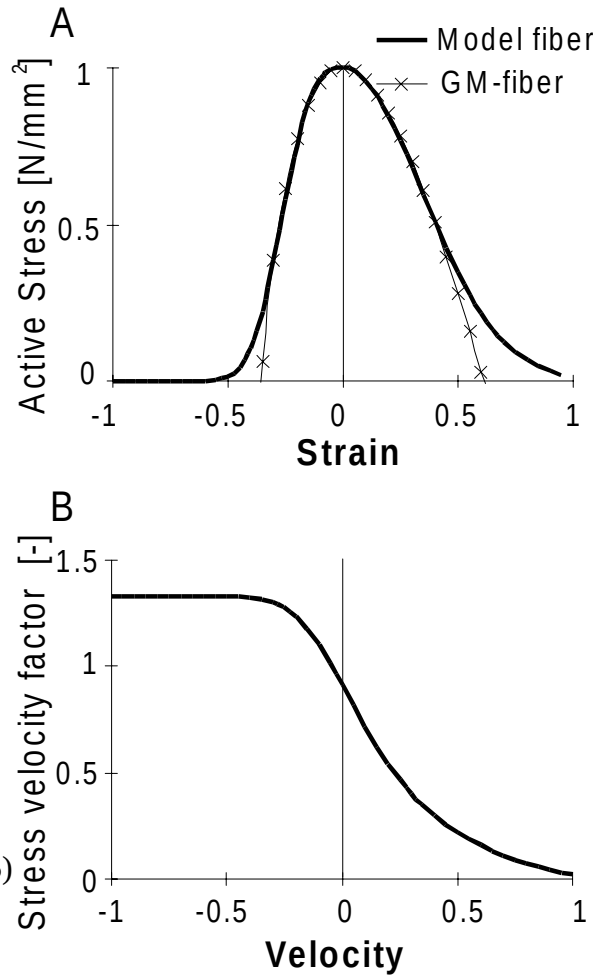

Figure 4-3 **A** Active stress-strain relationship normalized for the active stress at muscle fiber optimum length. Comparison of model-fiber with experimental GM-fiber data from Zuurbier *et al.* (1995) is made. **B**: Active stress-velocity relationship, fiber force normalized for the isometric force at given length and for maximal shortening velocity ($v_{max} \approx 1$) adapted from Hatze (1981). According to physiological custom positive velocity indicates shortening.

- For the dynamic behavior of activated skeletal muscle, a normalized force (stress)-velocity relation (S(v), Hatze, 1981), valid for maximally activated muscle, is implemented (see also fig. 4-3B):

$$S(v) = \frac{c_0}{c_1 + e^{-c_2 \cdot \mathrm{SINH}(c_3 \cdot v + \frac{1}{2} \cdot c_3)}} \quad (6)$$

Where v is the normalized shortening velocity and c_i are constants (Table 4-1). In accordance with physiological practice shortening is indicated by a positive velocity ($v = -\dot{\tilde{\varepsilon}}$, strain velocity in local fiber direction) and lengthening is negative. The constants c are chosen in such a way that under isometric conditions: S(v=0) = 1 and under the condition of maximal shortening velocity of the fibers, where is assumed $v_{max} = 1$, eq. 6 yields: $S(v_{max}) \approx 0$.

- Active fiber force is assumed to be generated by identical sarcomeres arranged in series within the fiber and therefore exerting the same force. Consequently, the active fiber stress is assumed to be constant over the length of the muscle fiber. The reference for the fiber stress is the strain in the middle of the muscle fiber. The strain of muscle fibers arranged in parallel is linearly distributed over the width of the muscle element as a result of a linear

displacement function chosen perpendicular to the fibers. This choice is made based on the expectation that there will not be large differences in deformations of adjacent muscle fibers.

- Active stress is generated in fiber direction only. Consequently, the active fiber stress is defined in the local fiber direction, regardless if the muscle fiber is curved or not. Hence, the difference in global and local element coordinates is accounted for in application of active fiber stiffness in the muscle element.
- No properties are incorporated that result in fatigue, potentiation and other time related force changes other than the properties described by eq. 6.

4.3.2. Tendinous tissue

Both tendon and tendon-sheet (aponeurosis) are of tendinous tissue. The elasticities of these structures are assumed to be linear. In the present two-dimensional model, the aponeurosis as well as the tendon are modeled by the same type of element. This element (BEAM54) is from the standard ANSYS element library and will serve the purpose of modeling tendinous structures. The BEAM54 element allows incorporation of thickness of the aponeurosis by applying a tapered shape for these elements. Hence a distribution of the normal stiffness, i.e. the resistance against length changes is introduced from point A to point B in figure 4 and yields in a constant strain over the aponeurosis (from A to B). To prevent the model from generating moments of force in the tendon element the bending stiffness is set to a small value (table 1). Hence, the modeled tendinous structures are allowed to curve under applied forces.

Ettema and Huijing (1993) measured a strain for the series elastic components of GM muscle-tendon complex of about 3 % for muscle optimum force. In this paper we assumed the tendon to be homogeneous. Consequently, tendon strain at muscle optimum force is taken to be about 3%. The stiffness of the model aponeurosis is calculated at the muscle-model optimum force. The aponeurosis stiffness (NS_{ap}) is chosen to be equal to the tendon stiffness at the tendon-end (point A) and NS_{ap} at point B is chosen such way that the aponeurosis strain is approximately constant and about 3 %.

4.3.3. FEM-muscle model

With the muscle and tendon elements presented any muscle-tendon complex can be constructed, under the condition that a (mid) longitudinal area can be defined in the direction of the line off pull, which is a good representation of the muscle geometry *in situ*. In this study we focus on functional characteristics of the medial gastrocnemius muscle (GM) of the rat (fig. 4-1). The model is a two-dimensional representation of the mid-longitudinal area of this muscle-tendon complex. The model simulations were performed using 16 muscle elements in parallel with respect to each other and 40 tendon elements for the representation of tendon (2 x 4 elements) and aponeurosis (2 x 16 elements) (fig. 4-4). The curvature of the aponeurosis is constructed of smooth curve with a start and end (point A and B) angle of 0º with respect to the muscle line of action and consequently an angle of about 20º is introduced with the most proximal or distal fiber. Initially, when the model muscle is not activated, all fibers are straight

and of identical length and the fiber angle (α) is the same for all fibers. This assumption is for heuristic purpose, because insights in complex muscle functioning are gathered more easily of homogeneous muscle geometries. When the model is activated, fibers will curve and the aponeurosis will bend under the applied load.

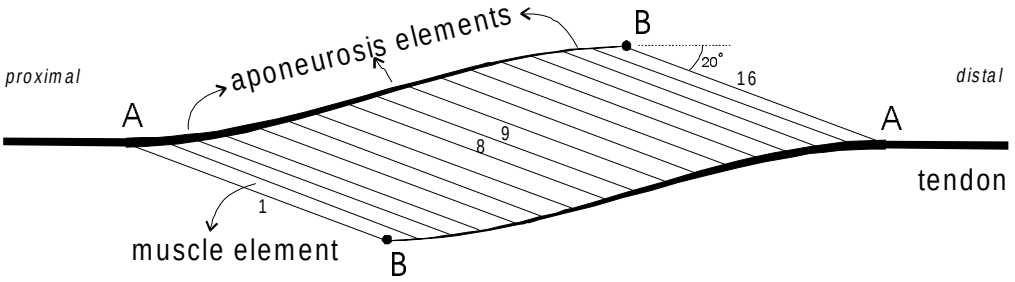

Figure 4-4 Representation of the finite element muscle model with 16 muscle elements in parallel. The muscle elements are numbered from left to right. The tendons are represented by 4 elements and the aponeurosis consists of 32 elements with linearly distributed normal stiffness, i.e. thickness. The beginning (A) and end (B) of the aponeurosis are marked. At point B the angle between the fiber and the aponeurosis is 20° as is marked in the figure. The geometry of the model presented is the initial shape where all fibers have identical length (ℓ_f = 12.5 mm) and are at muscle optimal length (ℓ_{mao} = 31.7 mm) under passive condition, with linearized aponeurosis length: ℓ_a = 21.1 mm.

The number of elements used serves the goal of this paper, more elements in parallel did not lead to different predicted muscle forces or significant changes in predicted muscle geometry. In fiber direction only one element is used, to preserve the fact that active fiber stress is constant for the length of the fiber. When in a muscle model more elements arranged in series representing a small bundle of fibers, the active stress would be distributed over these elements, which is in contradiction with the assumption that the fiber stress is constant over its length. Consequently, one muscle element represents a bundle of muscle fibers arranged in parallel.

In addition, material properties are defined for the muscular and tendinous tissue. The properties of all muscle elements are identical. Active fiber stress is described by equation (5) and (6) and presented in figure 4-3A&B. The values for constants of these equations are shown in Table 4-1. Passive stiffness of the fiber tissue in fiber longitudinal direction has been estimated from experimental data of rat GM (Meijer *et al.*, 1997). According to experiments of Strumpf *et al.* (1993) on dog diaphragm, the passive stiffness perpendicular to the fiber direction is larger than in fiber direction (Table 4-1). The incompressibility of skeletal muscle is modeled by equation (3). The constants for the fluid and solid parts are chosen in such a way that area loss is restricted to maximal 3% of the initial area. Large element deformation i.e. simulating migration of fluid, is restricted by constant λ (3).

The present model (fig. 4-4) is used to simulate isometric and isokinetic contractions. Under isometric conditions muscle force is calculated at different muscle lengths in a range from

active slack length (ℓ_{mas}), i.e. the length at which the active muscle exerts no external force, to about 4 mm above muscle optimum length (ℓ_{mao}). Simulation results are compared to experimental data of the rat GM (Meijer *et al.*, 1997). Under isometric conditions geometry of the modeled muscle and rat GM are compared. For this comparison rat GM as well as model geometry is linearized as is indicated in figure 4-1 (bottom part). Muscle geometry is expressed in the parameters: fiber length (ℓ_f), aponeurosis length (ℓ_a), fiber angle (α) and aponeurosis angle (β), which are plotted against muscle length (ℓ_m). For isokinetic contractions muscle force is calculated with different shortening velocities imposed at the tendon ends. ANSYS the FEM package used allows study of the internal strains and stresses as well as the morphology of the muscle-tendon complex during the contractions.

Although, FEM models a continuum and not individual fibers it is possible to study single fibers in a muscle belly. As a result of the fact that the longitudinal fiber direction is defined in the length direction of the muscle elements, single fibers can be addressed for example based on the distance to the most proximal/distal fiber.

4.4. Results

For verification, the model predictions under isometric and isokinetic conditions are compared to experimental data. Furthermore, the influences of passive properties on muscle functioning are presented.

4.4.1. Isometric conditions

Modeled and experimental results regarding isometric normalized force-length characteristics are shown in figure 4-5. The model predicts the force–length characteristics well for the length range from muscle active slack-length (ℓ_{mas}) to optimum length (ℓ_{mao}, see fig. 4-5A). For muscle lengths over ℓ_{mao} the total normalized muscle force is under-estimated by the model. Normalized passive muscle force is over-estimated by 5% of F_{mao} (muscle force at ℓ_{mao}) at ℓ_{mao}+4 mm.

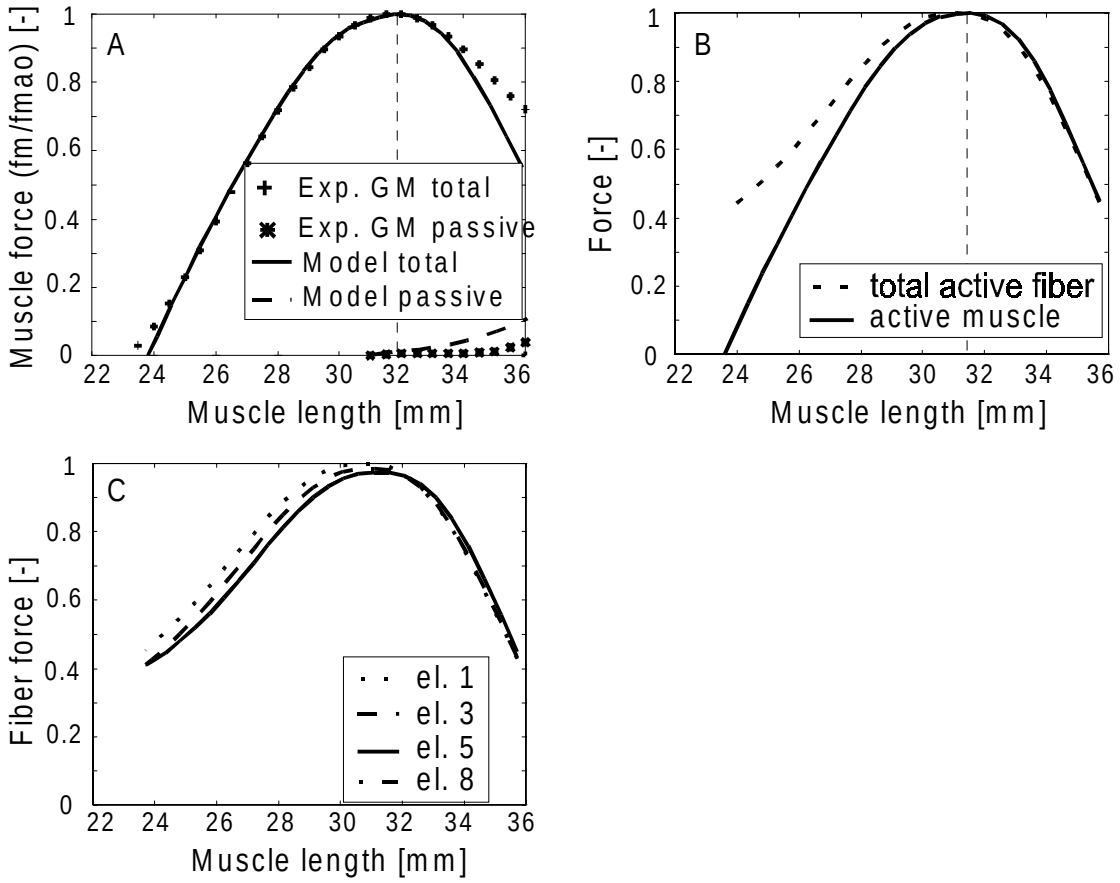

Figure 4-5 **A** Length-force relationships of the model is presented versus experimental data of rat GM. Experimental data is according to Meijer *et al.* (1997). The total and passive force is normalized for the maximal muscle force at muscle optimum length (ℓ_{mao}). **B** The active fiber force versus the active muscle force based on the subtraction of the total and the passive force calculated by the model. **C** The normalized forces of some muscle elements are presented versus muscle length. The most distal/ proximal elements (el. 1; el. 16 is identical as a result of symmetrical geometry, see fig. 4-4) exert the largest force below muscle optimum length.

To obtain an estimate for active force the passive length-force curve is subtracted from the total curve (fig. 4-5B). With the present model we are able to study actual active force, based on the exerted active fiber stress. In figure 4-5B the total normalized active fiber force is plotted against muscle length and compared to the estimate of active muscle force, based on the subtraction of the total and passive force. Note that at ℓ_{mas} a considerable active fiber force is exerted, despite the fact that no active force is exerted by the muscle. The actual fiber force of some fibers is presented in figure 4-5C. The contribution of the most distal and proximal fibers (element 1 and 16, fig. 4-4) to the total muscle force is largest at ℓ_{mas}. This phenomenon is a result of interactions of passive tissue stiffness perpendicular to the muscle fibers, the active fiber stiffness and the fact that fiber volume is constant during contraction.

The forces calculated are based on mechanical equilibrium of a continuum. The mechanical equilibrium results also in a specific geometry. Muscle geometry can be described during isometric contractions. A comparison is made of geometrical parameters (ℓ_f, ℓ_a, α and β versus ℓ_m) of the two-dimensional linearized muscle geometry to experimental data (fig. 4-6 A&B).

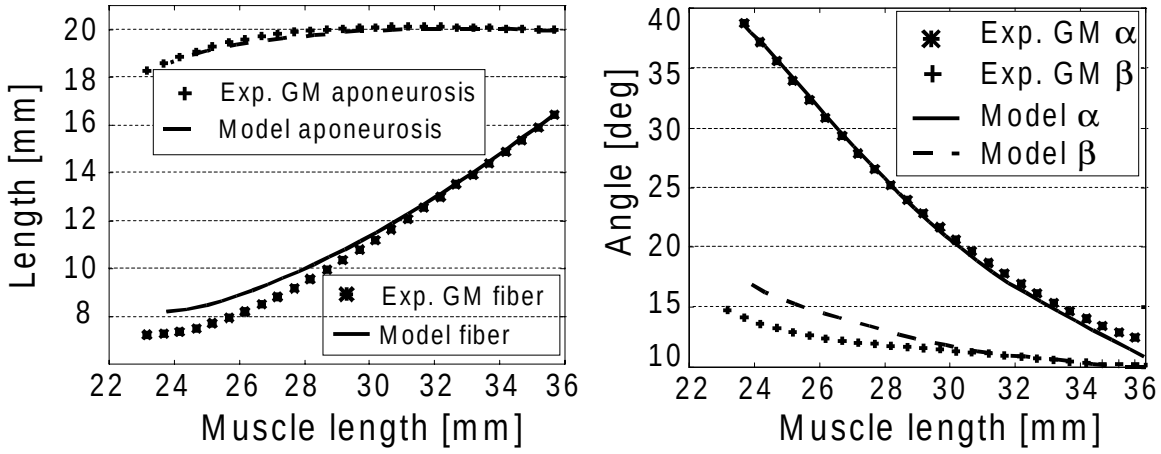

Figure 4-6 Prediction of linearized muscle geometry compared with experimental data of rat GM. **A** Fiber and aponeurosis length versus muscle length are predicted well. **B**: Fiber and aponeurosis angles versus muscle length, where the fiber angle (α) is predicted well and the maximal difference for the aponeurosis angle (β) is 2.5°.

Muscle geometry is predicted well for ℓ_f, ℓ_a and α, the maximal difference is: 6%, <1% and 8% respectively. The aponeurosis angle (β) is over-estimated by 20% ($\approx$ 2.5°) at ℓ_{mas}, this difference can be attributed to the fact that the rat GM has a distal fiber and a proximal aponeurosis of shorter length modeled (Zuurbier and Huijing, 1993) compared to the muscle geometry.

During an isometric contraction a fiber length distribution is developed as a result of change in curvature of the aponeurosis and curving and bulging of fibers. This so-called secondary fiber length distribution (Huijing, 1995) is quantified in figure 4-7A for all muscle elements at four different muscle lengths (ℓ_{mas}, ℓ_{mao}-4.5, ℓ_{mao} and ℓ_{mao}+4.5 mm). The largest difference occurs between the middle fibers (element 8 and 9) and the most distal/proximal fibers (element 1 and 16): 6 % of fiber optimum length (ℓ_{fao}) at muscle optimum length. At ℓ_{mas} the middle fibers have higher lengths compared to their neighbors, but are 5% shorter compared to the most distal/proximal fibers. It should be noted that these length differences are developed by fibers with identical material properties and are initially of identical lengths. As a result of a difference in length fibers exert different forces. The active fiber stress, related to muscle elements, is presented in figure 4-7B for four muscle lengths. The maximal difference in stress of the muscle elements compared to the middle element is 10% of maximal active stress. A large difference in length does not automatically lead to a large difference in active stress. The maximal fiber length difference at ℓ_{mao}-4.5 mm is 3% but the maximal difference in exerted fiber force equals 10% of the exerted stress in the middle fiber. This shows that the contribution of individual fibers to total muscle force is different.

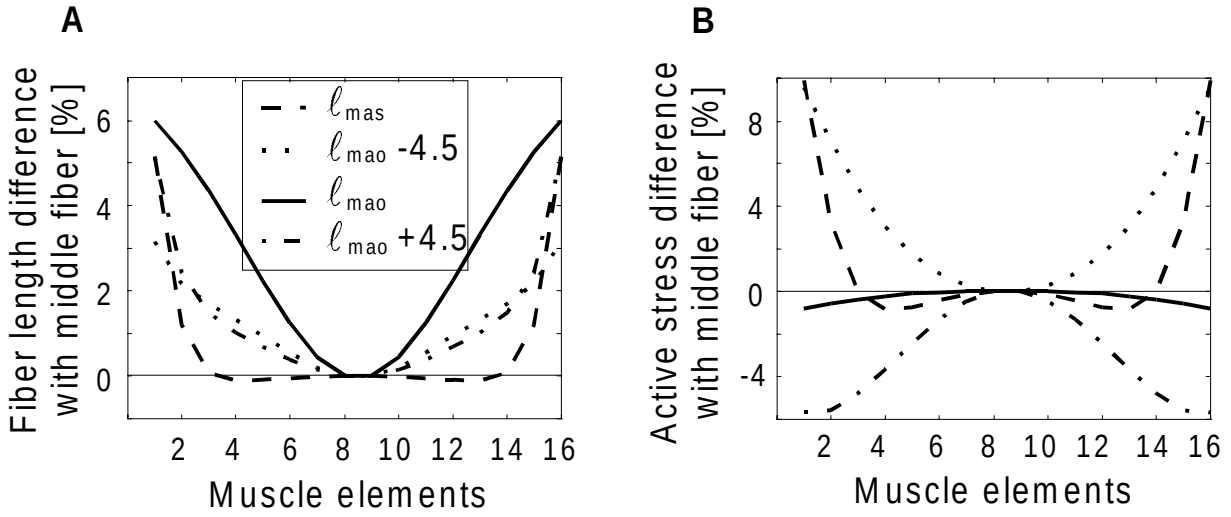

Figure 4-7 A: The difference in fiber strain in the elements compared to the middle element (el. 8 and 9) at four different muscle lengths (ℓ_{mas}, ℓ_{mao}-4.5, ℓ_{mao}, ℓ_{mao}+4.5 mm). The maximal difference of 6% is found at ℓ_{mao} for the most distal and proximal fibers (element 1 and 16). **B**: The difference in fiber active stress in the elements compared to the middle element at the same four muscle lengths. Note that at the descending limb (ℓ_{mao}+4.5) of the stress-strain relationship the longer middle fibers exert a larger stress compared to the fibers more located towards the outside of the muscle belly.

4.4.2. Concentric conditions

Simulations of isokinetic contractions were performed for a length range of 3 mm, started at ℓ_{mao}-3.5 mm and for a length range of 10 mm, started at ℓ_{mao}+3.5 mm with shortening velocities of 1 and 10 mm/s. Hence, the end-lengths of all contractions is ℓ_{mao}-6.5 mm (equals ℓ_{ma} = 25.5 mm). Muscle force during shortening is plotted versus muscle length (force length trajectories, fig. 4-8A). The isometric length-force curve is added for comparison. As expected, muscle force during shortening is lower and the difference in force depends on shortening velocity. In the early phase of shortening muscle force drops, which is a result of interaction of fibers and series elastic structures. In the final phase of shortening muscle force only depends on muscle length and on shortening velocity, and not on start length or shortening range. This is expressed by the fact that force length trajectories for v = 1 mm/s and for v = 10 mm/s coincide over a length range ℓ_{ma} = 27.5 to 25.5 mm and ℓ_{ma} = 26 to 25.5 mm respectively. After shortening muscle force re-develops to the isometric value (F_{ma} = 2.5 N at ℓ_{ma} = 25.5 mm).

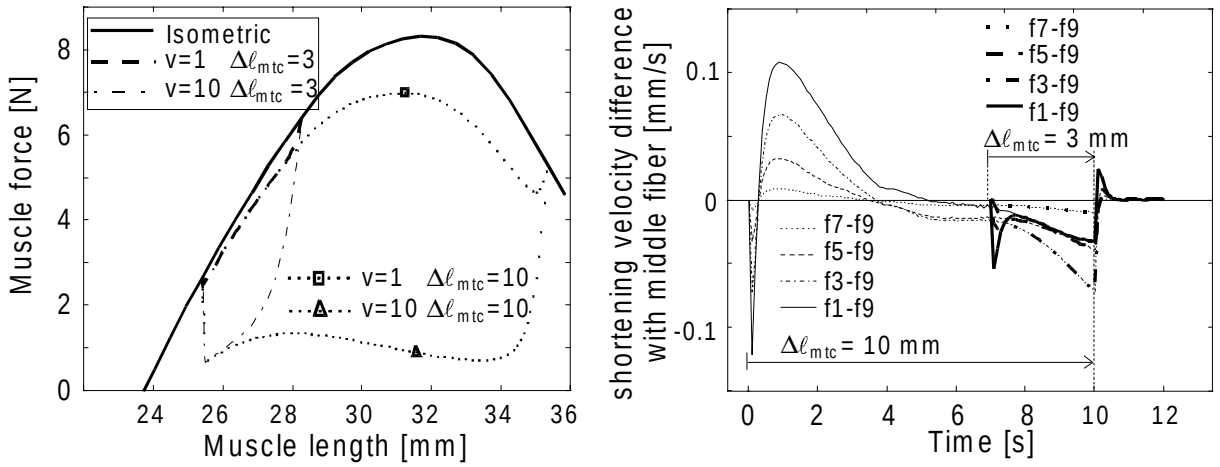

Figure 4-8 A: The force trajectories of the model during shortening with a shortening velocity of 1 and 10 mm/s over a muscle tendon complex range ($\Delta\ell_{mtc}$) of 3 and 10 mm versus muscle length compared with the isometric length-force curve. B: The shortening velocity of some fibers compared with the middle fiber during the above mentioned concentric contraction versus time. The contraction over $\Delta\ell_{mtc}$ = 3 mm (thick curves) are shifted over the time axis in order to coincide with the contractions of $\Delta\ell_{mtc}$ = 10mm at the same time (t = 14.6 s) when ℓ_{mao}-6.5 is reached. Consequently it is visible that the velocity trajectories are identical over the last seconds (t = 8 - 12s) of contraction.

Secondary fiber length distributions are observed during isometric contractions lead to differences in individual fiber velocities in concentric contractions. For concentric contractions at 1 mm/s, the differences of fiber velocities within the muscle are plotted versus time (fig. 4-8B). The contraction over a length range ($\Delta\ell_{mtc}$) of 3 mm is started at t = 7s, therefore both contraction over a range of 3 and 10 mm reach at the same time (t = 10 s) ℓ_{ma} = 25.5 mm. The shortening velocity of the middle fiber ('f9') is subtracted from the velocity of a fiber. The difference in shortening velocity between the most distal/proximal fiber ('f1') and the middle fiber is most extreme. The distal/proximal fiber reacts quicker to geometrical changes compared to the other fibers, see in the first phase of shortening as well as after shortening (t > 10s) when the tendon-ends are kept isometric. The differences in shortening velocity can be 10% (i.e. 0.1 of 1 mm/s) of the applied shortening velocity. In figure 4-8A the force length trajectories during shortening show that the start length of contractions did not lead to differences in muscle force predicted during end phase of the concentric contraction. In addition to the overlap of the force length trajectories (fig. 4-8A) the individual fiber velocities (fig. 4-8B) of contractions over a length range ($\Delta\ell_{mtc}$) of 3 and 10 mm for t > 8s, are identical as well.

During muscle shortening initiated from ℓ_{mao}+3.5 and velocity 1 mm/s, the muscle force increases (after a small decrease) from 4.5 to 8.5 N (ℓ_{ma} = 35 to 31 mm, see fig. 4-8A), consequently the aponeurosis increases in length ($v_a < 0$, lengthening) as a result of interactions of the muscle belly and the series elastic components. In addition, the muscle belly shortening velocity (v_m) is larger compared to the applied velocity on the muscle tendon complex (fig. 4-9). Experimental observations of Zuurbier and Huijing show similar results (their figure 4, 1993). Except that the aponeurosis *in vivo* does not lengthens due to an increase in muscle force during shortening started of ℓ_{mao}. The distal fiber velocity predicted ($v_{f,d}$) is consistent with rat GM distal fiber. However, the mean fiber velocity predicted ($v_{f,mn}$) is larger compared to the muscle shortening velocity.

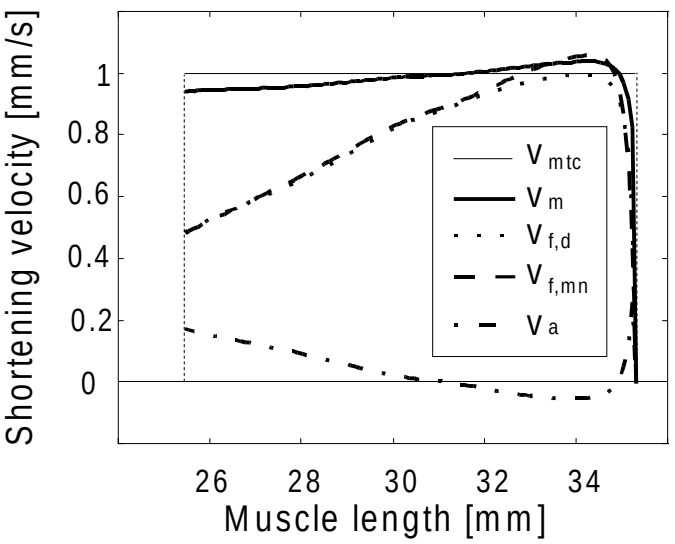

Figure 4-9 The shortening velocity of the muscle belly (v_m), distal fiber ($v_{f,d}$), mean fiber ($v_{f,mn}$) and aponeurosis (v_a) are plotted against muscle length of a concentric contraction with a velocity of 1 mm/s applied to the muscle tendon complex. The mean fiber shortening velocity is larger compared the velocity of the most distal fiber. In contrast with the trace of distal fiber predicted by the model which is in consistence with the experimental distal fiber observed by Zuurbier and Huijing (1993). The aponeuroses lengthen over a range of 35 to 31 mm ($v_a < 0$).

4.5. Discussion

Simulation of isometric contractions yielded good prediction of the length-force characteristic, below muscle optimum length as well as the linearized geometry of rat GM. The cause of prediction error in the length-force characteristic over muscle optimum length is unknown and needs further investigation.

The model presented is useful for the study of individual fiber functioning in whole muscle. The present study revealed that muscle fibers interact. Interactions of fibers are a result of the passive muscle tissue present, which has a specific, anisotropic, resistance against deformation. Two components of this passive resistance have a significant influence on muscle functioning. First, shear stiffness that is the resistance of fibers to slide along one another. Consequences of this property are the limited distributions in fiber length (fig. 4-7A) and fiber velocity (fig. 4-8B) of adjacent fibers, compared with the length and velocity differences of fibers far apart in the muscle belly. With different fiber lengths and velocities the contribution of individual fibers to the total muscle force is different. It is very likely that shear stiffness contributes to the fact that the regular striation pattern of skeletal muscle remains intact over a large muscle length range. Another consequence of shear stiffness is that fiber force is not only exerted at the fiber ends but also on adjacent fibers. In cardiac muscle shear is observed to be a moderator of stresses

(Horowitz, 1988b). Hence no large differences, i.e. peaks in stresses were found, which is consistent with findings of the present study. Experiments on specially prepared skeletal muscle fiber bundles (Street, 1983) showed the ability of fibers to transmit tension in lateral direction, which can also be attributed to shear stiffness.

The second passive property with great implication for muscle functioning is the stiffness of muscle tissue perpendicular to the fibers (x-fiber direction). Strumpf *et al.* (1993) showed in their bi-axial experiments on dog diaphragm that x-fiber stiffness in not negligible. The present model shows the functional consequences: as fiber shortens, the fibers get thicker, consequently the x-fiber strain increases, as well as x-fiber stress. This stress is compensated by the active fiber stress in fiber direction as a result of the following mechanism. Deformation in fiber direction is coupled with deformation in x-fiber direction because of the fact that muscle volume is constant. Imagine a cylinder with a constant volume which length is decreasing, consequently the diameter has to increase. If the cylinder wall is of elastic material, a force is needed to increase the diameter. The active fiber force is the only force to compensate for this force. At the ascending limb of the active fiber length-force curve the force decreases with shortening, the fiber diameter increase and also the x-fiber stress. At a certain fiber length an equilibrium is developed between the active fiber stress and the passive x-fiber stress where no force is exerted at the fiber ends. For the model presenting a whole GM a considerable active fiber force is exerted at muscle active slack length (fig. 4-5B). Therefore, is it concluded that an active muscle consumes energy at slack length where no force is exerted at the tendon ends. It is the mechanism that is important here and not the amount of active fiber force, because this amount depends entirely on the stiffness assumed in the direction perpendicular to the fibers. The mechanism described can also explain the experimentally observed shift of ℓ_{mas} to higher muscle lengths due to sub-maximal activation (Roszek *et al.*, 1994). Moreover, in studies on skinned fibers (e.g. Maughan and Godt, 1979; Brenner and Yu, 1991; Xu *et al.*, 1993) researcher found evidence for x-fiber stiffness under passive as well as active conditions. It should be noted that cautiousness is needed when observations on skinned fibers are extrapolated to muscle because in skinned fiber the demand of constant is not fulfilled any more (van der Linden *et al.*, 1997). This is in agreement with the observation of Horowitz *et al.* (1988a) that the incompressibility property results in a rather high compressive stiffness of cardiac muscle tissue due to an interaction of mechanical properties of fibers. This stresses the importance of the combined properties of passive tissue and the demand of constant volume. The results of the present model suggest that geometrical models such as the planimetric model (e.g. Huijing and Woittiez, 1984, Otten, 1988, van der Linden *et al.*, 1998) have no mechanical foundation. The planimetric model assumed a relationship between the fiber and the muscle force based entirely on the angular effect. Such a relationship leads to the erroneous assumption that at muscle active slack length, no active fiber force is exerted. The present model showed that as a result of mechanical equilibrium the fibers exert a considerable amount of force at muscle active slack length. Therefore, a relationship between fiber and muscle force should include contributions of passive tissue properties.

In the present model, we assumed the sarcomeres to act in series and therefore exert all the same active stress in series. Consequently, no in-homogeneous behavior of sarcomeres in series is allowed in the present model. As a result of this assumption, the model is not suitable to study the effects of sarcomere heterogeneities in muscle fiber (Julian and Morgan, 1979a,b; Edman et al, 1993). Preliminary results with another version of the model presented, a version where inhomogeneous behavior of sarcomeres is allowed, showed that sarcomeres in series do not necessarily have to exert the same force as a result of equilibrium in the continuum. The position of the sarcomere in the muscle belly defines the contribution of the sarcomere. This suggests that force exerted is passed through to neighboring structures in parallel as well as in series by shear and pulling forces.

In conclusion, the model in the present form is able to predict the length-force characteristic to some extent. Moreover, the predicted linearized geometry compares well with the experimental observed linearized geometry of the rat GM. Hence, the present model is a description of skeletal muscle as a mechanical continuum, incorporating properties such as shear and x-fiber stiffness as well as the conservation of muscle volume with important functional implications. Therefore, the present model is of great heuristic value in understanding skeletal muscle functioning. The model presented showed that a muscle can not be considered a ‘lumped’ fiber. Fibers in a muscle belly have different contribution to the functional characteristics of a whole muscle, which depends on their position in the muscle belly.

Chapter 5

A Reducing Cross-Bridge Model Explains Experimentally Observed Contraction History Effects

5.1. Abstract

A model based on the sliding-filament and cross-bridge theory is used to describe effects of contraction history during sustained contractions with phases where shortening or lengthening are imposed. The model presented has some modifications with respect to the general Huxley model, such as: a force-length relationship, a Kelvin element arranged in series with the contractile filaments and a cross-bridge detachment function for cross-bridges, stretched over their maximal binding length, that detach without consuming energy. The main model extension is the assumption that the number of available cross-bridges is reduced each cycle, thus introducing effects of fatigue. The obtained model is referred to as the reducing cross-bridge (RCB) model. The RCB-model is compared to the general Huxley model and to experimental observations under different conditions.

In accordance with experiments, the RCB-model is able to describe post-shortening force deficit in the entire sarcomere length range and post-lengthening force enhancement in the length range below sarcomere optimum length. Over optimum sarcomere length two RCB-models arranged in series are able to predict an enhanced force after lengthening. Furthermore, it is shown that exerted sarcomere force changes, due to superimposed high-frequency vibrations, compared to conditions without vibrations, as a result of changed cross-bridge distributions. A dissociation of force and number of attached cross-bridges is found, which implies that experimentally obtained stiffness, based on contractions with superimposed vibrations, does not relate to the number of attached cross-bridges.

(van der Linden *et al.*, 1998d, Biological Cybernetics, submitted)

5.2. Introduction

Many studies have shown that muscle fiber force does not solely depend on length and velocity of shortening or lengthening during maximal activation. Force changes in time seem therefore to depend on contraction history. Interactive effects that influence force exerted during sustained contraction are:

1. Fatigue related effects
2. A previous phase where shortening is applied
3. A previous phase where lengthening is applied
4. Velocity of shortening or lengthening
5. In-homogenous behavior of sarcomere in series.

A major factor of decrease in isometric force in time can be attributed to effects of fatigue, which has been defined historically as the failure to maintain force output, leading to a reduced performance and stiffness (Edman and Lou, 1990). Several authors (see reviews of Fitts, 1994 and McLester, 1997) attribute this reduction in performance to accumulation of metabolites. In the present paper, we focus on the effects of fatigue but not on the underlying mechanisms.

If an activated muscle is exposed to a stretch phase, enhancement of force can be observed in a subsequent isometric phase compared to the force at the same length of a sustained isometric contraction (e.g. Abbott and Aubert, 1952; Edman *et al.*, 1978; Sugi and Tsuchiya, 1988). When activation is sustained after the stretch phase, a part of the force enhancement is maintained; as is observed in frog (Edman *et al.*, 1978; van Atteveldt and Crowe, 1980; Edman and Tsuchiya, 1996); rat (Ettema *et al.* 1990; Meijer *et al.*, 1997) and human muscle (Cook *et al.*, 1995). The force enhancement after stretch is independent of the stretch velocity (Sugi and Tsuchiya, 1988).

For shortening this phenomenon is reversed, i.e. a force deficit is observed during and after a shortening phase (e.g. Buchthal and Kaiser, 1951; Edman, 1975; Edman *et al.*, 1993, Sugi and Tsuchiya, 1988; Granzier and Pollack, 1989). This deficit is inversely related to the shortening velocity. Length dependence of force reduction after shortening has been shown experimentally in rat gastrocnemius medialis muscle (Meijer *et al.*, 1997). Below muscle optimum length the force deficit after shortening is smaller compared to that of a contraction with the same distance of shortening (and velocity) over muscle optimum length. Meijer *et al.* (1997) found no evidence for differences in geometry of rat gastrocnemius muscle due to the force deficit after shortening and concluded that the force deficit has its origin at the intracellular level. Granzier and Pollack (1989) suggested that accumulation of metabolites during sustained contraction might underlie the deficit in force after shortening.

The sliding-filament theory (A.F. Huxley and Niedergerke, 1954; H.E. Huxley and Hanson, 1954) describes the sliding of myo-filaments during length changes in muscle fibers. Furthermore, the cross-bridge theory (Huxley, 1957) describes the motor behind this sliding of

filaments. This is expressed in a mathematical model that combines existing knowledge of structures, mechanics and energetics of muscle, by means of a partial differential equation (PDE). This combination of theories, generally referred to as the Huxley-model, is useful for comprehending muscle fiber dynamics during length changes as well as during isometric contractions. Subsequent modifications of this model were basically:

1. to increase the number of possible states a cross-bridge can have, which allows the study of force transients (e.g. Huxley and Simmons, 1971; Hill *et al.* 1975 and Eisenberg *et al.*, 1980);
2. to decrease numerical efforts by assuming Gaussian cross-bridge distributions (e.g. Zahalak, 1981, Ma and Zahalak, 1987) and consequently approximating the PDE proposed by Huxley (1957);
3. to extend the model with excitation dynamics (Zahalak and Ma, 1990). However, contraction history effects could not be explained.

In the present paper we propose that effects of contraction history during sustained contractions can be attributed to a change in cross-bridge cycling dynamics in such a way that effects of fatigue (Granzier and Pollack, 1990) and the change in stiffness, i.e. number of attached cross-bridges (Sugi and Tsuchiya, 1988) can be described. We assume that the number of cross-bridges available for force exertion is reduced is sustained contractions. The magnitude of this reduction is related to the number of cycles performed. The model thus obtained is an extended version of Huxley's model and referred to below, as the reducing cross-bridge (RCB) model. The model is applied to simulate sustained contractions with isometric and isokinetic phases and to study effects of altered contraction dynamics. The results of the model are compared to experimental data at sarcomere lengths below as well as over sarcomere active optimum length (ℓ_{sao}).

5.3. Methods

5.3.1. Huxley-model

Similar to Huxley (1957) a number of assumptions regarding cross-bridge dynamics were made:

1. Cross-bridges are independent elastic force generators arranged in parallel.
2. At any instant in time, each cross-bridge has access, with a certain probability, to only one actin-binding site.
3. Cross-bridge force is proportional to the bond length or stretch (x) from the neutral equilibrium position (x = 0) of the cross-bridge (fig. 5-1A).
4. Two cross-bridge states are assumed: one attached state and one detached state, where the probability of cross-bridge attachment is defined by a function f(x) and the probability of detachment by the function g(x) (fig. 5-1B). Two states are sufficient for studying steady state contractions. However, if force transients are studied more cross-bridge states are

necessary (e.g. Huxley and Simmons, 1971; Hill *et al.* 1975 and Eisenberg *et al.*, 1980). The rate constants 'f' and 'g_i' are rough estimates concerning cross-bridge cycling (Huxley, 1957). However, the relation between the 'f' and 'g_i' constants determines the maximal shortening velocity and the maintenance heat and work production under various conditions as experimentally observed by Hill (1938).

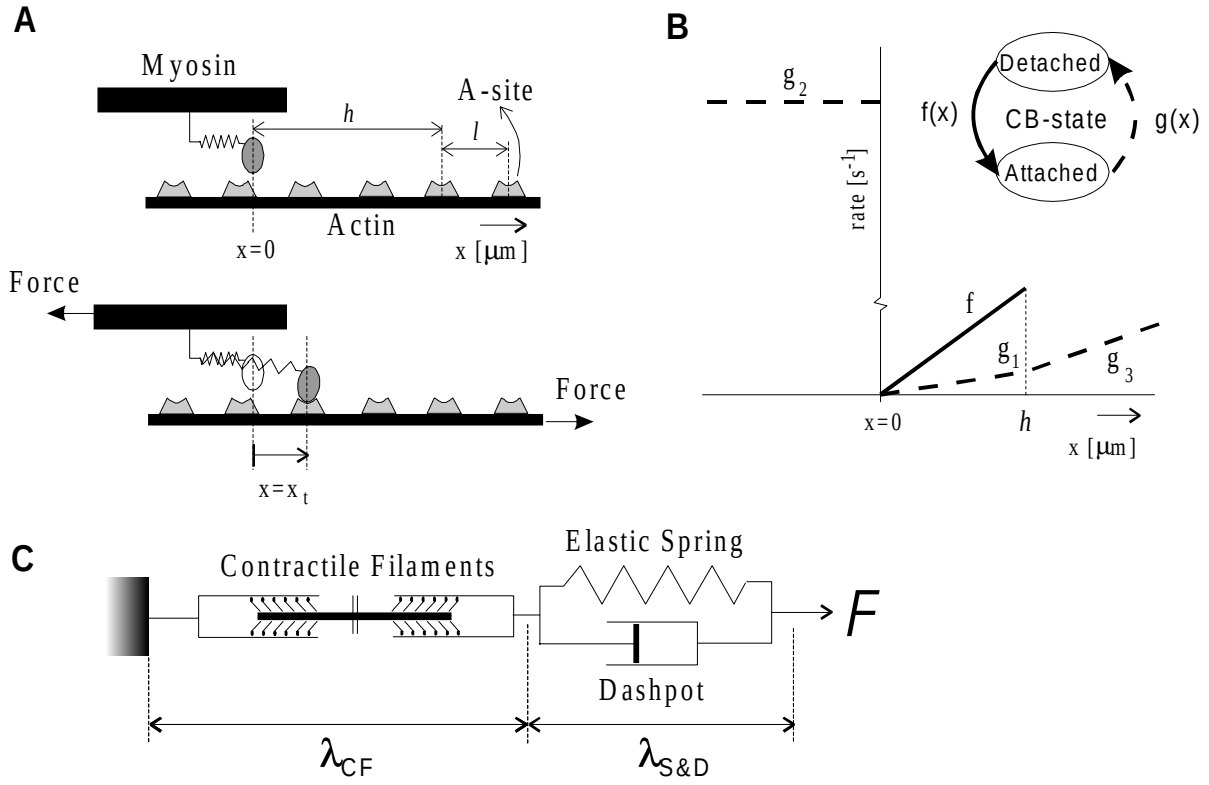

Figure 5-1 Schematic representation of the cross-bridge theory **A**: Several model parameters are shown, x indicates cross-bridge bond length, h*:* maximal bond length, *l:* distance between the locations on actin filament where cross-bridges heads can attach (A-sites). **B**: two cross-bridge states and a schematic representation of the rate function depending on bond length (x). Values for model parameters are given in Table 5-1. **C**: Representation of the model used, where the contractile filaments has the properties of the reducing cross-bridge model (RCB-model) and is arranged is series with a Kelvin element.

Mathematically this is formulated as follows. Let n(x,t) be the distribution function representing the fraction of attached cross-bridges with a displacement or binding length (x) at time t. The actin-myosin bonding kinetics satisfy the PDE:

$$\frac{d\,n(x,t)}{d\,t} = \frac{\partial n}{\partial t} + \frac{\partial n}{\partial x}\frac{\partial x}{\partial t} = f(x)\cdot\{N - n(x,t)\} - g(x)\cdot n(x,t) \qquad (1)$$

Where: $\frac{\partial x}{\partial t} = v$, is the sliding velocity of myofilaments with respect to each other and N is the maximal number of available cross-bridges. This equations describes the change of the number of attached cross-bridges (n) in time, and because n depends on x an t, n is partial differentiated to t and x. The right side describes the fraction of available cross-bridges that attach minus the

fraction of cross-bridges that detach at time t. Where these fraction of cross-bridges depend on the bonding length (x).

5.3.2. The reducing cross-bridge model

Basically the model presented in this paper is identical to the above described Huxley-model, but has been enlarged with the following extensions:

1. The model is extended with force length characteristics. According to the sliding-filament theory the amount of force exerted is proportional to the amount of myo-filament overlap for the length range over sarcomere optimum length (ℓ_{sao}). However, below ℓ_{sao} filament overlap remains maximal but force decrease is related to length decrease. A number of possible explanations have been proposed (e.g. Gordon *et al.*, 1966): 1. The actin filaments of one side in a sarcomere interacts with actin filaments on the other side, which result in less space for cross-bridges to attach. 2. Cross-bridges attach to an opposite (i.e. wrong) actin and exert an opposite force. 3. myosin filaments tend to penetrate the z-lines and will develop a resistive force. 4. Finite element analysis (van der Linden *et al.*, 1997) of muscle fiber mechanics showed that a resistance force is developed below optimum length as a result of mechanical interactions of passive properties parallel and perpendicular to the line of pull due to the demand of constant volume of muscle fiber. 5. Due to radial expansion at short fibers length myo-filament spacing increases and consequently the longitudinal force exerted by cross-bridges decreases as radial force increases (e.g. Xu *et al.* 1993). In any case, the amount of force exerted by a sarcomere below ℓ_{sao} is related to its length. Therefore, we incorporated an overlap function that is constant below ℓ_{sao} and decreases with increasing length (fig. 5-2A). A resistance function is multiplied with the overlap function and is assumed to be zero at sarcomere active slack-length and increases with length to attains unity at ℓ_{sao} (fig. 5-2B). The overlap and resistance functions together (fig. 5-2C) yield the 4th order polynomial fit of mean sarcomere force-length data of rat gastrocnemius medialus muscle (GM) (Zuurbier *et al.*, 1995). This distinction between an overlap and a resistance function is introduced to model length dependence of contraction history effects observed (e.g. Meijer et al, 1997). This specific force-length characteristic is used to allow the simulation of sustained

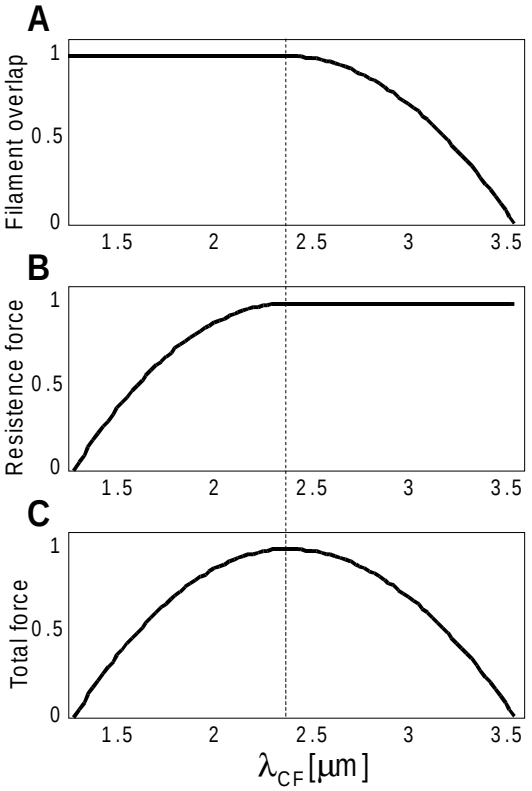

Figure 5-2 Determinants of sarcomere force-length characteristic. **A.** filament overlap function **B.** resistance function. **C.** In combination they yield the experimentally determined mean sarcomere force-length relationship of rat GM muscle (Zuurbier *et al.*, 1995).

contractions of sarcomeres, and model results will be compared to experimental data of single fibers and muscle. Implementation of such length dependence in the model causes the number of available cross-bridges (N) to depend on length of the contractile filaments (λ_{CF}), such that $N = N(\lambda_{CF})$.

2. We assume contraction history effects to be related to the number of cross-bridge cycles performed: after each cycle a percentage α of the cross-bridges available for attachment will no longer take part in the force generating process. Consequently, during sustained contraction the total amount of available cross-bridges decreases with the number of cycles. This is in accordance with observations of Edman and Lou (1990) on frog fibers that fatigue induces a decrease of stiffness as well as force. Therefore, the model presented is called the 'Reducing Cross-Bridge' (RCB) model. The percentage α is chosen such that force decrease during sustained isometric contractions is proportional to the force decrease per second observed in rat GM (figure 3 in Meijer *et al.*, 1997). Equation (1) becomes:

$$\frac{\partial n}{\partial t} + v \cdot \frac{\partial n}{\partial x} = f(x) \cdot \left\{ N(\lambda_{CF}) - n(x,t) - \alpha \cdot n_{recy}(x,t) \right\} - g(x) \cdot n(x,t) \qquad (2)$$

With $n_{recy}(x,t)$ is the distribution of detached cross-bridges from which a percentage α is taken out of the recycling process due to effects of contraction history. This equation is solved numerically with fixed time steps (Δt = 0.1 ms) and length step (Δx = 0.5 nm), see appendix A for details. This solution method is preferred above the approximation of PDE with quasi-static distribution moments as proposed by Zahalak (1981) based on Gaussian cross-bridge distributions. Length dependence of the effects of fatigue are ignored at this point, which are negligible in a range from -4 mm to +2 mm of muscle optimum length (Meijer *et al.*, 1998).

3. Huxley and Simmons (1971) showed experimentally the existence of two structural elements in series with the contractile element in isolated frog fiber with additional elastic and viscous properties. Incorporation of a Kelvin element, i.e. a parallel arrangement of linear spring and a dashpot, placed in series with the contractile filaments (fig. 5-1C) in the model results in slower responses to length changes. The implementation, especially the interaction of the contractile filaments and Kelvin element, is described in appendix B.

3. In order to describe low-energy cost during lengthening many authors (e.g. Sugi, 1972; Zahalak, 1981; T.L. Hill *et al.*, 1975) assumed that if cross-bridges stretched over their maximum bonding length (i.e. x>h), they detach without utilization of energy. Furthermore, it is assumed that the rate of detachment (g_3) for cross-bridges stretched over their maximal bonding length is larger compared to the rate (g_1) in the range from zero to h (i.e. 0<x<h, fig. 5-1B). This is implemented in the RCB-model. Since these force-fully detached cross-bridges (Sugi, 1972) do not contribute to the accumulation of metabolites, the reducing process (equation 2) is not applied to these cross-bridges. The parameters of RCB-model are listed in Table 5-1.

Table 5-1 Model parameters

s	2.4143 μm	f(0<x<h)	100 s^{-1} x/h	C	0.5	ℓ_{sao}	2.433 μm
h	15.6 nm	g_1(0<x<h)	25 s^{-1} x/h	D	0.007	$F_{max}(\ell_{sao})$	20.75
l	5.5 nm	g_2(x<0)	500 s^{-1}	α	1 %	$\lvert v_{max}\rvert$	4.13 μm/s
m, k	1	g_3(x>h)	30 s^{-1} x/h			#ACB(ℓ_{sao})	23.1

The model parameters as shown in figure 5-1 and eq. 3, parameters C and D (appendix B) represent constants of the in series arranged Kelvin element, i.e. the spring and dashpot, α is the percentage of cross-bridges that is taken out of the recycling process due to effects of contraction history. On the right in the table some values which are based on an isometric contraction at ℓ_{sao} and are used for normalization purposes.

The main output of the model is the distribution of attached cross-bridges in time. From this distribution, we determine force of the contractile element (F_{CF}) with the following equations (according to Huxley, 1957):

$$F_{CF}(t) = \frac{m \cdot s \cdot k}{2 \cdot l} \int_{-\infty}^{\infty} x \cdot n(x,t) \cdot dx \qquad (3)$$

With: m: number of cross-bridges
s: optimum length of contractile element in RCB-model ($\lambda_{CF,opt}$)
k: cross-bridge stiffness
l: distance between cross-bridge binding sites on actin filament

Only maximally activated sarcomeres are modeled and therefore activation dynamics are ignored. In addition, the effects of length dependence of Ca^{2+} sensitivity are assumed not to play a role of importance.

5.3.3. Stiffness

The general output of the model is the cross-bridge distribution, i.e. the number of attached cross-bridges (#ACB) and their bond length. Since cross-bridges are independent force generators the number of attached cross-bridges is a measure for sarcomere stiffness (Julian and Sollins, 1975). Experimentally #ACB is determined by measuring muscle stiffness. Therefore, high-frequency length perturbations are applied and the quotient of the length change of the contractile element (λ_{CF}, fig. 5-1C) and the force change is called 'quasi-stiffness' by Latash (1993). In present paper, it is referred to as high-frequency (HF) stiffness. With the present model a comparison is made between HF-stiffness and #ACB under isometric and isokinetic conditions. It is shown that application of high-frequency length perturbations on sarcomere have effect on the cross-bridge distribution when compared to the same contraction without perturbation.

5.3.4. Contractions modeled

The RCB-model is used to perform contractions with concentric and eccentric phases are performed below and over sarcomere optimum length (ℓ_{sao}) with different velocities and these are compared to sustained isometric contractions at the target length of the isokinetic contractions. Furthermore, the results are compared to data from the literature (Edman *et al.*, 1978, 1993; Sugi and Tsuchiya, 1988; Meijer *et al.*, 1997). Only experimental results of contraction on rat GM with a lengthening protocol are presented in figure 5-6. The results are obtained from an identical experimental setup and procedure followed as described by Meijer *et al.* (1997), except for the applied length protocol (figure 5-5A). Sustained isometric contractions are performed wit the RCB-model at 70%, 85%, 115% and 130% of ℓ_{sao} (i.e. 1.70, 2.07, 2.80 and 3.16 μm, respectively). Contractions with concentric phases are performed with 10% and 50% of maximal shortening speed (v_{max} = -4.125 μm/s) of the model (i.e. -0.4 and -2.1 μm/s respectively), during the eccentric phases lengthening is performed with velocities of 10% and 25% of v_{max}. Shortening velocities are indicated with negative values. Isokinetic phases are initiated at t = 0.5 s after a pre-isokinetic phase at the start length in which a fully isometric force is exerted, in figure 5-3A this is indicated for a sustained contraction with an concentric phase. The isokinetic phase ends when the sarcomere is shortened or lengthened with 15% of ℓ_{sao} and target length is reached. Finally, the model sarcomere is allowed to redevelop isometric force at target length during the post-isokinetic phase (for at least 1 s) up to t = 2.5 s, which is indicated in figure 5-3A as the post-concentric phase. Presented forces and number of attached cross-bridges (#ACB) are normalized for the respective maximal values determined from a sustained isometric contraction at ℓ_{sao} at about t = 0.3 s (table 5-1).

5.4. Results

5.4.1. Reducing cross-bridge-model versus Huxley-model

The reducing cross-bridge model (RCB) has a number of properties that are different from those of the Huxley-model. A comparison of results from both models for an isometric and concentric contraction is presented in figure 5-3, for lengths below sarcomere active optimum length (ℓ_{sao}). The effects of the additional properties of the RCB-model on sustained isometric contraction is clear as force decreases about 10% per second, compared to no decrease for the Huxley-model (fig. 5-3B). Responses to force and length changes (at t= 0, 0.5 and 1.4 s) by the RCB-model are slower when compared to the Huxley-model due to the additional structural elements arranged in series with the contractile element. The maximal tetanic isometric force exerted by the RCB-model is lower than that of the Huxley-model, as a result of the fact that the process of reducing cross-bridges is active from the very beginning of the contraction.

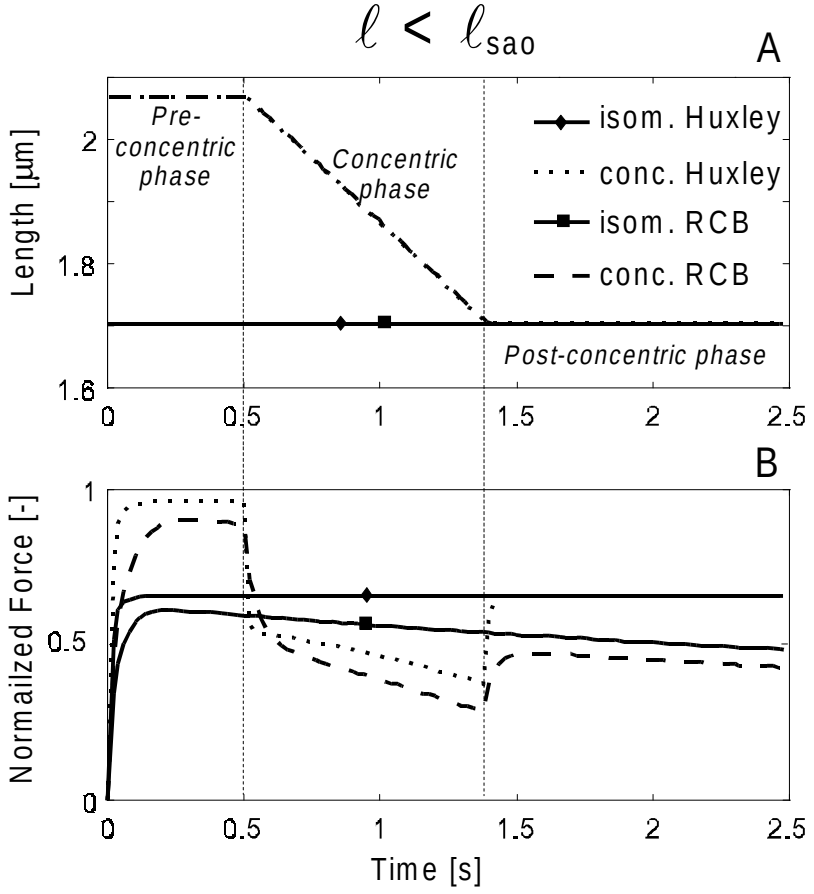

Figure 5-3 A comparison of result for the original Huxley model and the RCB-model

A. The length protocols applied to both models, two contractions were performed in a length range below ℓ_{sao}: 1. sustained isometric contraction 2. contraction with a pre-concentric phase, a concentric phase and a post-concentric phase. **B.** The corresponding forces of the Huxley and the RCB-model under both conditions. Force is normalized for the optimal force exerted at ℓ_{sao} under isometric conditions (tab. 1).

Furthermore, the deficit in force developed during a concentric contraction is not recovered during the post-concentric phase, despite the fact that target length is identical for the concentric contraction and the sustained isometric contraction. In contrast, the Huxley-model shows a force that recovers completely to the level corresponding the actual length during the post-concentric phase. In this way, effects of contraction history on force exerted were introduced in the RCB-model.

Table 5-1 Effects of contraction history in percentages.

Condition		Differences determined	
v [% v_{max}];	ℓ_i [% ℓ_{sao}]	Δ Force [%]	Δ #ACB [%]
-10	70	-11.9	-12.3
-50	70	-6.1	-6.0
-10	115	-7.6	-6.8
-50	115	-3.1	-2.3
10	85	4.8	4.6
25	85	2.9	3.1
10	130	-0.5	-1.3
25	130	-1.5	-1.7
two sarcomeres in series: $\Delta\ell_{initial}$ 0.1→ $\Delta\ell_{t=2.5s}$ 1.6%			
10	125	3.5	

The differences at t = 2.5 s between isometric contractions and contractions with an isokinetic phase. The velocity during the isokinetic phase and target-length (ℓ_i, length at which isometric contraction is performed) are presented in the first two columns, the force difference in percentages in the third and the change in the number of attached cross-bridges (#ACB) in the last column. In the bottom rows, the differences of two RCB-models (sarcomeres) arranged in series at t = 2.5s of the sustained isometric contractions (ℓ_i = 125% ℓ_{sao}) and contraction with eccentric phase (v = 10% v_{max}). An initial sarcomere length difference of 0.1 % increases to 1.6 % length difference.

5.4.2. Effects of shortening velocity

In addition to contractions shown in figure 5-3, concentric contractions are modeled with the RCB-model with two different speeds of shortening (-10% and -50% of v_{max}) (fig. 5-4). A comparison is made between sustained isometric contraction at target length and contractions with a concentric phase. During the concentric phase force depends on velocity of shortening (fig. 5-4B). During the post-concentric phase force recovers but a deficit of force is maintained compared to the sustained isometric force at the target length. A high velocity of shortening results in a smaller deficit (-6%, see tab. 2) compared to low velocity of shortening (-12%, tab. 2). These observations are in agreement with experimental results on rat GM of Meijer *et al.* (1997) as well as on frog fibers Edman *et al.* (1993). If the same length protocol is applied for contractions over ℓ_{sao}, quantitatively similar patterns are found (not shown), although the differences in post-concentric force are smaller compared to the contractions performed below ℓ_{sao}. The force deficit after shortening at 50% of v_{max} and 10% of v_{max} are -3% and -8%, respectively (tab. 2). The pattern of force in time matches that of the number of attached cross-bridges (#ACB) (fig. 5-4B+C). It is concluded that force decrease during shortening is a result of decrease in number of attached cross-bridges. Moreover, during shortening cross-bridge bond-length decreases and can be negative for some cross-bridges, i.e. negative forces are exerted by these cross-bridges. Furthermore, the rate of detachment is higher for these cross-bridges and therefore the number of cross-bridge cycles per unit time increases, which results in a decrease in number of cross-bridges attending the cycling process due to the reduction factor α. Finally, this results in smaller amount of #ACB in the post-concentric phase and therefore, less force is exerted. The final difference in #ACB at t = 2.5s (tab. 2) between the two concentric contractions is a measure for the difference in number of cross-bridge cycles performed during shortening. The concentric phase with a high velocity of shortening needs fewer cross-bridge cycles to reach the target length compared to a low velocity of shortening and therefore the force deficit at t=2.5s is smaller compared to the sustained isometric contraction.

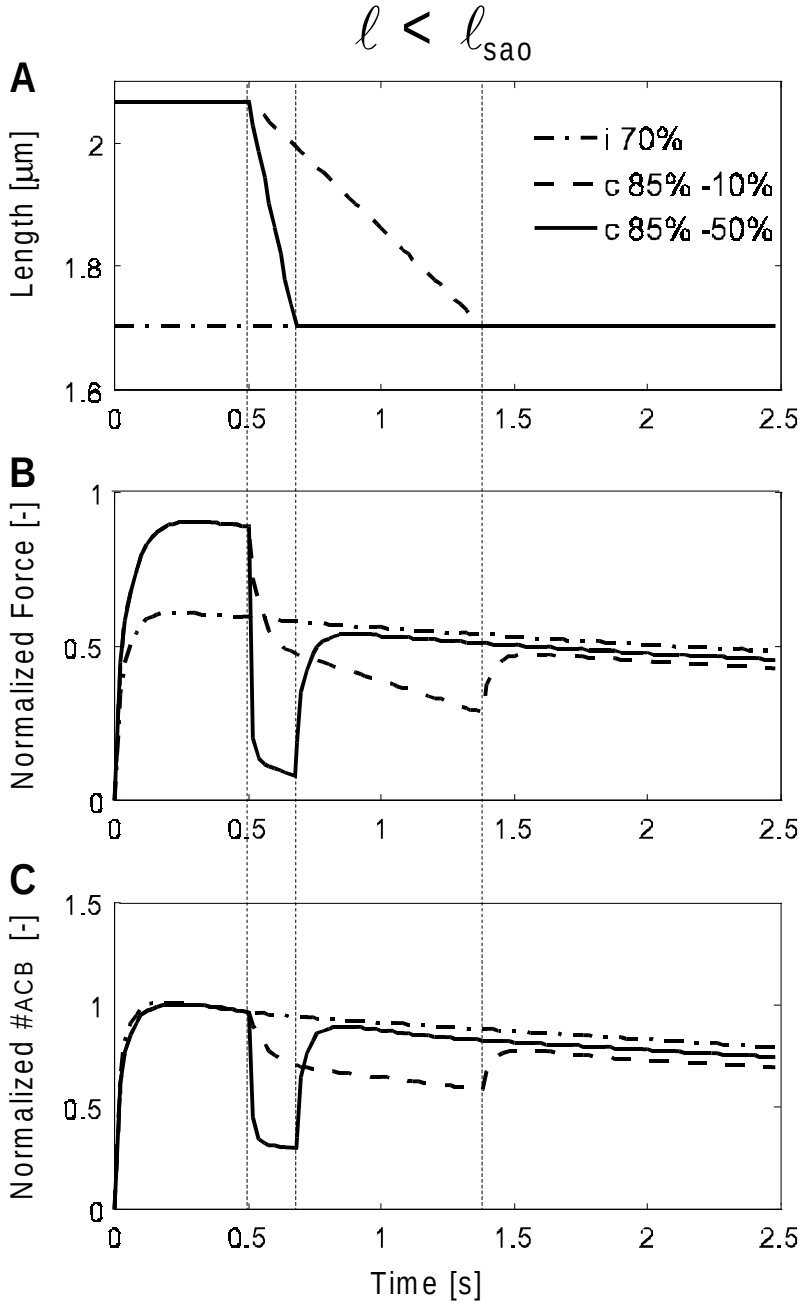

Figure 5-4 Effects of shortening according the RCB-model in a length range below ℓ_{sao}.

A. The length protocol applied to the RCB-model. Three contractions are simulated: a sustained isometric contraction at 70% of ℓ_{sao} ('i 70%') and two contractions with a concentric phase, with start length 85% of ℓ_{sao} and two different shortening velocities (-10 and -50% of v_{max}) ('c 85% -10%' and 'c 85% -50%'), with identical target lengths at 70% of ℓ_{sao}. **B.** The corresponding force traces. The RCB-model predicts a force deficit after shortening, which depends inversely on velocity of shortening **C.** The corresponding number of attached cross-bridges (#ACB) during these contractions. The decrease in force is clearly caused by the change in number of attached cross-bridges for post-concentric conditions.

5.4.3. Effects of eccentric velocity

The lengthening protocol imposed on the model is presented in figure 5-5A for contractions within a length range below ℓ_{sao}. Force is enhanced during eccentric phase (fig. 5-5B). The increase in force exerted during stretch depends on the velocity of lengthening as is expected from the eccentric part of the force-velocity curve. An enhancement in force remains after the eccentric phase below ℓ_{sao} (fig. 5-5B) compared to force of the sustained isometric contraction.

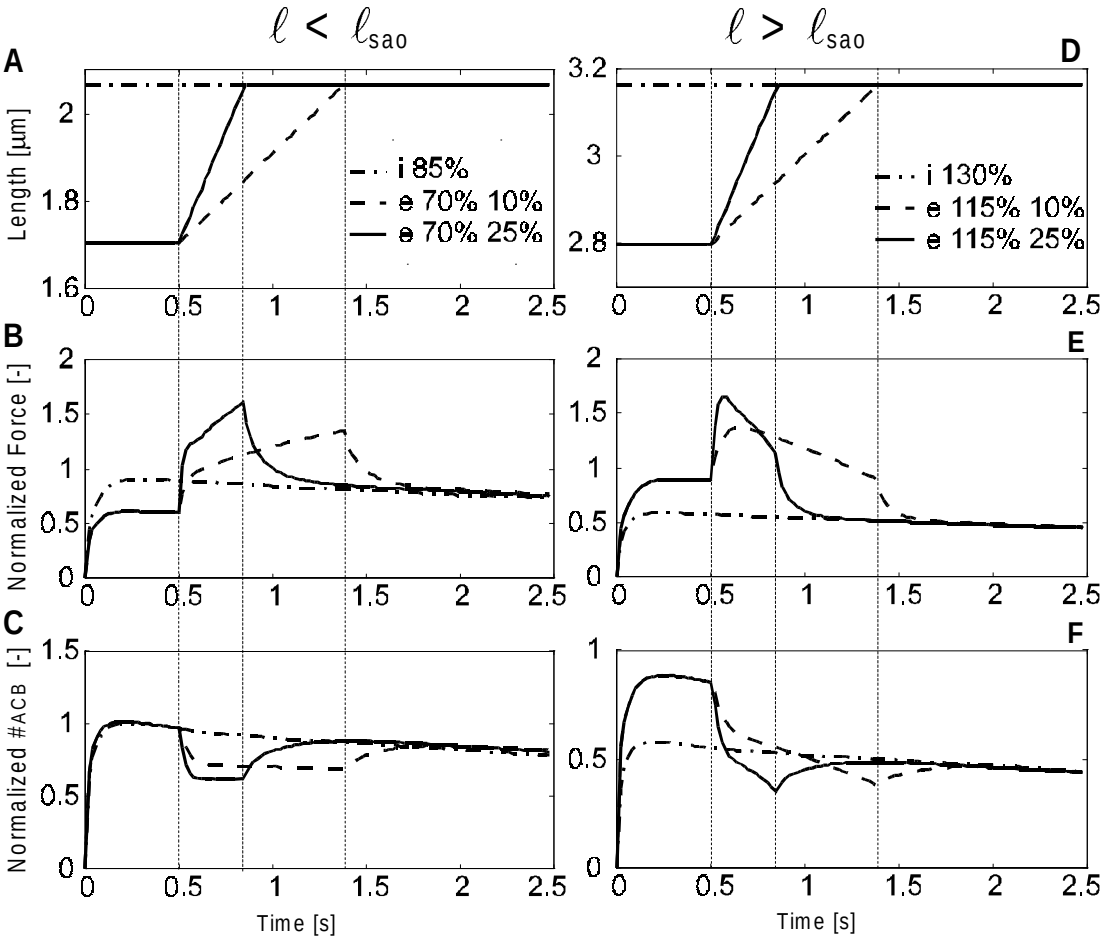

Figure 5-5 Effects of lengthening according the RCB-model. The left panel indicates effects for a length range below ℓ_{sao} and the right panel length range over ℓ_{sao} **A.** The lengthening protocol applied to the RCB-model. Three contractions are simulated: a sustained isometric contraction at 85% of ℓ_{sao} ('i 85%') and two contractions with an eccentric phase, with start length 70% of ℓ_{sao} and with two different lengthening velocities (10 and 25% of v_{max}) ('e 70% 10%' and 'e 70% 25%'), with identical target lengths at 85% of ℓ_{sao}. **B.** The corresponding force traces. The RCB-model predicts a force enhancement after lengthening which depends on velocity of lengthening below ℓ_{sao}. **C.** The corresponding number of attached cross-bridges (#ACB) during the contractions. The post-eccentric #ACB is proportional with force. However, during lengthening #ACB is not proportional to the force exerted. **D.** An identical length protocol is applied to the model over ℓ_{sao}. A sustained isometric contraction at 130% of ℓ_{sao} ('i 130%') and two contractions with an eccentric phase, with start length 115% of ℓ_{sao} and with two different lengthening velocities (10 and 25% of v_{max}) ('e 115% 10%' and 'e 115% 25%')., with identical target lengths at 130% of ℓ_{sao} **E.** The forces determined after the eccentric phase do not show an enhancement compared to the force of sustained isometric contraction at target length, the small deficit is hardly visible, see table 5-2 for details. **F.** The #ACB is less than for the sustained isometric contraction during the post-eccentric phase, (see also tab. 2).

The surplus of force at t = 2.5s depends on a previous velocity of lengthening in such a way that lower velocity leads to a greater increase (4%, tab. 2) of force compared high velocity of lengthening (2%, tab. 2). These findings are in agreement with experimental observations on rat GM (fig. 5-6) and on frog (e.g. Edman et al, 1978, Sugi and Tsuchiya, 1988).

During lengthening the force exerted increases, even though #ACB decreases as is predicted by the model, it must be concluded that the average bond length of the attached cross-bridges is increased. For more details about this finding is referred to the section on stiffness below. Force enhancement observed after an eccentric phase at t=2.5s is caused by a larger #ACB compared to #ACB of the sustained isometric contraction (fig. 5-5C). Moreover, higher velocity of stretch result in fewer attached cross-bridges at t=2.5s.

A post-eccentric force deficit (-3% and -4%, tab. 2) is found for modeled eccentric contractions performed in a length range over ℓ_{sao} (fig. 5-5E), which is in contrast with observations (e.g. Edman *et al.*, 1978; Sugi and Tsuchiya (1988). The #ACB is smaller compared to that of sustained isometric contraction (fig. 5-5F, and tab. 2).

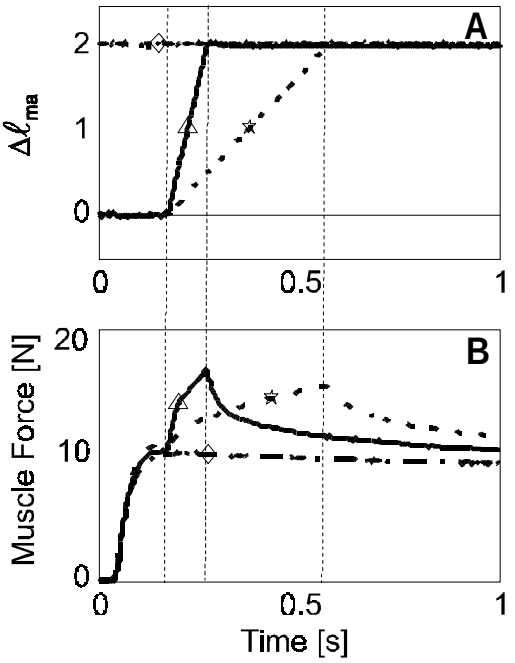

Figure 5-6 Experimental results regarding effects of lengthening.

A. Experimental protocol applied to rat GM with phases of muscle lengthening and a sustained isometric condition. **B**. Measured muscle forces under three conditions. An enhancement of force is observed after a contraction with an eccentric phase. Furthermore, this enhancement depends inversely on the velocity of lengthening. An identical experimental setup is used as is described by Meijer *et al.* (1997).

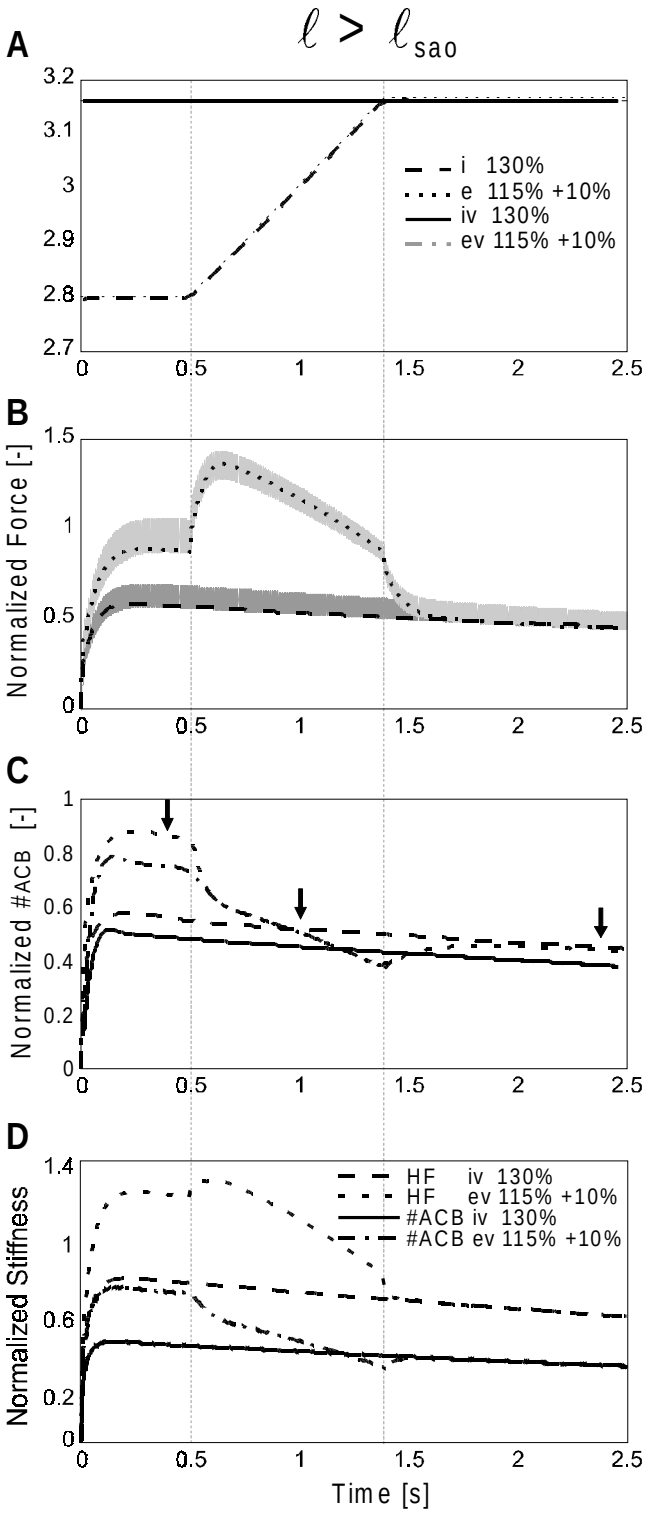

Figure 5-7 Effects of superimposed high-frequency perturbations vibrations. **A.** Contraction performed with superimposed high-frequency length perturbations on the protocol shown in figure 5-5A. A comparison is made between these contractions performed without ('i 130%', 'e 115% +10%') and with high-frequency vibrations ('iv 130%', 'ev 115% +10%'). **B.** The exerted forces are increase as a result of applied vibration, under isometric conditions. **C.** The corresponding number of attached cross-bridges (#ACB). #ACB is decreased as a result of applied vibration under isometric conditions. Arrows indicate moments at which the cross-bridge distribution is plotted in figure 5-8A. **D.** Comparison of #ACB and HF-perturbations is made and it is clear that during the eccentric phases an increase of HF-stiffness is observed, which is in contrast with a decrease in #ACB.

5.4.4. Stiffness

Sarcomere stiffness is determined by modeling an identical protocol as is shown in figure 5-5D, with additional high frequency length perturbation (frequency: 500 Hz; amplitude: 1 nm and Δt = 0.05 ms) (fig. 5-7A). It should be mentioned that the frequency and amplitude applied had no periodical effect on the #ACB, i.e. the ripple found on the #ACB curve is negligible. In contrast to experimental observations (Sugi and Tsuchiya, 1988; Edman and Lou, 1990), the length perturbations applied to the mode effect the force exerted (fig. 5-7B). Modeled pre-eccentric force increases with about 10% (fig. 5-7B). However, #ACB is decreased about 20% during isometric phases (fig. 5-7C). This can be explained as follows: due to additional length perturbations applied bond length of attached cross-bridges changes with higher detachment rates ($x<0$ and $x>h$, fig. 5-1B). Below $x = 0$ detachment rate (g_2) is much higher than g_3 for $x>h$, therefore relatively more cross-bridges with small length detach. In figure 5-8A cross-bridge distributions are shown during the contractions with an eccentric phase at three moments (t=0.4, 1 and 2.4 s) indicated with an arrow in figure 5-7C. The effect of the applied length perturbation is best visible during the isometric phases (t = 0.4 and 2.4), where a wider range of cross-bridges bond lengths is found, with a small shift to larger bond lengths. Consequently, the mean cross-bridge bond length increases (fig. 5-8B) and more force is exerted. Therefore, despite the fact that #ACB is decreased during high-frequency length perturbations, the force is increased, and consequently force is not proportional to #ACB. A similar effect is observed during lengthening under non-perturbed conditions, as force increases and #ACB decreases, a shift to longer bond-length of attached cross-bridges is found (fig. 5-8A, middle) and consequently, the mean bond length increases (fig. 5-8B). In contrast with stiffness based on #ACB, HF-stiffness is proportional to the amount of force exerted and increases during lengthening (fig. 5-7B&D).

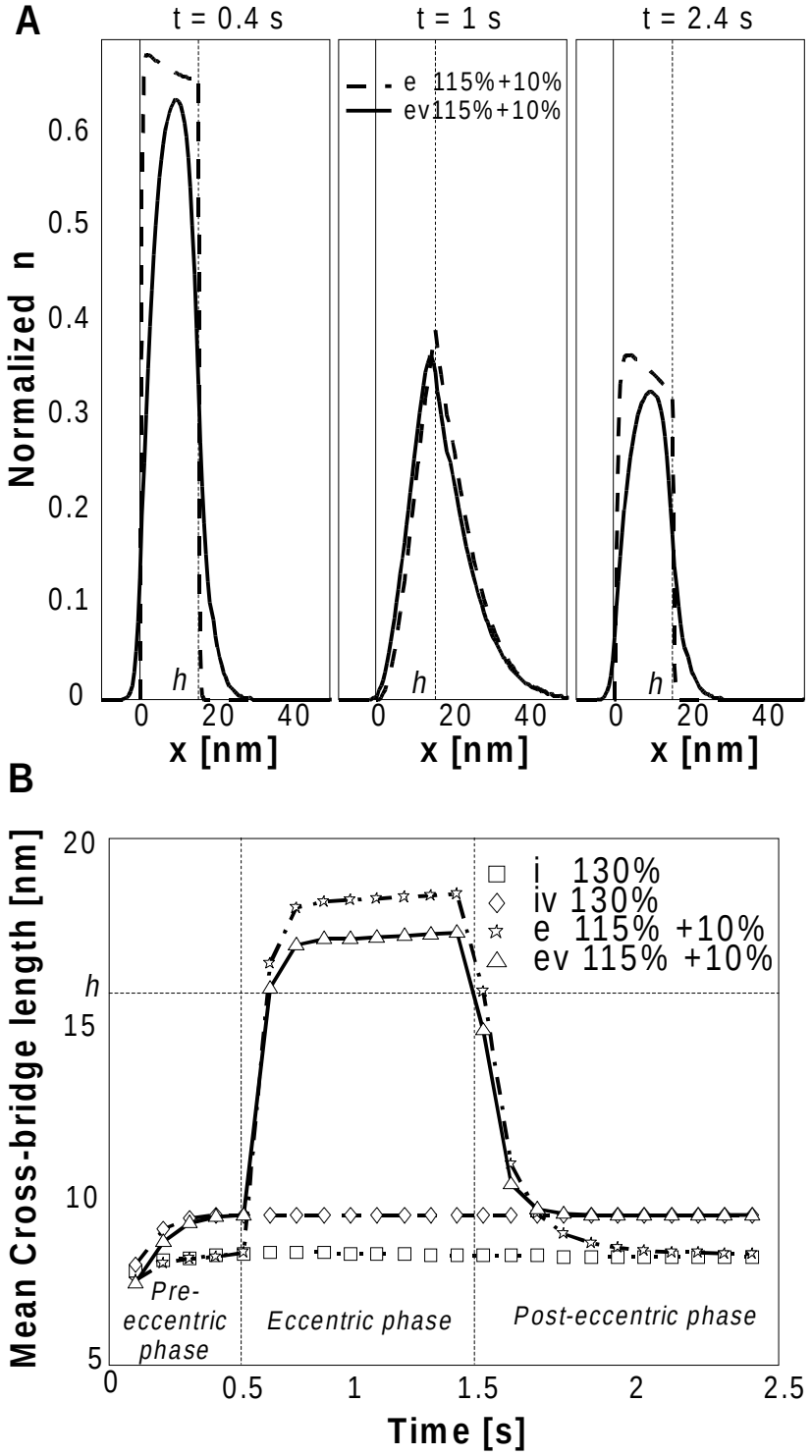

Figure 5-8 Effects of lengthening on cross-bridge distributions.

A. The cross-bridge distribution (n(x,t)) at three moments in time (0.4, 1 and 2.4 s), indicated with and arrow in figure 5-7C, are presented for contractions with and without an applied length perturbation. The left and the right panel are under isometric conditions and the middle panel shows the distribution during the eccentric phase. **B.** The average cross-bridge bond length during the sustained contractions at 0.1 s intervals, based on the cross-bridge distribution. The applied high-frequency vibrations result in an increase of the average bond length of the cross-bridges under isometric conditions. Note that during the eccentric phase the average bond length is larger than the maximal bond length (h).

Figure 5-8B presents the mean cross-bridge bond length at intervals of 0.1 s. It should be noted that at these specific moments in time the force is at its minimal value of the periodically changing force. Therefore, under isometric conditions cross-bridges are extended at least an additional 1 nm due to the length perturbations imposed. At the maximal value of the periodically changing force (1 ms later, due to 500 Hz frequency) cross-bridges are extended even more. During the eccentric phase the extension of cross-bridges is fluctuating between minus 1 nm (see fig. 5-8B) and about plus 1 nm at 1 ms later (not shown in fig. 5-8B).

5.4.5. Sarcomeres in series

The RCB-model, i.e. one sarcomere, is not able to predict isometric force well after the eccentric phase, for contractions performed over ℓ_{sao} (fig. 5-5E), which is in contrast with experimental observations on rat GM (figure 5-6) and on fibers (e.g. Julian and Morgan, 1979a,b; Morgan and Proske, 1984; Sugi and Tsuchiya, 1988). However, if two RCB-models are arranged in series such enhancement of force is found due to initial length inhomogeneity of sarcomeres. The length difference between the two RCB-models slowly increases from initially 0.1% to 1.6% at the final time t = 2.5s. During isometric condition the length difference increases continuously and is therefore a (slow) dynamic condition. The post-eccentric force is enhanced 3.5% compared to the force of sustained isometric contraction at the same target-length (table 5-2). For contractions below ℓ_{sao} performed with two RCB-models arranged in series an initial length difference will disappear during the contractions.

5.5. Discussion

In contrast with original Huxley model, the RCB-model predicts: 1. force enhancement during and after lengthening, 2. force decrease during and after shortening, as well as 3. effects of fatigue. Thus effects of contraction history are introduced in a Huxley based model. In the model presented, coupling of cross-bridge cycling to effects of contraction history leads to a better prediction of force during sustained contractions of sarcomeres. Recycle rates increase under isokinetic conditions when compared to isometric conditions, which results in a larger reduction of the maximal available number of cross-bridges in time and consequently a force deficit after shortening (fig. 5-4) is introduced. This is consistent with observations of Sugi and Tsuchiya (1988) that fiber stiffness is decreased after shortening. However, during lengthening the process of reducing available cross-bridges is influenced by the fact that more cross-bridges are stretched beyond maximal bond-length (h, see figure 5-8A middle panel) and these cross-bridges are forcefully detached (with rate g_3) and without consuming energy. Therefore, the reduction in number of available cross-bridges by the factor α is depressed, consequently an enhancement of force after an eccentric phase is observed (fig. 5-6B). If larger velocities are applied, concentric as well as eccentric, the cross-bridge cycle rate increases in time, and consequently the reduction of available cross-bridges increases. However, fewer cross-bridge cycles are needed to reach target length. Finally, the force deficit found is smaller compared to the deficit of contractions with slow concentric phases.

The above described mechanism shows good predictions for contractions performed within a length range below optimum length. However, for contractions performed within a length range over optimum length another process is involved as well, namely the change in filament overlap. For sustained contractions with a concentric phase this results in smaller force deficits (see table 5-2), than for similar contractions performed within a length range below optimum length. During lengthening, filament overlap decreases and therefore the number of available cross-bridges decreases more dramatically than can be 'saved' for the force generation by forceful detaching of cross-bridges at a length higher than the maximal bond length. Based on present results it is concluded that, an another mechanism is responsible for the observed force enhancement after lengthening over optimum length. A mechanism, thoroughly discussed in literature (e.g. Morgan *et al.* 1990, Edman *et al.*, 1978 and Sugi and Tsuchiya, 1988) is the interaction of sarcomeres in series in such a way that heterogeneities of sarcomere lengths are found. When length differences between two RCB-models arranged in series are allowed, this mechanism causes a force enhancement after an eccentric phase over ℓ_{sao}, although only a small increase in exerted force is observed (tab. 2).

5.5.1. Length dependence

The length dependence of force was introduced by assuming an overlap function and a resistance function, which together yield the (mean) sarcomere force-length curve (fig. 5-2). This results in different behavior of the sarcomere under dynamic conditions below and over optimum length. In case no distinction is made between an overlap and resistance function, the maximum number of available cross-bridges would depend entirely on the force-length relationship, unlike the constant overlap function in the present model. The force deficit after a concentric phase in a sustained contraction would be smaller below optimum length than for a contraction with the same amplitude and velocity over optimum length. This would be in agreement with results of Meijer *et al.* (1997) on whole rat GM muscle and implies that some other mechanism is involved, if the number of available cross-bridges below ℓ_{sao} is smaller than the maximum assumed in the present model. In case of stretch this process is also influenced by the forcefully detachment of cross-bridges. This results in larger enhancements in force when the number of available cross-bridges increases (length range below ℓ_{sao}), due to a combined effort of this increase and no reduction in available cross-bridges, compared to the situation that these processes counteract each other, which is the case for a length range over ℓ_{sao}.

5.5.2. Other model adjustments

The assumption that the reduction of the number of available cross-bridges, due to the effects of contraction history, appears to be not enough to explain the force enhancement after stretch. Based on experimental observations Edman and Lou (1990) suggested, that the force per cross-bridge decreases due to effects of fatigue as well as the number of available cross-bridges. When the assumption that force per attached cross-bridge decreases in time is incorporated in the present model, result will show proportional lower force instead of an additional difference. Therefore, force decrease per cross-bridge will not account for the

differences found between the experiments and the present model for contraction performed in a length range over ℓ_{sao}.

Another process proposed in literature (Colomo *et al.*, 1986; Edman 1975, 1980) that may be responsible for observed post-shortening force deficits, is de-activation of the contractile machinery. With the presented model only, maximally stimulated sarcomeres were studied. Effects of sub-maximally stimulation, such as the de-activation machinery, are ignored without making large errors, because it is not expected to play a role of importance in tetanic contractions (Edman, 1975, 1980; Colomo *et al.*, 1986).

The fact that high-frequency perturbations affects force is in contrast with experimental observations of Sugi and Tsuchiya (1988) who found identical forces with and without applied high-frequency perturbations. This suggests that the RCB-model is conceptually different from the real situation, because sinusoidal perturbed cross-bridges will, according to the cross-bridge theory shorten and extend to lengths with higher rates of detachment. Alternative models are needed to explain this behavior. Such models may be based on helix-coil transactions (e.g. Flory, 1956; Pollack 1990). These models assume that contraction is initiated by helix-coil transitions of a small segment of the myosin rod (S-2). Another alternative is a model with more different cross-bridges states with rate functions that depend different on contraction history. Mijailovich *et al.* (1996) reported in their model study that filament extension under applied forces results in a dissociation of force and stiffness in such a way that stiffness develops before force, suggesting that cross-bridges are attached but exert no force. Without incorporating elastic filaments in the RCB-model this model shows a dissociation as well, which is caused by the presence of the in series arranged Kelvin element. Our model shows a remarkable dissociation between force and number of attached cross-bridges during lengthening, unless HF-stiffness is calculated, which is proportional to force (van der Linden *et al.*, 1996). Models with extensible filaments are not likely to be able to overcome the discrepancies found between the RCB-model and experimental results. With regard to statements about stiffness in which a relation is assumed between force, stiffness and number of attached cross-bridges, one should interpret these statements with great care, as is shown is the present study.

5.5.3. Conclusions

Coupling of contraction history effects to the cross-bridge recycle process describes experimentally observed phenomena like force enhancement after lengthening and force deficit after shortening as well as velocity dependence of these phenomena to some extent. The assumption of forcefully detached cross-bridges has already proven its value in the energy approach of muscle contraction (e.g. T.L. Hill at al., 1975; Ma and Zahalak, 1990). In the present work it explains force enhancement after stretch. The distinction between an overlap function and a resistance function was an attempt to predict the length dependence of force generation after contraction with isokinetic phases, and is debatable based on the present results. A refinement of the model in a sense of more cross-bridge states may lead to better results. The present study showed that, due to the reduction of the number of available cross-

bridge per cycle, several different effects of contraction history during sustained contractions can be predicted better.

5.6. Appendix A

The equation to be solved is a first order, linear and partial differential equation (2). After rewriting and discretizating it becomes:

$$\frac{\Delta n(x,t)}{\Delta t} = f(x)\cdot\left\{N(\lambda_{CF}) - n(x,t) - \alpha\cdot n_{recy}(x,t)\right\} - g(x)\cdot n(x,t) - v\cdot\frac{\Delta n(x,t)}{\Delta x} \qquad \text{(A. 1)}$$

The distribution of cross-bridges (n) at time t is kept in an array over a large range of bond lengths (x). Finally, at every time instant (t+Δt) n(x) is numerically determined:

$$\begin{aligned} n(x,t+\Delta t) = \quad & n(x,t) + \left[f(x)\cdot\left\{N(\lambda_{CF}) - n(x,t) - \alpha\cdot n_{recy}(x,t)\right\}\right]\cdot\Delta t \\ & - \left[g(x)\cdot n(x,t) - v\cdot\frac{\Delta n(x,t)}{\Delta x}\right]\cdot\Delta t \end{aligned} \qquad \text{(A. 2)}$$

To prevent the term $v\cdot\frac{\Delta n(x,t)}{\Delta x}\cdot\Delta t$ to become larger than n(x,t), which is the case for large velocities, the time step (Δt) becomes: $\Delta t^{*} = \left|\frac{0.5\cdot\Delta x}{v}\right|$.

Force exerted by the contractile element is numerically determined based on eq. (3) over de range of bond lengths from x_{min} to x_{max}:

$$F(t) = \frac{m\cdot s\cdot k}{2\cdot l}\sum_{i=x_{min}}^{x_{max}} x_i\cdot n(x_i,t)\cdot\Delta x \qquad \text{(A. 3)}$$

The RCB-model is programmed in C-language and linked to MATLAB[2].

5.7. Appendix B

Force equilibrium of the linear spring, dashpot and the contractile element is determined by an iterative procedure where the following continuity conditions are valid at any t:

$$\begin{aligned} \ell &= \lambda_{CF} + \lambda_{S\&D} \\ v &= \dot{\lambda}_{CF} + \dot{\lambda}_{S\&D} \\ F_{CF}(\lambda_{CF}) &= F_{S\&D} = C\cdot\lambda_{S\&D} + D\cdot\dot{\lambda}_{S\&D} \end{aligned} \qquad \text{(B. 1)}$$

For description of symbols is referred to figure 5-1C, parameters C and D represent the elastic spring and dashpot respectively (table 5-1). To find the length of the spring and dashpot combination at the next time step($\lambda_{S\&D}(t+\Delta t)$) the root finding method of "Wijngaarden-

[2] MATLAB® is Copyright© of The Mathworks, Inc.

Dekker-Brent" is used (Press *et al.*, 1992). Therefore, $\dot{\lambda}_{CF}(t+\Delta t)$ is substituted for v in eq. A.2, a new cross-bridge distribution is determined, which results in a new F_{CE} (eq. A.3). Finally, the root ($\lambda_{S\&D}(t+\Delta t)$) is found, when the error (B. 2) is minimized.

$$error = \lambda_{S\&D}(t+\Delta t) - \frac{F_{CF}(t+\Delta t) - D\cdot\dot{\lambda}_{S\&D}(t+\Delta t)}{C} \qquad \text{(B. 2)}$$

Chapter 6

Acute Effects of Tenotomy, Aponeurotomy and Myotomy Modeled to Study Intramuscular Force Transmission in Skeletal Muscle

6.1. Abstract

The present study focuses on force transmission in a model of uni-pennate extensor digitorum longus of the rat. In addition, the role of the aponeurosis and shear stiffness are addressed. A distinction is made between myotendinous and myofascial force transmission, where force is transmitted from fibers to aponeurosis and from fibers in sideward direction, respectively. The two dimensional model is based on the finite element method. Surgical interventions such as tenotomy, aponeurotomy and myotomy are performed to study the effects on the force-length characteristic, fiber length, active fiber stress, shear stress and fiber strain. The interventions implicated removal at several locations of direct myotendinous connection to insertion of a considerable amount of muscle fibers. In addition is in two stages myofascial connection removed of sideward connected fibers.

After surgical intervention a considerable amount of the fibers had no direct myofascial connection to insertion but force decrease was only minor. The shortening of these fibers was small and not enough to explain the decrease in muscle force. The force decrease found is caused by a decrease in active fiber stress just distally of the invention in the intact part of the muscle as a result of high local fiber strain. The results indicated that up to 48% of the force exerted, was transmitted through myofascial pathways under specific conditions. Due to myofascial force transmission fibers without direct myotendinous connection to insertion are prevented to shorten much, and generate a substantial amount of active fiber stress. The force decrease found after interventions performed is strongly related to the amount of deformations. If muscle integrity is thoroughly disturbed by myotomy or by removal of a large part of the aponeurosis, the force reduction is significant. The results indicated that the role of the aponeurosis is besides transmitting force form fibers to origin and insertion, extended with the maintenance of muscle integrity in such a way that muscle is capable of producing optimal force. On the basis of the present results an explanation for the success of intramuscular aponeurotomy performed on spastic muscle is suggested.

6.2. Introduction

In a classical view of skeletal muscle, fibers are considered to transmit force, generated in the sarcomeres, to aponeuroses and through the tendons onto the bony structures. How force is transmitted from sarcomeres through fibers, aponeurosis and tendons is not fully understood. Myotendinous connections at the ends of muscle fibers are held responsible for the longitudinal force transmission to the tendinous tissue, i.e. the aponeuroses or tendons (e.g. Schippel and Reissig, 1968; Trotter, 1993).

Experimental observations on isolated muscle fibers (Street and Ramsey, 1965; Street, 1983) and on whole muscle (Huijing *et al.*, 1998) indicate that this classical view is over simplified (Huijing, 1998b). Moreover, Trotter (1990, 1993) found evidence of fibers with gradual tapered endings, which do not run from one tendon to the other tendon or aponeurosis. They suggested that force is transmitted from one fiber onto a neighboring fiber.

These studies indicate that force produced within muscle fibers is not only transmitted in longitudinal direction within the muscle fiber but also in sideward direction onto the intramuscular connective tissue. Such transmission has been referred to as myofascial force transmission (Huijing *et al.*, 1998; Huijing, 1998a). Force transmission in sideward direction between the intracellular elements and the extracellular space is made possible by transsarcolemmal connections (see review by Patel and Lieber, 1997).

The role of myofascial force transmission in muscle functioning is not fully understood, neither for intact muscle, nor for specific experimental conditions and surgical interventions such as tenotomy, aponeurotomy or myotomy. Despite such lack of detailed knowledge of these phenomena, surgical interventions such as intramuscular aponeurotomy (Bauman and Koch, 1989) are performed with success on spastic children for restoration of a more natural gait (e.g. Reimers, 1990; Barnes and Herring, 1991). More detailed knowledge about the mechanisms responsible for such results and their effects on muscle characteristics are highly desirable and a major goal of this study.

In an experimental approach access to muscle fibers is very limited and therefore detailed interpretation of results is severely hampered. The use of a model allows identification of the contributions of structures responsible for force transmission, without modeling every anatomical detail of muscle. Such an approach may be based on the Finite Element Method (FEM). This method showed its value in the study of mechanical properties in intact cardiac muscle (e.g. Huyghe, 1984; Horowitz et al, 1988; Hunter *et al.*, 1988; McCulloch *et al.*, 1992) as well as skeletal muscle (van der Linden *et al.*, 1998a). Therefore, is in the present study a model based on this method, used to model surgical and experimental interventions such as tenotomy, aponeurotomy and myotomy. Furthermore, the contribution of material properties, such as shear stiffness for muscle performance is studied under different conditions. The role of the aponeurosis for muscle integrity and characteristics is also considered. The effects of these interventions are studied by considering changes of force-length characteristics, fiber stress and

strain. The variety of conditions are compared to each other and to those of the model of intact muscle.

6.3. Method

6.3.1. FEM-skeletal muscle element

The muscle element used, representing muscle tissue in the model, is a modification of that presented by van der Linden *et al.* (1998a). Muscle tissue is modeled as a two-dimensional anisotropic and incompressible continuum with non-linear material properties. The total stress generated equals to the sum of active and passive stress. Active stress is developed only in fiber direction, if the muscle is activated. Active stress depends on strain of the muscle fiber (fig. 6-1). The active stress-strain curve is an exponential fit of the experimental data for mean sarcomere force-length characteristic of the rat gastrocnemius medialis (GM) (Zuurbier *et al.*, 1995). In the present study only passive and maximally activated muscles are studied.

Passive stress consists of two parts. The first part of the passive stress is defined by strain in directions in relation to the fiber orientation, i.e. along fibers (y), perpendicular to the fibers (x) and shear (xy) (fig. 6-1). Positive strain in fiber direction represents fiber lengthening. The second part yields the contribution of a penalty function. The penalty function depends on change of muscle element area compared to the initial area. In this way the constant volume of muscle (Swammerdam, 1737) is modeled in the present two-dimensional model. In the model, the mid-longitudinal area representing the muscle belly is assumed constant in accordance with to experimental observations (Zuurbier and Huijing, 1992).

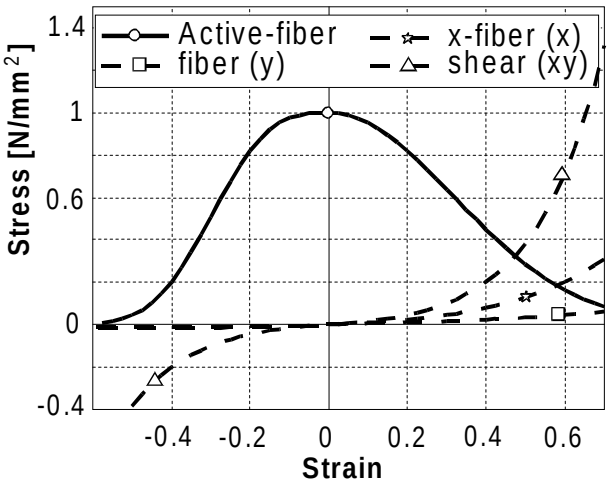

Figure 6-1 Stress-strain relationship

The passive and active stress-strain relationships of used by the model. Active fiber stress is only defined in the fiber direction (y), the curve is an exponential fit of the experimentally determined mean sarcomere force-length characteristic of the rat GM (Zuurbier *et al.*, 1995). Passive stress is defined in directions in reference to the fibers. Consequently, a component is defined in fiber direction (y), perpendicular to the fibers (x) and a component for shear (xy).

An important modification of muscle element characteristics compared to previous work (van der Linden *et al.*, 1998a) is the assumption that active fiber stress need not to be constant over the length of the fiber. In the present model the active fiber stress is dependent on the local fiber strain. The assumption that active stress is exerted only in the longitudinal direction is unaltered. If fiber stress is based on local strain a fiber bundle can be modeled as more muscle elements in series. This modification allows us to use length-width ratios for the muscle elements, which result in more liable

interpolations of element deformations. Consequently, local area of a fiber bundle is preserved, large deformations in a part of a fiber bundle are compensated for within this local part instead of somewhere else in the fiber bundle. With more elements is series the non-linear displacement function in fiber direction is simplified to a linear function, i.e. displacements of points between the nodes are linearly interpolated, to reduce the muscle element complexity: the muscle element is converted from a 6-nodal point element to a 4-nodal point element. The muscle element is programmed in FORTRAN and linked to the standard ANSYS[3] software as a user-defined element.

The tendinous structures, i.e. aponeuroses and tendons, are represented by tapered shape beam elements (BEAM54) from the standard ANSYS element library. These elements have linear material properties. The fact that they are tapered is used to decrease the normal stiffness, i.e. resistance against elongation, towards the end of the aponeurosis. Due to the nature of this element, it can resist compressive forces, which is not expected to occur in tendinous tissue. Compressive forces in the aponeurosis can be expected at low muscle length and will have a reducing effect on the total muscle force. It is assumed that these compressive forces will not affect the general results of the present study.

6.3.2. The EDL model

The rat extensor digitorum longus (EDL) is an unipennate muscle with a special morphology (Ballice-Gordon and Thompson, 1988). Rat EDL has 4 different muscle heads connected each by their own aponeurosis and distal tendon to one of the four digits of the rat foot (fig. 6-2). The numbers assigned to the digits (II, III, IV and V), to which the tendons are connected, indicate the muscle heads. Proximally the muscle heads have one collective aponeurosis as well

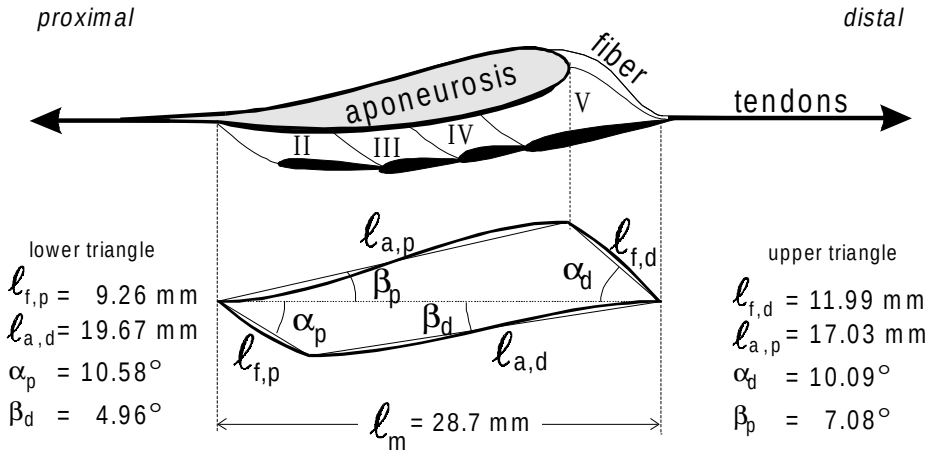

Figure 6-2 Extensor digitorum longus (EDL) muscle of the rat

Schematic representation of geometry of rat EDL, with the muscle heads connected to digits II to V of the rat hindlimb. In bottom panel are indicated the linearized length of proximal and distal aponeurosis and fibers and total muscle belly length.

[3] ANSYS © revision 5.3 (1996) is a FEM program of Swanson Analysis Systems Inc. (SASI) under an ANSYS

as one proximal tendon. The muscle heads are not equal in size, their relative mass as determined experimentally is shown in Table 6-1 (Huijing *et al.*, 1998). These values are reasonable estimates for the respective physiological cross-sectional areas (A_f) of the heads. In a rat EDL the tendons of the different muscle heads are arranged in parallel. It is assumed that the strain in the EDL tendons is constant. The four separate tendons are modeled by one continuous distal aponeurosis. Increasing the normal stiffness of the beam-elements (representing the aponeurosis) from proximal to distal end preserves a constant strain of this aponeurosis. In this way is compensated for the removal of the separate tendons.

Linearized muscle-tendon complex geometry of the mid-longitudinal area of EDL (fig. 6-3A) is modeled according to a pilot study for the work presented in Huijing *et al.* (1998). The lengths and angles of the linearized muscle geometry are shown in figure 6-2. The curved aponeuroses are described by splines with a zero angle with line of pull of the muscle at both ends. Initially the fibers have a distributed length range from 9.3 mm for the proximal fiber to 12 mm for the distal fiber and all fibers are modeled initially as straight lines. This initial distribution in fiber length is referred as a primary fiber length distribution (Huijing, 1995). The stress-strain properties of all fibers are assumed identical. Zero fiber strain corresponds to fiber optimum length. Consequently the short (proximal) fibers have fewer but identical sarcomeres arranged in series compared to the longer distal fibers. The muscle belly is constructed of 51 muscle elements, in 3 elements arranged in series, representing a small bundle of muscle fibers. 17 of those groups of elements are arranged in parallel (fig. 6-3A). The relative number of muscle elements arranged in parallel per muscle head, is a measure for the cross-sectional area (Table 6-1&2).

As force is transmitted in sideward direction, it is difficult to identify the contribution to the total force. However, for tenotomy, aponeurotomy and myotomy conditions, an estimate of a minimal value can be made. The enhancements in force found ($\Delta F_{MF,min}$), compared the expected force based on the physiological cross sectional area (A_f) with direct myotendinous connection, is attributed to myofascial transmitted force (eq. 1). Therefore, the force (F_{mao}) produced at muscle optimum length (ℓ_{mao}) is compared to A_f with a direct myotendinous connection to the tendons under several conditions. The minimal relative contribution of the myofascial force to the total force in a specific condition, is thus estimated as follows:

$$\left(\Delta F_{MF,\min}\right)_{condition} = \left(\frac{\frac{F_{mao,condition}}{F_{mao,\text{int act}}} - \frac{A_{f,condition}}{A_{f,\text{int act}}}}{\frac{F_{mao,condition}}{F_{mao,\text{int act}}}} \right) \cdot 100\% = \left[1 - \left(\frac{A_f}{F_{mao}} \right)_{condition} \cdot \left(\frac{F_{mao}}{A_f} \right)_{\text{int act}} \right] \cdot 100\% \qquad (1)$$

Where:
- $F_{mao,intact}$: force at muscle optimum length of the intact model
- $F_{mao,condition}$: force at muscle optimum length under a specific conditions
- $A_{f,intact}$: cross-sectional area of the whole intact muscle
- $A_{f,condition}$: cross-sectional area with direct myotendinous condition to origin and insertion of the muscle

For comparison of experimental and model data, A_f is represented by mass of the rat EDL muscle heads determined in the experiments (Table 6-1) and in the model A_f is represented by the number of elements arranged in parallel per muscle head (Table 6-2).

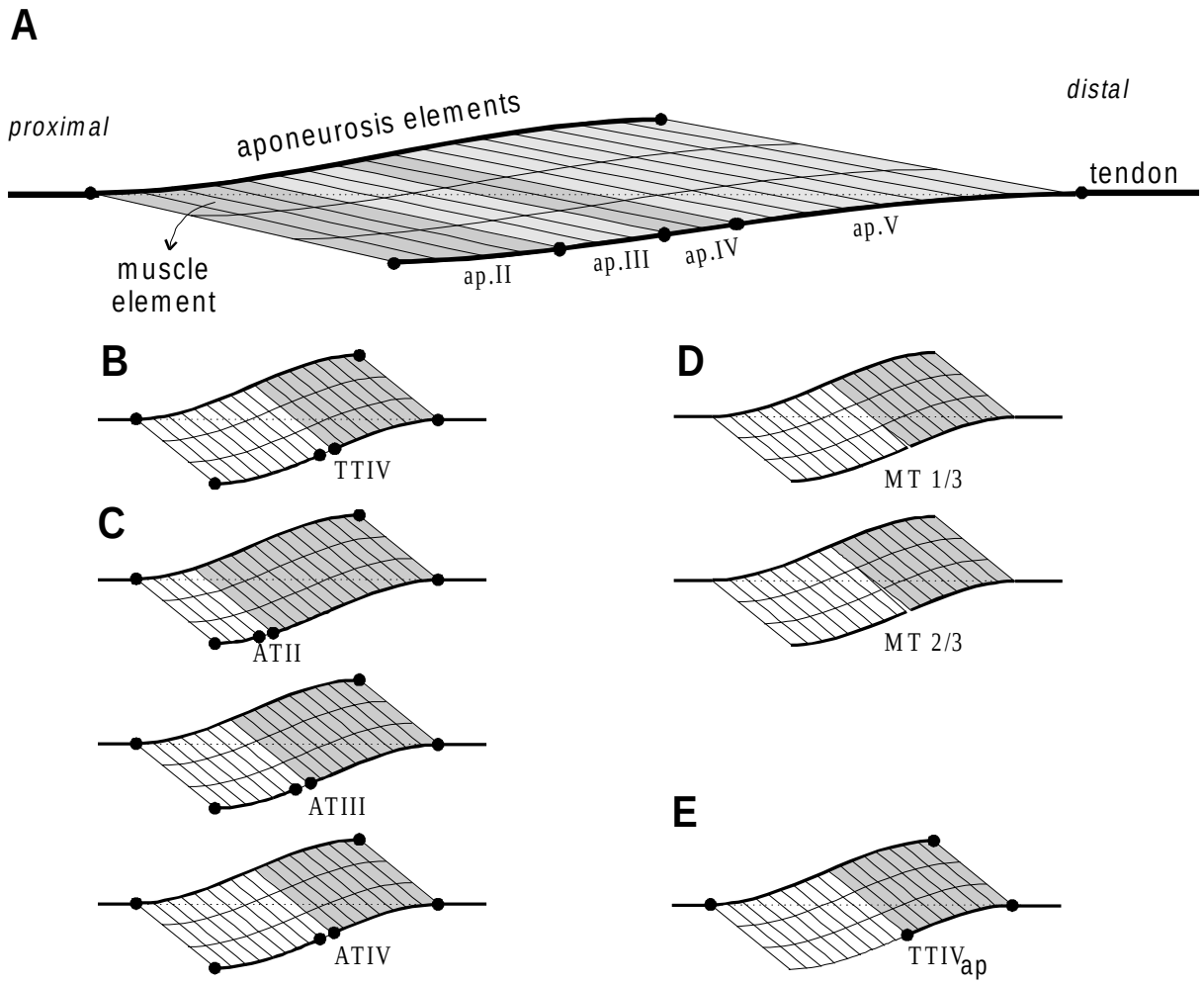

Figure 6-3 Model of rat EDL

A. Finite element mesh of rat EDL in 2D, with the aponeurosis and muscle elements as well as the location of the separate aponeurosis of the muscle heads ap.II, ap.III, ap.IV and ap.V indicated . The distinction made for muscle heads II to V in gray scales is only for clarity reasons. **B.** Schematic representation of tenotomy IV as performed to the model (TTIV), by removing one aponeurosis element. The gray area indicates the A_f of the muscle that has direct myotendinous connection to both tendons. The white area has no direct myotendinous connection to the distal tendon. **C.** Aponeurotomy at the location of heads II, III and IV performed to the model, by removing one aponeurosis element (ATII, ATIII and ATIV). **D.** Two phases of myotomy performed to the model between muscle head IV and V, under condition MT1/3 one element of these heads is sideward disconnected, in contrast with MT2/3 where two elements are disconnected. The aponeurosis of the disconnected heads is left intact. **E.** Aponeurotomy at the location of head IV ($ATIV_{ap}$) performed by removing all aponeurosis elements of the heads II, III and IV.

Table 6-1 Rat EDL data

	EDL mass [%]	EDL F_{mao}	$\Delta F_{MF,min}$ [%]	$\Delta \ell_{mao}$ [mm]
Intact	100	100	0	
TTII	77	99	22	0.3
TTIII	60	92	35	1.0
TTVI	45	84	46	1.6
MT1/3	45	67	33	3.4
MT2/3	45	52	14	5.3

Experimental data of rat EDL (Huijing *et al.*, 1998). For each condition the amount of mass with a direct myotendious connection to origin and insertion, the force at ℓ_{mao}, the minimal amount attribute to myofascial force transmission according eq. 1. In the last column is the shift of ℓ_{mao} indicated.

6.3.3. Tenotomy

Tenotomy (TTIV) is modeled by removing the most distal aponeurosis element of a muscle head IV (fig. 6-3B). Consequently no force is transmitted from the disconnected aponeurosis of heads II, III and IV to the intact head V and the distal tendon. Only muscle fibers of head V have a direct myotendinous connection to origin and insertion of the muscle. The aponeurosis of head V is left intact. Fibers without a direct myotendinous connection to muscle insertion (heads II, III and IV) can only contribute to muscle force, if force is transmitted in sideward direction by the connective tissue. This simplification of tenotomy is based on the assumption that the effects of only one element of the disconnected aponeurosis are negligible.

6.3.4. Aponeurotomy

The distal aponeurosis of the model EDL is continuous and is therefore suitable for performing aponeurotomy at different locations. For convenience these locations are chosen such that they match the interfaces of the identified muscle heads of EDL. In fact this is model of an imaginary muscle with geometry of the rat EDL. Aponeurotomy implies cutting the aponeurosis and is modeled by removing a aponeurosis element as is done for tenotomy. Aponeurotomy applied to the several locations (ATII, ATIII and ATIV) is shown in figure 6-3C. The condition of aponeurotomy at location IV is in fact identical to modeled tenotomy of head IV.

6.3.5. Myotomy

One of the acute effects of stretch and activation after aponeurotomy is progressive tearing of muscle connective tissue along the direction of the fibers at the location where the aponeurosis is cut (Brunner *et al.*, 1998). The present model is used to study two phases of the rupture. First, the rupture is modeled with a depth of one-third of the fiber length. A rupture with a depth of two-thirds of local fiber length models the second phase of myotomy. Myotomy is applied at the interface between heads IV and V by sideward disconnecting muscle elements

arranged in parallel. Myotomy is modeled in the first phase by disconnecting sideward one element and in the second phase two elements in series are disconnected (fig. 6-3D). Consequently, no force can be transmitted from the aponeurosis of heads II, III and IV to the intact aponeurosis of head V. Furthermore, over a considerable length, is sideward connection of fibers and thus myofascial force transmission between heads IV and V removed.

6.3.6. Shear stiffness

The ability of transmitting force in sideward direction is attributed (e.g., Street, 1983; Trotter, Richmond and Purslow, 1995; Huijing, 1998a) to the resistance against shear. The present model allows studying the effects of reduced shear stiffness of muscle tissue on the force-length characteristics and the contribution of myofascial force transmission. Aponeurotomy is applied at the location of head IV to the model with a 50% reduced shear stiffness ($ATIV_{½S}$) compared to the original model.

6.3.7. Role of the aponeurosis

After aponeurotomy is applied, the remaining but disconnected part of the aponeurosis may seem without function if it is considered as an elastic structure arranged at an angle with the muscle fibers. To test if this is the case, we removed all aponeurosis elements of muscle heads II, III and IV following aponeurotomy IV ($ATIV_{ap}$, see fig. 6-3E) and determined the effects on force-length characteristics, fiber stress and strain.

We determined force-length characteristics of passive and active muscle for each modeled intervention. The total and passive force-length characteristics are fitted with 4^{th}-order polynomial functions, and subtracted to obtain an estimate of the active force-length curve. Though this procedure is commonly accepted particularly in an experimental context, an error is made. Due to different muscle geometry under passive and active conditions at the same muscle length, the contribution of the total passive stress to muscle force is different in passive and active muscle.

Under all active conditions all fibers, i.e. muscle elements are uniformly activated, the maximal fiber stress is unity. Depending on their length, fibers have an active fiber stress in the range from 0 to 1. Local fiber active stress, strain and shear stress are presented in the deformed mesh of the muscle in 9 intervals of gray scales. A dashed line indicates the contour of the undeformed mesh. For reasons of comparison is chosen to present these values in a limited range. If a value in a specific condition is out of the range defined, the maximal or minimal value is presented separately in the figure.

The lengths of 17 fibers spread equally distanced over the muscle belly are determined based on the lengths of three muscle elements arranged in series. For reasons of comparison only the length changes of fibers are presented with respect to their initial length, i.e. optimal length.

Table 6-1 EDL model data

	# elements	A_f [%]	F_{mao} [N]	F_{mao} [%]	$\Delta F_{MF,min}$ [%]	$\Delta \ell_{mao}$ [mm]
Intact	17	100	2.4	100		
ATII	13	77	2.2	95	20	-0.1
ATIII	10	59	2.1	92	36	0
TTVI / ATVI	8	47	2.1	90	48	0.1
MT1/3	8	47	1.6	68	31	1.7
MT2/3	8	47	1.1	47	0	-0.5
$ATIV_{ap}$	8	47	1.6	70	33	-0.5
$ATVI_{½S}$	8	47	2.0	86	46	0

For each condition the number of muscle elements arranged in parallel with a direct myotendious connection to origin and insertion, the relative cross-sectional area corresponding to the number of elements in the previous column, the force at ℓ_{mao}, the relative F_{mao}, the minimal amount attribute to myofascial force transmission according eq. 1. In the last column is the shift of ℓ_{mao} indicated.

6.4. Results

6.4.1. Model of intact EDL

Figure 6-4 shows model results for the intact muscle. These results will be used below as reference for comparison for the surgical interventions modeled. In agreement with common practice in myology, force-length characteristics (fig. 6-4A) are presented as passive force and active force. The length at which the muscle exerts optimal force (F_{mao}) is identified by muscle active optimum length (ℓ_{mao}).

The modeled primary fiber length distribution, results in a larger active fiber length range for the most proximal fibers (-27% to +20%, for ℓ_{mao}-4 to ℓ_{mao}+2) compared to the active length range of the most distal fibers (-23% to +15%, for ℓ_{mao}-4 to ℓ_{mao}+2) (not shown). On activation, the primary fiber length distribution is modified in a secondary fiber length distribution (Huijing, 1995) (fig. 6-4B), due to bulging of the fibers (van der Linden *et al.*, 1995). At $\ell_{mao,}$ the maximal difference in active fiber length is 3% of the fiber's initial length (see also fig. 6-5B, right panel). That at ℓ_{mao} the secondary fiber length distribution is symmetrical with respect to the central fiber, suggests that though initially the fiber have distributed lengths, the same pattern in the secondary distribution is found as was observed for initial homogeneous muscle (van der Linden *et al.*, 1998). The different active length ranges of the fibers found, suggests that the active length range of sarcomeres of the short proximal fibers is larger compared to length range of sarcomeres in the distal fiber, which are larger in number.

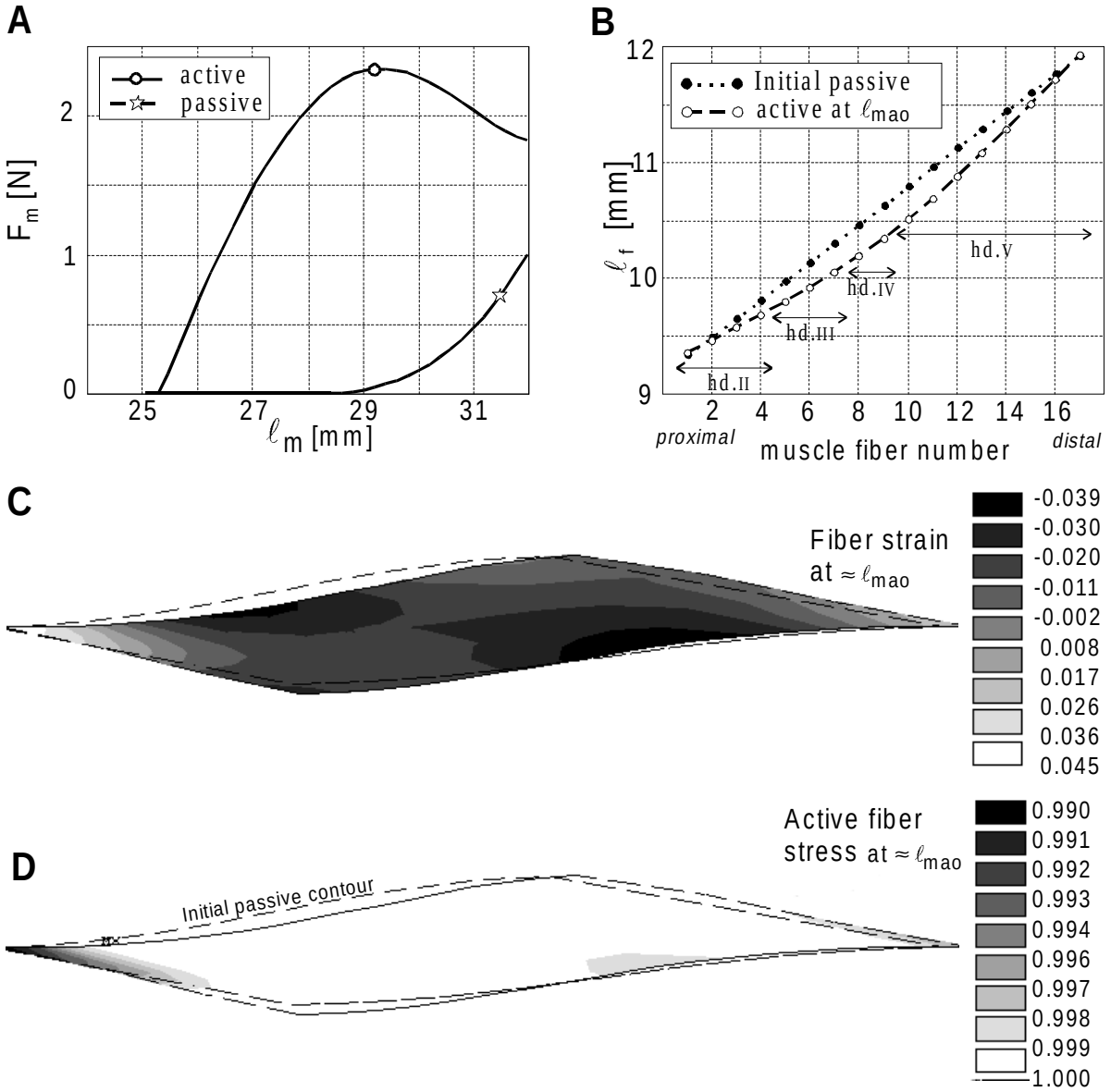

Figure 6-4 Model results of the intact EDL **A.** The active and passive muscle force length characteristic. **B.** The lengths (ℓ_f) of 17 fibers spread equally distanced from proximal to distal over the muscle heads (hd.II, hd.III, hd.IV and hd.V) in their initial passive condition and at active muscle optimum length (ℓ_{mao}). Note the primary and the secondary fiber length distribution. **C.** The local fiber strain plotted in the deformed mesh of the active model at ℓ_{mao}. The initial passive contour is indicated with a dashed line. The strain is presented in 9 ranges of gray scales. Negative strain represents local shorter fiber, i.e. sarcomeres. **D.** The active fiber stress corresponding to the local fiber strain of figure C. The small strain differences near zero strain and the plateau of the active stress-strain relationship (fig. 6-1) result in a nearly homogeneous active fiber stress. In most parts of the muscle the active stress is between 99.9 and 100% of the active stress, indicated in white.

Local fiber strain at ℓ_{mao} is imaged in figure 6-4C. This figure shows that a distribution of lengths of sarcomeres in series within muscle fibers is found. This suggests that force generated in sarcomeres is transmitted not only from sarcomere to sarcomere but also in sideward

direction (myofascial force transmission). However it should be noted that, at ℓ_{mao}, the combined effects of the secondary fiber length distribution and length distribution of sarcomeres in series are relatively small, so that the active stress deviates less than 1% of the optimal active stress (fig. 6-4D). In most sarcomeres an active fiber stress larger than 99.9% of the maximal active stress (white color).

6.4.2. Effects of tenotomy

By tenotomy of head IV (TTIV) the direct tendinous connections of nearly 55% of the muscle fibers to the insertion of the muscle is removed. Compared to the intact condition, the geometry of the active muscle at ℓ_{mao} is not affected much as a result of tenotomy IV (fig. 6-5E&F). The effect of TTIV on muscle force-length characteristics is shown in figure 6-5A. Optimum force (F_{mao}) is decreased by only 10% compared to the intact condition. Thus F_{mao} is 48% higher than expected from the muscle mass that has direct myotendinous connections with both proximal and distal tendons (Table 6-2). This 'extra' force can only reach the distal tendon by myofascial force transmission and thus represents the minimal amount that can be attributed to this type of transmission. Tenotomy IV did not lead to a change of ℓ_{mao}. In contrast, muscle active slack length (ℓ_{mas}) shifted to lower lengths. This can be explained on the basis of changes in fiber length. The relative length changes of 17 fibers spread equally over the whole muscle belly with respect to their initial length, is plotted in figure 6-5B. Near $\ell_{mas,}$ the fibers of head II, III and IV, have higher lengths compared to the intact condition.

Consequently a higher force is exerted at low muscle length. Near ℓ_{mao} (i.e. 29.3 mm) the length of fibers of head II, III and IV is 6% shorter compared to their lengths in the intact muscle. This means that these fibers are prevented from shortening and still contribute a considerable amount of force to the total muscle force. Note that, despite the difference in fiber lengths, the secondary distribution of lengths within these heads (II, III and IV) shows a pattern similar to that found in the intact muscle (parallel curves): at ℓ_{mao}, the most proximal fiber (# 1)

Figure 6-5 Modeled effects of tenotomy on EDL muscle (TTIV) **A.** The active and passive muscle force exerted normalized for F_{mao} of intact muscle after tenotomy of head IV (TTIV) compared to the intact EDL. Note that optimum force is decreased by 10%. **B.** The difference in length of 17 selected fibers compared to their initial length ($\Delta\ell_{fa}$), at muscle lengths near ℓ_{mas} and ℓ_{mao}. The length of both modeled conditions is identical: 25.6 and 29.3 mm. The relative F_{mao} exerted at these lengths is presented in the legend. The location of intervention is indicated with a gray bar (TTIV). Note that in the proximal part (fiber nr 1 to 8) a distribution of fiber lengths is developed. **C.** The active fiber stress near ℓ_{mao} (ℓ_m = 29.3 mm) plotted in the deformed mesh under intact condition is indicated in gray scales from 0.6 to 1. The initial passive contour is indicated with a dashed line. Due to the limited range (95 - 100%) differences in active fiber stress shown in figure 6-3D are not visible. **D.** Active fiber stress after tenotomy. The locations of intervention are indicated with an arrow head. **E.** The local fiber strain presented in the deformed mesh after TTIV. One fiber is indicated by a dashed line in the intact part of the muscle. The different gray scales along this fiber show a strain distribution which indicate short sarcomeres at the proximal end to long sarcomeres at the distal end near the location of intervention.

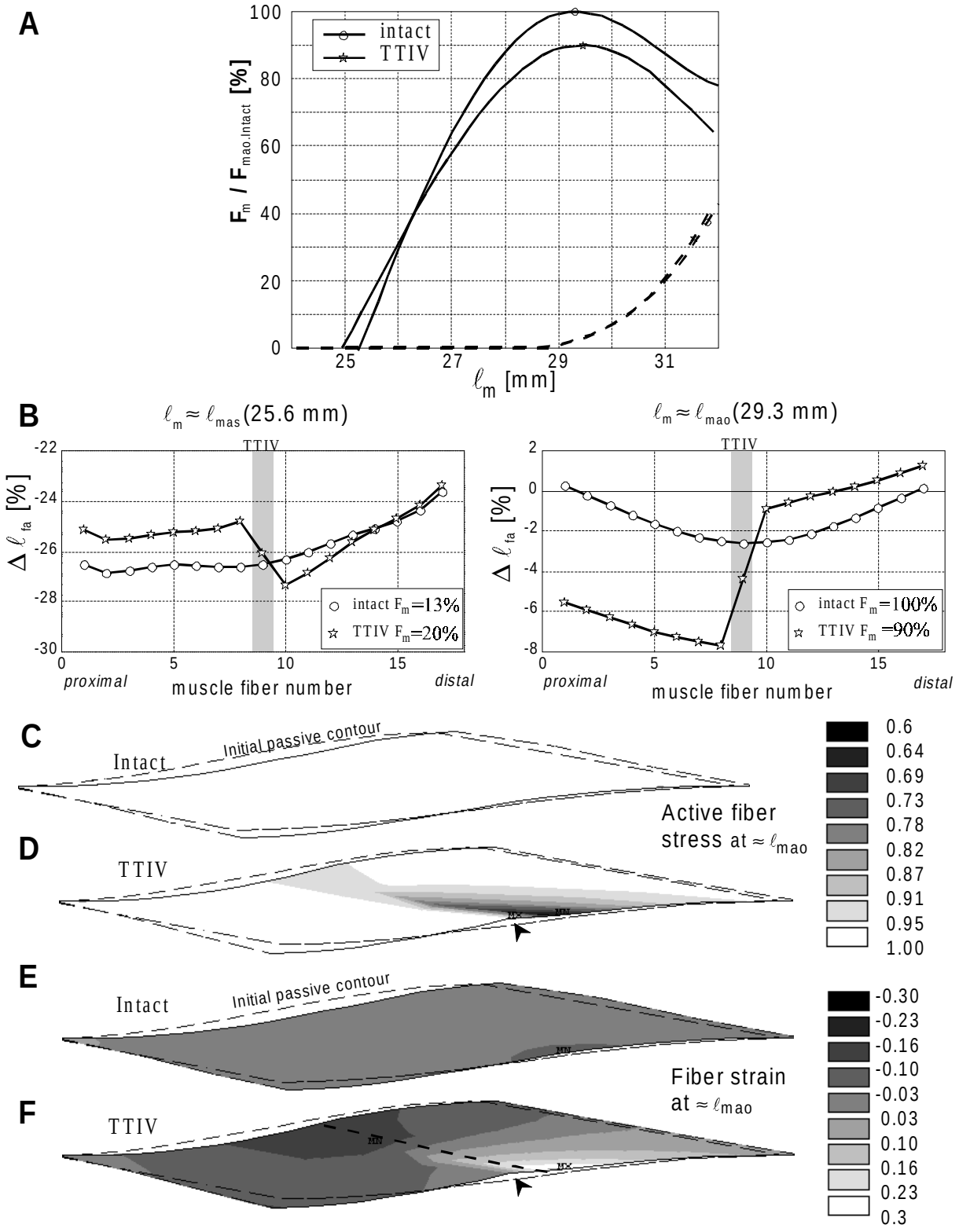
A
intact
TTIV
F_m / $F_{mao.Intact}$ [%]
ℓ_m [mm]
B
$\ell_m \approx \ell_{mas}$ (25.6 mm)
$\ell_m \approx \ell_{mao}$ (29.3 mm)
TTIV
$\Delta \ell_{fa}$ [%]
intact F_m=13%
TTIV F_m=20%
intact F_m=100%
TTIV F_m =90%
proximal
distal
muscle fiber number
C
Intact
Initial passive contour
Active fiber stress at $\approx \ell_{mao}$
D
TTIV
E
Intact
Initial passive contour
Fiber strain at $\approx \ell_{mao}$
F
TTIV
0.6
0.64
0.69
0.73
0.78
0.82
0.87
0.91
0.95
1.00
-0.30
-0.23
-0.16
-0.10
-0.03
0.03
0.10
0.16
0.23
0.3

Figure 6-5

is 2% longer compared to the most distal fiber of head IV (# 8) (fig. 6-5B). Note that the fibers of head V distal to the location of intervention are approximately 1% longer than in the intact muscle. These results regarding fiber lengths account for a reduction of muscle force by only 2% compared to the intact condition, leaving 80% of decrease of optimum force to be explained.

If active fiber stress is imaged within the deformed muscle contour, additional effects of tenotomy become clear (fig. 6-5D): Tenotomy causes a substantial reduction of the active fiber stress within the intact part of the muscle (head V). The minimal active stress expressed, as fraction (0.7) of stress in the intact condition (fig. 6-5C) is located just *distally* of the location of intervention (indicated by the arrowhead, fig. 6-5D). Note that this highest decrease in active muscle fiber stress is found predominantly at the distal end of the fibers. The reduced active stress found at this location is a result of an increased local fiber strain there (fig. 6-5F).

A compensating shortening at the proximal end of these fibers causes the fact that the total length of fibers, near the location of intervention, is not increased. See for example the strain along one fiber, indicated by a dashed line in fig. 6-5F: Proximally the relative fiber strain is -0.20 and distally it is +0.3. Furthermore, it should be noted that after TTIV the local fiber strain in a large area of the muscle is decreased from a range {-0.03 .. 0.03} in the intact condition to {-0.1 .. -0.03} (fig. 6-5F). This is an indication that a large amount of sarcomeres have a lower length. However, within the proximal half of the muscle (head II through IV) any deviation from the intact condition is very small (fig. 6-5D, active stress 0.95 - 1.0, white color).

It is concluded that myofascial force transmission prevents the proximal fibers to shorten and allow them to contribute very substantially to the total muscle force. The small decrease in muscle force found, is caused predominantly by a localized increase of sarcomere lengths just distally of the location of intervention, thus in the intact part of the muscle.

Figure 6-6 Modeled effects of aponeurotomy on EDL muscle **A.** Normalized muscle force-length characteristics after aponeurotomy applied to three locations (ATII, ATIII and ATIV) at the distal aponeurosis compared to the intact condition. Note, the more the intervention is located to the distal side of the aponeurosis, the more F_{mao} is reduced. **B.** The difference in length of 17 selected fibers compared to their initial length ($\Delta\ell_{fa}$), at muscle lengths near ℓ_{mas} and ℓ_{mao}. The length of both modeled conditions is identical: 25.6 and 29.3 mm. The relative F_{mao} exerted at these lengths is presented in the legend. The location of intervention is indicated with a gray bar (ATII, ATIII and ATIV). **C.** The active fiber stress near ℓ_{mao} (ℓ_m = 29.3 mm) plotted in the deformed mesh under intact condition is indicated in gray scales from 0.6 to 1. The initial passive contour is indicated with a dashed line. **D.** Active fiber stress after ATII: a reduction is found locally on the distal side of the intervention. The locations of intervention are indicated with an arrow head. **E.** Active fiber stress after ATIII. Note, the reduction found locally on the distal side of the intervention is increased compared to ATII. **F.** Active fiber stress after ATIV. Note the reduction found locally on the distal side of the intervention is increased compared to ATIII, in combination with the increase of area with reduced stress.

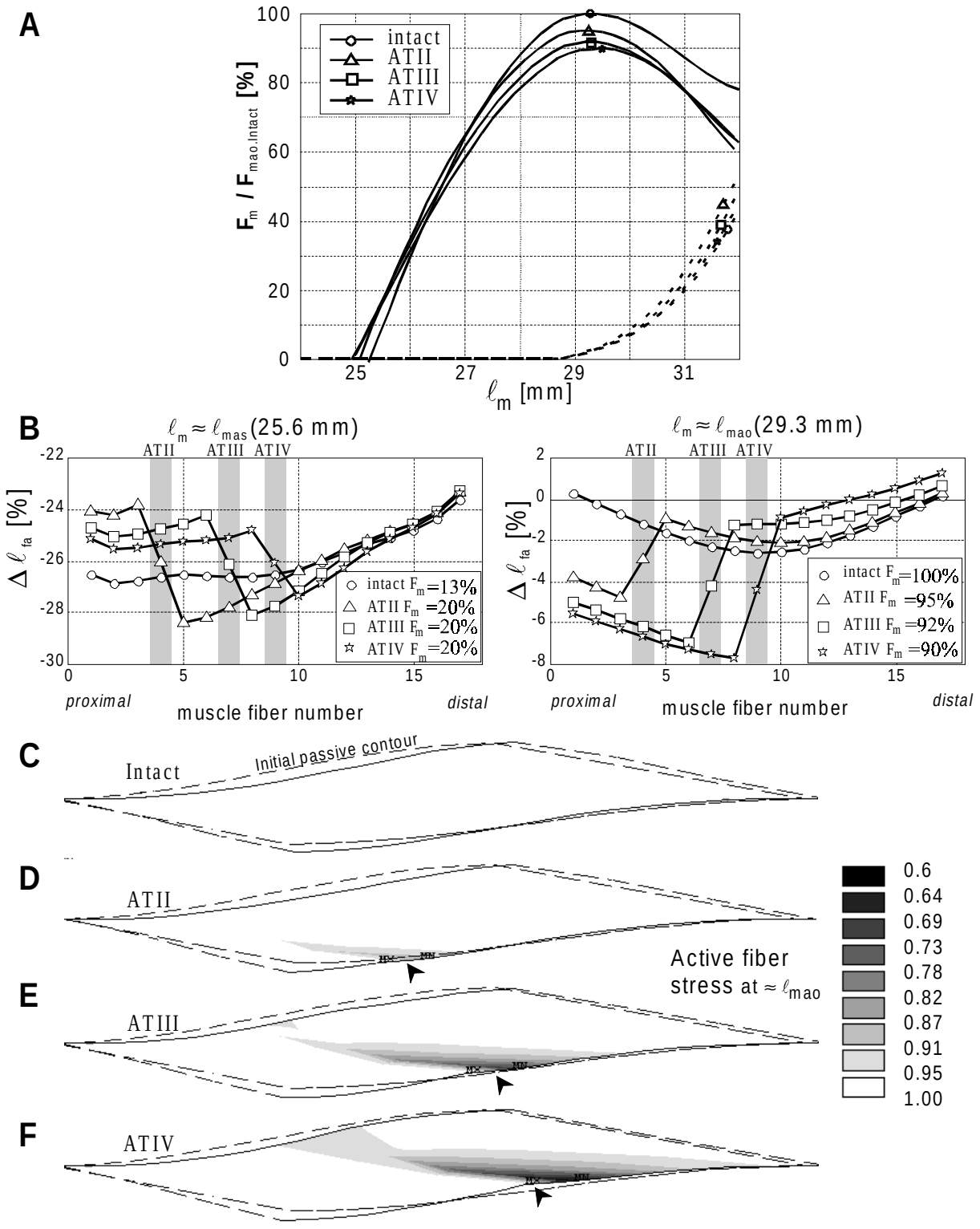
A
intact
ATII
ATIII
ATIV
F_m / $F_{mao.Intact}$ [%]
ℓ_m [mm]
B
$\ell_m \approx \ell_{mas}$ (25.6 mm)
$\ell_m \approx \ell_{mao}$ (29.3 mm)
ATII ATIII ATIV
$\Delta \ell_{fa}$ [%]
intact F_m=13%
ATII F_m =20%
ATIII F_m =20%
ATIV F_m =20%
intact F_m=100%
ATII F_m =95%
ATIII F_m =92%
ATIV F_m =90%
proximal
muscle fiber number
distal
C
Intact
Initial passive contour
D
ATII
E
ATIII
F
ATIV
Active fiber stress at $\approx \ell_{mao}$
0.6
0.64
0.69
0.73
0.78
0.82
0.87
0.91
0.95
1.00

Figure 6-6

6.4.3. Effects of aponeurotomy per se

Aponeurotomy performed in experimental setting has as a secondary consequence: tearing of the muscle along the direction of the muscle fibers below the location of aponeurotomy. The model allows to study the isolated effects of aponeurotomy.

At three different locations on the distal aponeurosis, aponeurotomy is modeled (ATII, ATIII and ATIV). If the intervention is located more to the distal end of aponeurosis, an increasing number of fibers (23, 41 and 53 % for ATII, ATIII and ATIV respectively) is no longer connected directly to the distal tendon. Despite that fact, the reduction in optimum force (F_{mao}) compared to that of the intact muscle is only minor: 5, 8 and 10 % respectively (fig. 6-6A). At ℓ_{mao}, the minimal force that can be attributed to myofascial force transmission is 20, 36 and 48% for ATII, ATIII and ATIV respectively (table 6-2). Only a small shift in ℓ_{mao} is found (table 6-2). The shift of ℓ_{mas} to lower muscle lengths is similar for all aponeurotomy locations and is explained by the fact that the proximal fibers attain a higher length for low muscle lengths (fig 6B, left panel).

At ℓ_{mao}, the fibers attached to the disconnected aponeurosis are somewhat shorter than they were in the intact muscle at that length, and those within the intact parts of the muscle somewhat longer (Figure 6-6B, right panel). Between conditions ATII, ATIII and ATIV , differences in length of these fibers are small (0-2%), but the number of fibers with a lower length increases progressively with a more distal location of intervention (i.e. ATIII, ATIV). These results for fiber length can explain a reduction in optimum force after aponeurotomy by 1-2% only, leaving 80-90% of the decrease in force to be explained.

The plots of the active fiber stress (fig. 6-6C to F) reveal that the area with lower local active stress is increasing with a more distal location of the intervention. These areas are always located just distal to the location of aponeurotomy. The minimal active stress in the muscle fiber direction decreases from 0.86 for ATII to 0.6 for ATIV. Note that just proximal to the location of intervention active fiber stress is not decreased by more than 5%. This creates a very high gradient of stress across the intramuscular interface of heads.

Due to the local decrease in active fiber stress as well as the increase of the area with lower active stress, less force is exerted by the muscle after aponeurotomy. If aponeurotomy is modeled at a more distal location, the decrease in force augmented. This is due to an increase in a small deformation of the muscle at the location of the intervention. For ℓ_{mao}, this is visualized in figure 6-6C to F, by comparing the deformation of the muscle as a result of ATII, ATIII and ATIV in relation to the initial passive contour (dashed lines).

It is concluded that fibers attached to a disconnected aponeurosis are prevented from shortening substantially and are contributing considerably to the muscle force. The main part of the reduction in force after aponeurotomy is caused by local deformation of the muscle just distal to the location of intervention in the intact muscle parts.

6.4.4. Effects of myotomy

The tearing a of the muscle along the direction of the muscle fibers seen in experiments and patients' muscles below the location of aponeurotomy was modeled as myotomy in the present model. Myotomy was performed on the model muscle for 1/3 and 2/3 along the length of the fibers at the interface head IV and V.

Effects of myotomy on force length characteristics are shown in figure 6-7A. Optimal muscle force (F_{mao}) is decreased by 32 and 53% for conditions with one and two muscle elements disconnected sideward, respectively. For both conditions this force is produced with only 47% of the muscle volume connected directly to the origin and insertion of the muscle. At muscle lengths over ℓ_{mao} of the intact muscle, passive force is reduced considerable compared to that of the intact muscle. The gap developed between heads IV and V allows muscle lengthening to be accompanied by a much reduced increase in passive force. The shift of ℓ_{mao} to higher length after MT1/3 is caused by the operation of proximal fibers near their optimum fiber length at higher muscle length. Consequently, at a higher muscle length F_{mao} is reached.

At ℓ_{mao}, the *minimal* fraction of force that can be attributed to myofascial force transmission is reduced to 31% and 1% for MT1/3 and MT2/3 respectively. However this should *not* be taken as a suggestion that, in the MT2/3 condition, the contribution to muscle force by the fibers proximal to the myotomy without a direct tendinous connection to distal tendon, has nearly disappeared. It merely indicates that muscle force has dropped close to values expected on the basis of cross-sectional area. Figure 6-7C still shows that for those proximal fibers considerable active stress in the fiber direction is found. Therefore, the decrease of force is the net result of two opposing effects: (1) a decreased contribution of the intact distal part and (2) a remaining contribution (albeit much decreased compared to ATIV and MT1/3 conditions) via myofascial force transmission by the proximal muscle fibers of approximately absolute value. A rough estimate of this absolute value was obtained by integration of active fiber stress on the basis of gray scales. This estimate indicates that the force produced by the intact muscle part is reduced by about 10% of the force expected from physiological cross-sectional area. Therefore it is concluded that maximal force compensated for by contributions from the proximal part via myofascial force transmission less than 10% for this condition. It is concluded that myofascial force transmission is dependent on the length of intact interface between muscle fibers and is limited to a value between 1 and 10% in the MT2/3 condition.

A general feature of a myotomized or torn muscle is a shift of muscle mass away form the line of pull (e.g. see muscle contours of fig. 6-8E) to allow the line of pull to pass through the remaining intact segment of the interface of muscle parts. As a consequence, in the distal part of the muscle, fiber angles and aponeurosis angles with the line of pull are decreased at any muscle length. In the proximal muscle part this is also true for the aponeurosis angle but muscle fiber angle is not lowered.

The effects of myotomy on the fiber lengths are more pronounced compared to those of aponeurotomy (ATIV) (compare fig. 6-7B and fig. 6-6B). The length range of the active

proximal fibers is decreased dramatically but remained well above zero: For example in the MT1/3 condition the active fiber length range encompasses values of -15% (of the initial fiber length) at high muscle length (ℓ_m = 31 mm, not shown) and -25% at ℓ_{mas}. Note that, if the modeled rupture is twice as deep (MT2/3 condition), the active fibers of the proximal muscle part without direct myotendinous connection to the distal tendon, remain at a nearly constant length (of approximately -26% of their initial length, compare fig. 6-7B for $\Delta\ell_{fa}$ at ℓ_{mas} and ℓ_{mao}) for this muscle length range. However, at higher muscle lengths (not shown) a small increase of lengths of proximal fibers was seen. This is an independent indication of the occurrence of some myofascial force transfer even in this condition at higher muscle lengths.

At low muscle lengths the fibers of the proximal muscle part have higher lengths compared to their length in the intact muscle, consequently ℓ_{mas} shifts to lower muscle length. Maximal local fiber strain in the fiber direction at ℓ_{mao} is limited to -0.3% (Fig. 6-7F).

Figure 6-7 Modeled effects of myotomy on EDL muscle **A.** Normalized muscle force-length characteristics of myotomized EDL model at the interface of head IV and V in depths: 1/3 and 2/3 of the fiber length (MT1/3 and MT2/3) compared to ATIV and the intact condition. The development of the gap between heads IV and V allows muscle lengthening with a reduced increase in passive tension. **B.** The difference in length of 17 selected fibers compared to their initial length ($\Delta\ell_{fa}$), at muscle lengths near ℓ_{mas} and ℓ_{mao}. The length of both modeled conditions is identical: 25.6 and 29.3 mm. The relative F_{mao} exerted at these lengths is presented in the legend. The location of intervention is indicated with a dashed line (MT). Note that MT1/3 in not near ℓ_{mao} at this length (fig. 6-A). **C.** The active fiber stress near ℓ_{mao} (ℓ_m = 29.3 mm) plotted in the deformed mesh under intact condition is indicated in gray scales from 0.6 to 1. The initial passive contour is indicated with a dashed line. **D.** The active fiber stress after MT1/3. In general the location of maximal (MX) and minimal (MN) active stresses are indicated, if these values exceed the color range in the legend, these are mentioned separately. **E.** The active fiber stress after MT2/3. Note, the original location of the modeled rupture is closed, after activation a gap is developed. **F.** Local fiber strain after MT2/3 in deformed muscle mesh. Note, a reduced length of sarcomeres in the proximal muscle half and sarcomeres with an increased length is found distally of the rupture.

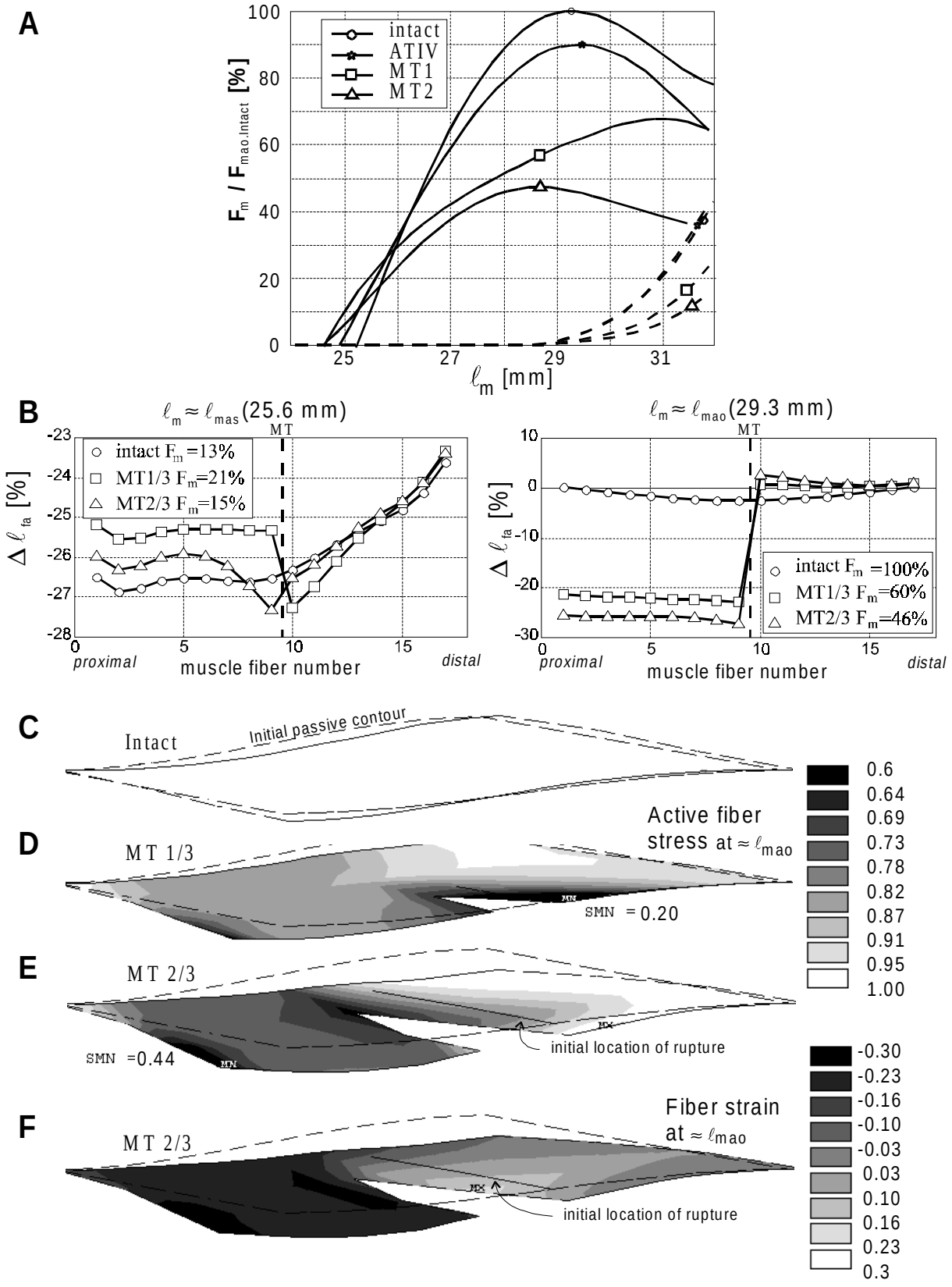
A
intact
ATIV
MT1
MT2
$F_m / F_{mao.Intact}$ [%]
ℓ_m [mm]
B
$\ell_m \approx \ell_{mas}$ (25.6 mm)
$\ell_m \approx \ell_{mao}$ (29.3 mm)
MT
intact F_m =13%
MT1/3 F_m=21%
MT2/3 F_m=15%
intact F_m =100%
MT1/3 F_m=60%
MT2/3 F_m=46%
$\Delta \ell_{fa}$ [%]
proximal
distal
muscle fiber number
C
Intact
Initial passive contour
Active fiber stress at $\approx \ell_{mao}$
D
MT 1/3
SMN = 0.20
E
MT 2/3
SMN =0.44
initial location of rupture
F
MT 2/3
Fiber strain at $\approx \ell_{mao}$
initial location of rupture

Figure 6-7

6.4.5. The role of shear stress and effects of decreased shear stiffness

Shear stiffness is supposed to play an important role in myofascial force transmission. In figure 6-8 the shear stress is imaged within the muscle contour found at ℓ_{mao} after modeled tenotomy, aponeurotomy and myotomy. In intact active muscle at that length, shear stress is rather homogeneous and slightly positive (Fig. 6-8A). However after the intervention, surrounding the location of aponeurotomy and myotomy (i.e. immediately distally as well as proximally to it) shear stress is altered dramatically to relative large values (fig. 6-8B to E). Such shear stress concentrations are consistent with experimental and surgical observations that the muscle tears at this point in the direction of the fibers. Note that at the tip of the modeled rupture, for the MT1/3 condition, shear stress has a relative maximal value, i.e. very negative value (fig. 6-8E). In contrast to the MT2/3condition (fig. 6-8F), where no shear stress concentration is found at this tip. It is therefore concluded that the rupture has stabilized and will not increase up to the proximal aponeurosis at this muscle length. However, it is expected that rupture continue at higher muscle lengths.

In the rest of the muscle no large deviations in shear stress are found compared to the intact condition. Forces transmitted by the intact distal aponeurosis are higher at the distal end compared to the proximal end, due to number of fibers with direct myotendinous connection to this aponeurosis. Because of this larger force a larger deformation after ATIV (fig. 6-8D) is found, compared to ATII and ATIII (fig. 6-8B&C). Consequently higher stresses and stress differences are found near the location of the intervention.

Figure 6-8 Shear stress at $\ell_m \approx 29.2$ mm (ℓ_{mao}) of EDL muscle after modeled surgical interventions

The shear stress under conditions studied, is indicated in gray scales from -0.1 to 0.035. The muscle belly is presented in deformed shape, where a dashed line indicates the outline of initial passive shape (fig. 6-2A). In general the location of maximal (MX) and minimal (MN) shear stresses are indicated, if these values exceed the color range in the legend, they are mentioned separately. **A.** Shear stress under intact condition. **B, C, D.** Shear stress after aponeurotomy is applied to head II, III and IV (ATII, ATIII and ATIV, respectively), the latter is identical to tenotomy of head IV (TTIV). The locations of intervention are indicated with an arrow head. The minimal shear stress value is found just proximal situated of the location of intervention, this value decreases with the intervention is located more in distal direction. **E.** Shear stress after MT1/3. Noted the maximal shear stress is located at the tip of the rupture, which suggests that it is not stable. **F.** Shear stress after MT2/3. **G.** Shear stress after ATIV with a reduced shear stiffness ($ATIV_{½S}$). The overall shear stress in the muscle is reduced. The minimal value (SMN) is reduced with 75% compared to minimal value in ATIV (fig. 6-D). Note the somewhat increased deformation compared to ATIV (fig. 6-D). **H.** Shear stress after aponeurotomy with partial removed aponeurosis ($TTIV_{ap}$). All shear stress extremes are found on the distal end of the fibers, minimal stresses (MN) on the side without aponeurosis and maximal stresses (MX) at the intact side. also visible if initial muscle contour is compared to the deformed shape.

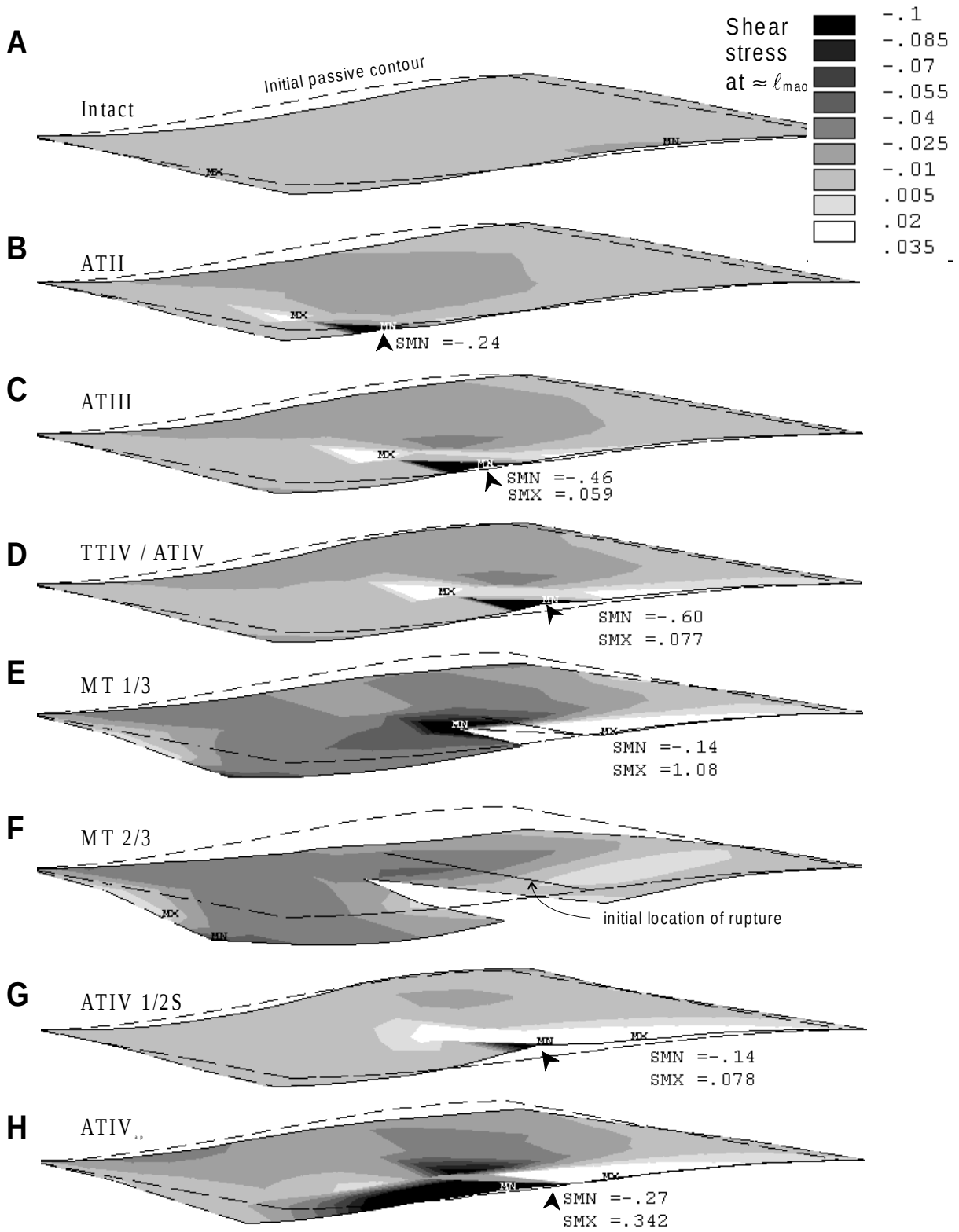
A
Intact
Initial passive contour
Shear stress at ≈ ℓmao
-.1
-.085
-.07
-.055
-.04
-.025
-.01
.005
.02
.035
B
ATII
SMN =-.24
C
ATIII
SMN =-.46
SMX =.059
D
TTIV / ATIV
SMN =-.60
SMX =.077
E
MT 1/3
SMN =-.14
SMX =1.08
F
MT 2/3
initial location of rupture
G
ATIV 1/2S
SMN =-.14
SMX =.078
H
ATIV
SMN =-.27
SMX =.342

Figure 6-8

If tenotomy IV is applied to the model with reduced shear stiffness (50%), an additional 4% decrease of F_{mao} (90 → 86%) is found (fig. 6-9A). Consequently the minimal amount of force that can be attributed to myofascial force transmission is not altered much (from 48% to 45.6%, Table 6-2). Throughout the muscle, reduced shear stiffness results in somewhat smaller negative values of shear stress (compare fig. 6-8D&G). However, a reduction of shear stiffness has a sizable effect on passive force (fig. 6-9A). It seems that with reduced shear stiffness the model lengthens due to shear deformation, more than when shear stiffness is not reduced. Passive lengthening of the muscle is accompanied by increase of fiber strain and shear. If the resistance of one of these deformations is reduced, that will dominate lengthening of the muscle, as is the case for shear under the condition of $ATIV_{½S}$. Passive fiber stress is increased less compared to the large decrease of shear stress, and therefore is passive muscle force decreased.

Figure 6-9 Role of shear stiffness and aponeurosis in EDL model

A. The normalized muscle force-length characteristics of the model under conditions ATIV, partial removed aponeurosis ($ATIV_{ap}$) and with reduced shear stiffness ($ATIV_{½S}$). Passive force after $ATIV_{½S}$ and $ATIV_{ap}$ are decreased about 50% compared to the intact and ATIV conditions. **B.** The difference in length of 17 selected fibers compared to their initial length ($\Delta\ell_{fa}$), at muscle lengths near ℓ_{mas} and ℓ_{mao}. The length of both modeled conditions is identical: 25.6 and 29.3 mm. The relative F_{mao} exerted at these lengths is presented in the legend. The location of intervention is indicated with a gray bar (ATIV). **C.** The active fiber stress near ℓ_{mao} (ℓ_m = 29.3 mm) plotted in the deformed mesh after ATIV condition is indicated in gray scales from 0.6 to 1. The locations of intervention are indicated with an arrow head. The initial passive contour is indicated with a dashed line. **D.** Active fiber stress after $ATIV_{ap}$. In the proximal muscle half less active fiber stress is found. **E.** Active fiber stress after $ATIV_{½S}$. The area of decreased active stress has increased in the distal half of the muscle. **F.** Fiber strain after $ATIV_{ap}$ plotted in the deformed mesh, indicated in gray scales from -0.3 to 0.3. Negative strain represents local lower length than optimal length for sarcomeres.

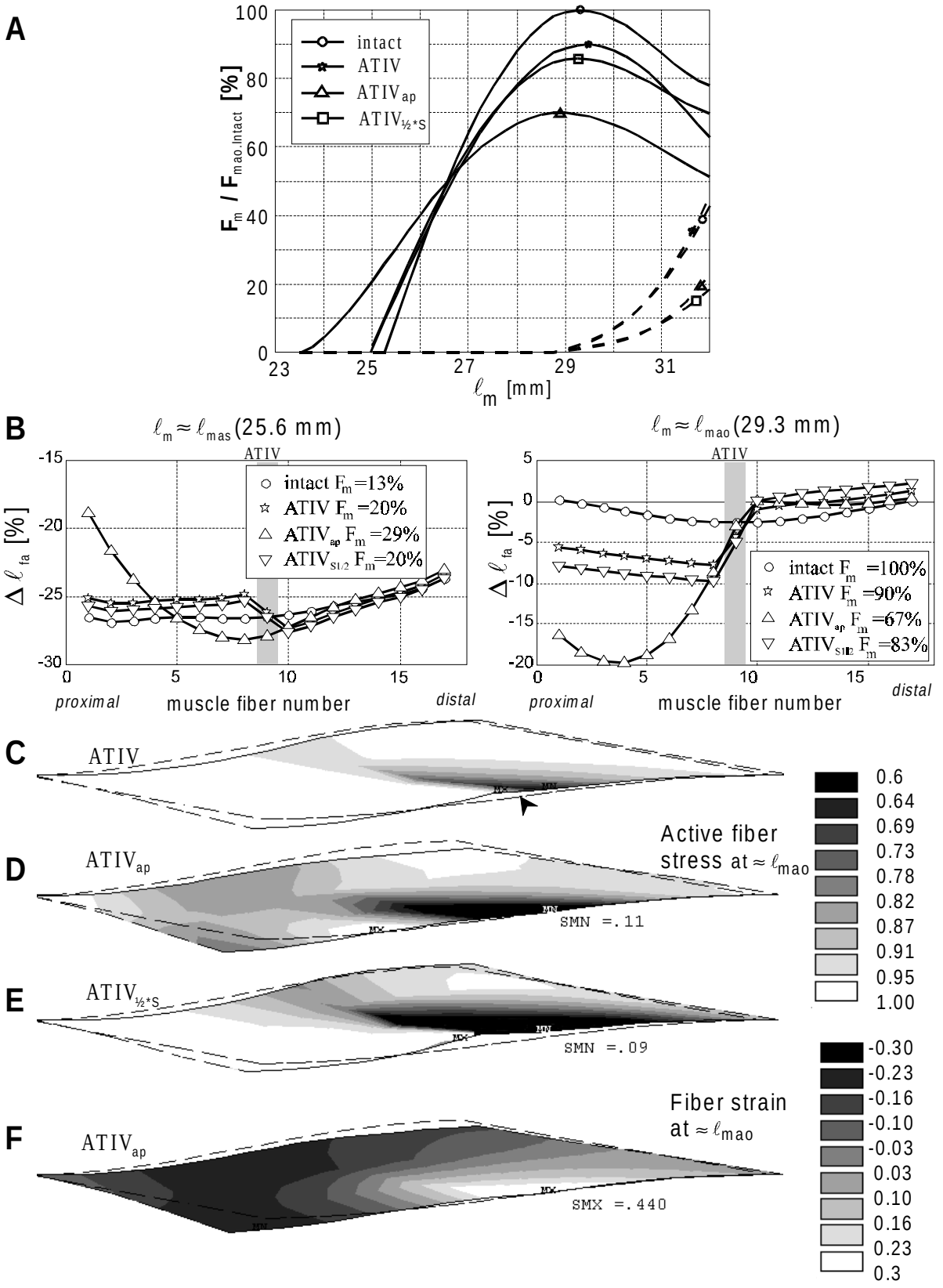
A
intact
ATIV
ATIV_ap
ATIV_½*S
F_m / F_mao.Intact [%]
ℓ_m [mm]
B
ℓ_m ≈ ℓ_mas (25.6 mm)
ATIV
intact F_m =13%
ATIV F_m =20%
ATIV_ap F_m =29%
ATIV_S1/2 F_m=20%
Δ ℓ_fa [%]
proximal
muscle fiber number
distal
ℓ_m ≈ ℓ_mao (29.3 mm)
ATIV
intact F_m =100%
ATIV F_m =90%
ATIV_ap F_m =67%
ATIV_S1/2 F_m=83%
C
ATIV
D
ATIV_ap
SMN =.11
E
ATIV_½*S
SMN =.09
Active fiber stress at ≈ ℓ_mao
F
ATIV_ap
SMX =.440
Fiber strain at ≈ ℓ_mao

Figure 6-9

6.4.6. The role of the disconnected aponeuroses after aponeurotomy

If all aponeurosis elements in the model are removed from muscle heads II, III and IV (condition $ATIV_{ap}$), we have effectively removed any possibility for myotendinous force transmission in this part of the muscle. In contrast to results in the ATIV condition a large effect on muscle force is found (fig. 6-9A): Optimal muscle force (F_{mao}) decreased by an additional 20%, to 70% of F_{mao} of the intact muscle. The passive force is decreased, due to the reduced contribution of the distal aponeurosis as well as of the fibers without myotendinous connection to the distal tendon as a result of a reduced passive stretch. The minimal contribution to muscle optimum force of the proximal fibers, without myotendinous force transmission, is reduced by an additional 15% (48 → 33%, tab. 2), based on the expected muscle force from the PCSA of the intact muscle part. It should be noted that the length of the interface of heads IV and V is unaltered compared to the intact and ATIV conditions.

Total removal of the aponeurosis is also responsible for a substantial shortening the fibers of the proximal muscle part at ℓ_{mao} (fig 9B, right panel) explaining most of the reduction of optimum force. The increase in length of the most proximal fibers (# 1-3) near ℓ_{mas} after removal of the aponeurosis (fig 9B, left panel) is a result of an increased local fiber stretch at the proximal end near the proximal tendon. This local fiber stretch is ascribed to myofascial force transmission.

It should be noted that the lengths of all proximal fibers still increase by approximately 2-17% (comparing values at ℓ_{mas} and ℓ_{mao}, fig. 6-9B left & right panel) with increasing the length of the active muscle, depending on their location within the muscle part. This also indicates that some myofascial force transmission is still present. However total removal, of the already disconnected, aponeurosis from the proximal fibers decreased the amount of force transmitted via myofascial pathways. Plots of active fiber stress show that, at ℓ_{mao}, in a large part of the proximal half of the muscle belly active stress is reduced by removal of the aponeurosis (fig. 6-9D) and therefore less force is exerted. This is also evident from higher negative values of local fiber strain (fig. 6-9F).

An additional factor responsible for the force reduction after removal of the aponeurosis is to be found in the distal muscle part. The area of low local active fiber stress in this part of the muscle increased at ℓ_{mao}, as did the minimal active fiber stress located just distally with respect to the interventions (compare fig. 6-9C&D).

After removal of the aponeurosis, at ℓ_{mao} an increased deformation of the muscle is seen (compare fig. 6-9C&D). This is accompanied by increased proximal fiber angles ($\alpha_{f,p}$) and decreased distal fiber angles ($\alpha_{f,d}$) with the line of pull.

It is concluded that even after severing the direct myotendinous connection of fibers to the insertion, an important influence of intact but disconnected aponeuroses on muscle characteristics is still present. This disconnected aponeurosis prevents the fibers from

shortening extremely and limits deviations of muscle geometry. After removal of large parts of the aponeurosis ($ATIV_{ap}$) muscle integrity is compromised resulting in quite different forces.

6.5. Discussion

6.5.1. Muscle integrity and role of aponeurosis

In general the aponeurosis is viewed to be an elastic structure, arranged in series at an angle with the muscle fibers. The major role of this structure is thought to be transmission of force, exerted by the fibers, to the tendons. However, the results of present study lead to an extension of the role ascribed to aponeuroses in muscle functioning. In addition to force transmission, the aponeurosis also affects the morphological integrity of the muscle. Removing it or parts of it, results in large local deformations of fibers. This brings them to less effective length ranges of force generation, compared to the intact muscle. Therefore, the aponeurosis of unipennate muscle should be considered an important boundary condition for the muscle enhancing the capability to produce force optimally.

The role of the aponeurosis in the intact muscle is different over the active muscle length range. Due to the angle at which fibers are attached to the aponeurosis, at low fiber lengths, the fibers compress the aponeurosis. For muscle length just below ℓ_{mao} the point where no force is transmitted by the aponeurosis is found at the end of the aponeurosis. At ℓ_{mas} this point is located at the other end of the aponeurosis where it is connected to the tendon. It should be noted that the compressed parts of the aponeurosis do not transmit force from muscle fibers to the tendons. Therefore, it seems likely that at low muscle length, force is transmitted predominantly by myofascial pathways. However, at length over ℓ_{mao} force exerted by the fibers is also transmitted through myotendinous structures to the aponeuroses and to origin and insertion. Compression of aponeuroses at low muscle length is also observed in rat GM (Zuurbier *et al.*, 1994). These authors reported that at ℓ_{mas} an aponeurosis was found of a 10% shorter length compared to the aponeurosis passive slack length.

It should be mentioned that in the present model aponeuroses are modeled by simple beam elements with linear (stiffness) properties. To bring these elements to lower lengths than their initial passive length, i.e. negative strain, compression forces are needed. These compression forces counteract the muscle force, so that at ℓ_{mas} these two forces are in equilibrium. Without this counteraction by aponeuroses, it is expected that ℓ_{mas} shifts to lower muscle length. This extra shortening may allow a decrease of fiber length. Consequently, a lower active fiber stress may be found compared to 40% active stress at ℓ_{mas} reported for a muscle fiber (van der Linden *et al.*, 1997).

Tenotomy

Comparison of model results and experimental data

In the present study we modeled tenotomy by removing a small part of an aponeurosis, as is done for modeling of aponeurotomy. This assumption is justified due to the modification made to the distal aponeurosis. The stiffness of the separate tendons is added to the continuous aponeurosis to preserve a constant strain. Consequently, a larger stiffness is implemented in distal direction of the distal aponeurosis. If no increase of normal stiffness was assumed, the aponeurosis of head V for example would have been more stretched compared to the condition where the distal tendons were modeled separately. In intact condition this assumption seems reasonable. The EDL model in intact condition is therefore a sound representation of the rat EDL. However, after surgical interventions applied (tenotomy), the stiffness of an aponeurosis distally of the intervention is too high and consequently the strain too low. Nevertheless, an aponeurosis with high stiffness will not lead to other patterns in force transmission and therefore the modeled aponeurotomy can serve as a condition of tenotomy.

The present model results for muscle force in ATII, ATIII ATIV conditions are in agreement with results of experimental distal tenotomy performed on rat EDL muscle (Huijing *et al.*, 1998): Optimal muscle force (F_{mao}) of rat EDL after experimental TTII, TTIII and TTIV is 99, 92 and 84% respectively of F_{mao} in intact EDL, versus 96, 92 and 90% for modeling conditions ATII, ATIII, and ATIV respectively. Also for estimates of minimal contributions of myofascial force transmission, the model results are in good agreement with experimental data with differences of only a few percents (Table 6-1&2). The consistence is striking, but it should be noted that for the EDL model, the three distal tendons of the separate muscle heads (II, III and IV) were integrated within one continuous distal aponeurosis. This possibly suggests that the role of the separate distal tendons in rat EDL do not play an important role for variables considered in the present study. For instance, for control of movement of separate digits the influence of this factor is expected to be quite determining. Knowing the role of the aponeurosis is more than that of a force transmitter only it is more surprising these model and experimental results are so consistent.

However, due to the continuous distal aponeurosis with increasing stiffness to the distal end, deformations of the aponeurosis of head V are reduced after tenotomy IV (or aponeurotomy), compared to the experimental TTIV. This may explain why no shift of ℓ_{mao} is found after ATIV in the model, as is observed in experiments (TTIV). A similar explanation yields for ATII and ATIII, consequently a shift of ℓ_{mao} under these conditions is expected as well.

In contrast to experimental observations on rat EDL (Huijing *et al.*, 1998), proximal fibers of the model did not decrease in length with aponeurotomy performed at a location more distally situated on the distal aponeurosis (fig. 6-6B, right panel). That the aponeurosis elements of head III, IV and V have a higher normal stiffness, will reduce lengthening of the distal aponeurosis at higher muscle length and therefore the proximal fibers are lengthened with higher muscle length. Reduced normal stiffness of the aponeurosis will lead to shortening of

the proximal fibers as is showed unambiguously in the condition where the aponeurosis is removed over a considerable amount ($ATIV_{ap}$), consequently, this part has no normal stiffness (fig. 6-9B, right panel).

Following distal tenotomies performed on rat EDL intramuscular ruptures do occur only exceptionally (Huijing *et al.*, 1998). This is in contrast with a acute rupture occurring after aponeurotomy on rat EDL (unpublished) and GM (Jaspers *et al.*, 1998). This suggests that EDL, due to its specific function, may be specially adapted to avoid high stress concentrations at the interface of muscle heads. Such adaptations may be in a sense of locally weaker connective tissue that allows large deformations without tearing or stronger, i.e. stiffer to prevent tearing at high stress concentrations.

On the basis of length measurements of the most proximal and distal fiber, Huijing (1998a) hypothesized that the fiber at higher distances from the location of intervention would have progressively shorter length. Myofascial force transmission would prevent the most distal fiber without direct connection to insertion from shortening to its slack length, however due to shear it is allowed to shorten somewhat, the next fiber further away would be shortening some more. The present study showed the opposite phenomenon, the fiber located far from the intervention has a higher length, due to curving and bulging, compared to the fiber located nearer the intervention. Furthermore, suggested Huijing (1998a) that force decrease observed in the experiments can be assigned entirely to the reduced length of the fibers in the proximal muscle part without myotendinous connection to origin and insertion. However, the present study indicates that the reduction in length of these fibers explained only a small part of the force decrease. Most of the force reduction is explained in the intact muscle part where just distally of the intervention less active force is produced, due to an increased local fiber stretch.

Integrated effects of aponeurotomy

Aponeurotomy is performed on human muscle to lengthen an overactive muscle due to spasticity (Baumann and Koch, 1989). Before and after aponeurotomy performed on the gastrocnemius muscle the ankle angle is measured under passive condition. A decrease of this angle is an indication for muscle lengthening. This procedure of measuring the angle is in our opinion not a solid evidence of muscle lengthening. 1. It is not clear what is meant with a passive condition of a spastic muscle. If such a muscle is passive, and no spastic reactions are observed, the passive force found in the present model after MT1/3 and MT2/3 should be used for comparison. Due to the reduction of passive force after MT1/3 and MT2/3 it is concluded that with the same force higher muscle length could be found and the impression is a lengthened muscle. 2. Is a shift of ℓ_{mao} an indication for muscle lengthening, due to fact optimal force is reached at a higher muscle length? A shift of ℓ_{mao} is not found in the present study, expect for MT1/3 a shift of 1.7 mm is found, however this shift is not maintained for MT2/3. The shift of ℓ_{mao} to higher length after MT1/3 is caused by the fact that the proximal fibers reach their optimum fiber length at higher muscle length. 3. An increase of active muscle length range is found, due to the shift of ℓ_{mas} to smaller length. However, that seems not logical to be addressed as muscle lengthening.

On the basis of the present results an explanation for the success of the operation performed on human is found elsewhere. The fibers without direct myotendinous connection to the distal tendon are 10 to 20% *shorter* (MT1/3, MT2/3, fig. 6-7B) compared to the intact condition. Moreover, in the present study is found that after aponeurotomy per se (ATIV) the overall fiber strain, i.e. sarcomere is decreased in almost the whole muscle (fig. 6-5F). The consequence of the reduced fiber strain will be that muscle spindles at specific locations are less excited. Particularly this effect of aponeurotomy will create a less spastic muscle and could realize a smaller ankle angle.

However, present results are based on the acute effects of the operation performed. Success of operations on human muscle is found after a recovery period of at least several weeks. By that time muscle may adapted to its new situation. The situation found after performing MT2/3 is the situation where adaptations during the recovery start. The adaptation process hypothesized by Herring *et al.* (1984) is that sarcomere number in series is adjusted so as to achieve an optimum sarcomere length when the muscle is experiencing a high level of tension. For fibers just distally located from the rupture with an extreme sarcomere length distribution this hypothesis yields adding sarcomeres at one end and removing sarcomeres at the other end. This suggests a complicated process and the outcome is hard to predict based on the present study.

Muscle integrity is thoroughly disturbed by myotomy or tearing of the muscle, due to high shear stress concentrations at the location of aponeurotomy, and an increase in deformation of muscle geometry is observed. At optimum muscle length, fibers without direct myotendinous connection to origin and insertion shorten and consequently generate less force. If aponeurotomy is applied to rat GM it causes acutely a decrease of F_{mao} to 55% (Brunner *et al.*, 1998; Huijing, 1998a). This is in agreement with the present model results (MT1/3, fig. 6-7A). Full recovery of F_{mao}, as is found in normal rat GM (Brunner *et al.*, 1998), is expected when the muscle integrity is restored, as a result of filling the rupture with connective tissue or reconnecting the severed aponeuroses ends.

The results indicated that the location at which aponeurotomy is performed has implications for the force exerted. This location can be optimized, if the goal of the surgical operation is formulated well. Moving the location in more distal direction, compared to ATIV will lead to a larger reduction in muscle force. Increasing the number of locations for interventions will result in more fibers proximally located, with decreased lengths compared to the results of the present study. More fibers with a reduced fiber strain may lead to less active muscle spindles and less active spastic muscle.

6.5.2. Force transmission and shear

An elastic continuum such as intact muscle, does not allow for large local deformations and consequently stress concentrations are limited. This suggests that in skeletal muscle, as in cardiac muscle (Horowitz *et al.*, 1988), shear stiffness plays an important role in controlling stress concentrations. However, this study revealed that the model is not very sensitive for the

value of shear stiffness, as myofascial force transmission is changed only minimally under the condition of considerably reduced shear stiffness ($ATIV_{½S}$).

In conclusion, the present study showed that pathways of force transmission are complex. In intact muscle at low muscle lengths, force is mainly transmitted by the connective tissue, in contrast to higher muscle lengths where force is also transmitted by the aponeuroses. After surgical interventions a considerable amount of force is transmitted through myofascial pathways with as a consequence high local stretch distally of the intervention, in the intact muscle part. This local stretch causes a decrease in active muscle force. However, the decrease in muscle force is not proportional to the number of fibers without a direct myotendinous connection to origin or insertion. A substantial force decrease is found if muscle integrity is thoroughly disturbed by myotomy or partly removal of the aponeurosis. Nevertheless, after two thirds of the sideward connection of fibers is removed by myotomy some force is still transmitted by myofascial pathways. Furthermore, the results indicated that the role of the aponeurosis is more than a simple transmitter of force but also responsible for maintenance of muscle integrity. Muscle integrity is necessary for optimal performance of the muscle.

Chapter 7

General Discussion

7.1. Introduction

In order to answer questions regarding muscle function, several models have been used to gain insights in mechanism of force transmission at different levels of detail in muscle. Insight is gained in how force is generated in the sarcomeres and is transmitted, due to interactions of structures. Furthermore, is indicated how well muscle performance can be predicted. Most of the results are extensively discussed in the individual chapters.

7.2. Transmission of force

7.2.1. Sarcomere, the force generator

In most of this thesis, the force-length and force-velocity characteristics are assumed independent. However, as is indicated in several experimental studies (mentioned in chapter 5), force depends on previous length changes and fatigue during a sustained contraction. For example the decrease of force during isometric sustained contractions, due to effects of fatigue; An isometric force deficit is found after a phase of muscle shortening and an enhancement after a phase of lengthening during sustained contraction.

The reducing cross-bridge (RCB) model is able to incorporate qualitatively the phenomena as observed in experimental studies, such as a force deficit after shortening and force enhancement after lengthening during sustained contractions. A shortcoming of the model in the present form is that it is not able to predict the length dependence of these phenomena. If this model is assumed to be a good representation of the mechanism involved, an additional mechanism exists in muscle to overcome these discrepancies. Such as the one discussed in the next section.

7.2.2. Sarcomere-sarcomere interaction in series

Mechanical interactions of sarcomeres in series are the second mechanism that can describe effects of contraction history phenomena. This mechanism yields non-uniform length and velocities of sarcomere in series. Due to small differences in sarcomere material properties or to different initial conditions, considerable sarcomere length distributions can be developed. After length changes during a sustained contraction the sarcomere length distribution is different from length distribution after a sustained isometric contraction at identical fiber length. This difference in sarcomere length distribution leads to a different force at the same fiber length (e.g. Morgan *et al.* 1990; Edman *et al.*, 1978, 1993; Sugi and Tsuchiya, 1988). This mechanism is addressed by Meijer *et al.* (1998). In their Hill-based fiber model with a large number of sarcomeres arranged in series, experimentally observed phenomena could be described based on interaction of sarcomere in series. That these interactions of sarcomeres in series result in force changes, is caused by in-stable behavior of sarcomeres on the descending limb of this force-length curve. However, Meijer *et al.* (1998) reported that this mechanism was not able to predict quantitatively the force changes found in experiments. This result

indicates that a combination of the RCB-model and sarcomere non-uniformities, is a promising approach. Such a combination is presented in chapter 5 by arranging two RCB-models in series and can describe length dependence of the effects of contraction history to some extent (chapter 5). As two RCB-models arranged in series incorporated force enhancement after lengthening over optimum length.

Though, effects of contraction history are observed in single fiber as well as in whole muscle, model results are of single fibers. If non-uniformities of sarcomeres occur in whole muscle to such an extent as where necessary in single model fiber (Meijer *et al.*, 1998) to predict the effects of contraction history, is discussed in the next section.

7.2.3. Myofascial force transmission

Force transmission by the myofascial connections is addressed when force is transmitted by fibers to adjacent fibers through the connective tissue. In their single fiber model Meijer *et al.* (1998) had to introduce initial differences in sarcomeres in series, either in length or in material properties, to allow for a sarcomere length distribution in series to be developed. The FEM-model indicate that in muscle, differences in sarcomere lengths are found, based on their location (chapter 4 and 6). This is in spite of the fact that fibers in the FEM-model have identical material properties. However, in muscle a large number of fibers are arranged in parallel. Myofascial force transmission will prevent large differences in length of elastic sideward connection of fibers to the connective tissue. This suggests that sarcomere non-uniformities should be similar in adjacent fibers, which is not so surprising with the observation of the regular striation pattern in skeletal muscle. That, the small differences in fiber strain distribution seem large enough to result in force differences, as is confirmed by a preliminary study (de Vries, 1998) performed with a FEM muscle-tendon complex. Force differences are found over muscle optimum length if very slow eccentric and concentric contractions are compared. The velocities during these modeled contractions were too small to explain the differences in force found, however a different strain distribution in both conditions could explain the observed force differences. These model results suggest that force of whole muscle depends on contraction history, as a result of strain distributions developed during a sustained contraction. Furthermore, is suggested that for muscle length over optimum length at least two states can be found with a different fiber strain distribution at the same muscle length. The force differences diminish quickly during a post-isometric phase, in contrast with experimental observations where effects are maintained for several seconds (e.g. Meijer *et al.*, 1997; Herzog and Leonard, 1997).

More research is necessary to identify the mechanism responsible for these results as found in FEM-modeling. Difference in lengths of sarcomeres or fibers in parallel are restricted by the resistance against shear. It is possible that reducing the coupling of fibers and the connective tissue in muscle, by modeling these structures separate with elastic connections, will lead to an increase in fiber strain distributions under conditions of different contraction history.

Another option is incorporating properties that result in effects of contraction history in the FEM-model by implementing RCB-model. However, it will make the FEM-model unnecessarily complex, since the observed effects of contraction history can also be implemented by a descriptive function as is proposed by Meijer *et al.* (1998). This function is determined by experimental observations of concentric contractions performed by rat GM. With this function, effects of shortening history can be described. Due to the linear character of this function, effects of lengthening history can be described to some extent as well (Meijer *et al.*, 1997b). Implementing such a function in the FEM-model to account for these effects, in combination with in the FEM-model observed fiber strain distributions, may lead to better modeling of muscle force during sustained contractions.

A major finding of the present work is that the contribution to total muscle force of fibers or sarcomeres, depends on its location in the muscle. Due to shear stiffness the difference in length of adjacent sarcomeres is small compared to sarcomeres located far apart. This is a result of the fact that muscle is modeled as a continuum. Along with the development of sarcomere length distributions in fiber, a secondary distribution of fiber lengths is developed within the muscle during activation, both depending on the location in the muscle belly. These distributions are developed from an initial homogeneous situation, at which all sarcomeres have the same material properties. Consequently, the contribution of fibers to the total force exerted is different per fiber. Furthermore, it is concluded that if non-uniform sarcomere lengths are found in series, force produced by sarcomeres is transmitted by myofascial connections in sideward direction in addition to the general excepted longitudinal fiber direction.

Fibers have different lengths in activated muscle. This suggests that different forces are exerted by fibers if the number of sarcomeres in series is identical. An intriguing question is: Do different fiber forces appear in real muscle, when assuming that the number of sarcomeres in series adjusts according to the hypothesis of Herring *et al.* (1984). This hypothesis postulates that the number of sarcomeres adjusts to achieve an optimum length when a high tension is experienced by the fiber. This suggests the making of sarcomeres in the outer fibers with high fiber length, due to the secondary fiber length distribution. However, there is no experimental evidence for a larger number of sarcomeres in series in the fibers on the outside of the muscle belly. It is therefore concluded that the hypothesis of Herring in not correct based on the results of this thesis.

Modeling muscle with FEM-models indicates that shear stiffness as well as stiffness perpendicular to the fiber has consequences for the muscle force exerted. A notable result is that at ℓ_{mas}, i.e. muscle length at which no force is exerted by the muscle, substantial active fiber stress is found. This suggests that muscle fibers are active and consuming energy at a muscle length at which no force is produced. Due to the limited knowledge of properties in the model, such as shear stiffness and stiffness perpendicular to the fibers, the amount of active fiber stress generated is difficult to estimate. The model properties responsible for this active stress are the passive stiffness perpendicular to the fibers and the demand of a constant muscle area. Constant muscle area is assumed a good approximation of a constant muscle volume

(chapter 2). The stiffness perpendicular to the fibers seems be more complex than is indicated by Strumpf *et al.* (1993). They only found a passive contribution of stiffness in directions perpendicular to the fibers. For skinned muscle fibers several authors (e.g. Maughan and Godt, 1979; Xu and Brenner, 1993) showed experimentally on that stiffness perpendicular to the fibers depends on activation. This suggests that cross-bridges generate radial as well as longitudinal forces. Consequently, an active force is generated perpendicular to the fibers at low fiber lengths in addition to the passive force found, as a result of stretch of the connective tissue surrounding the fiber at low muscle length. Nevertheless, an active fiber stress at muscle active slack length is a result of mechanical equilibrium of the continuum and is expected to occur *in situ* as well. However, for quantification of the active fiber stress at this muscle length more research is necessary for the quantification of the parameters. For this reason, it is expected that muscle will not operate at these inefficient low muscle lengths.

7.2.4. Motor-unit interactions

Muscles in this thesis are modeled homogeneously and maximally activated. However, muscle can also be sub-maximally or partly activated, due to recruitment of one or more motor units. A motor unit is a number of fibers spread or clustered in the muscle belly and innervated by a single nerve branch. If the muscle is activated partly, a passive fiber from one motor unit will resist an active neighbor fiber from another motor unit in its movements. Moreover, experimental evidence indicates that fibers of single motor units can appear in series, as is observed in parallel fibered muscle (e.g., Loeb *et al.*, 1987; Bodine *et al.*, 1988). Based on the present study seem in series arranged motor units in parallel fibered muscle to be rather inefficient. Because of the fact that myofascial force transmission will not prevent shortening of activated fibers at the cost of in series arranged passive fibers. However, fibers from one motor unit are randomly distributed in series as well as in parallel, as is experimentally observed by staining end-plate zones (Loeb *et al.*, 1987). This may be efficient because active fibers will not shorten at cost of passive fibers arranged in series due to the resistance of activated fibers that are arranged in parallel to the passive fibers. Shortening of active fibers at cost of lengthening passive fibers arranged in series will depend on the distances of these passive fibers and the active fibers arranged in sideward direction. Loeb *et al.* (1987) found that in series arranged fibers of a single motor unit appear in strips with a length of the whole muscle length. Consequently, the effects of shear will reduce the loss of efficiency over small distances. This suggests that based on the results of the present study it is not necessary for in series arranged fibers belonging to one motor unit to be aligned exactly, as is questioned by Loeb *et al.* (1987), resistence against shear will prevent passive fibers in a small strip with active fibers arranged in parallel from shortening (chapter 6; Huijing, 1998a).

7.2.5. Myo-tendinous force transmission

The force generated by the fibers is transmitted through the myo-tendinous connections to the aponeurosis and tendons. Force exerted by the fibers causes lengthening of the aponeuroses (chapter 2). If aponeuroses are assumed elastic, the prediction of muscle force and linearized muscle geometry improved, which indicates that these structures are of some importance. However, in chapter 6 is indicated that interactions of fibers and aponeuroses can also result in a shortening of aponeuroses as well. Under such conditions, the aponeuroses do not transmit force from fibers to origin and insertion of the muscle. At this point, the aponeurosis can not be considered a series elastic structure in the classical sense. However, if the aponeurosis is not transmitting force, it is not without function, as is indicated when the aponeurosis removed (chapter 6). A considerable deformation of the muscle is observed and consequently force exerted is reduced, suggesting that aponeuroses are of considerable importance to preserve muscle integrity.

An experimental study on two dimensional strain distributions on the surface of the passive aponeurosis of rat gastrocnemius medialis (GM), did not show compression in the direction of the line of pull (van Bavel *et al.*, 1996). However, they found during passive stretch away from the central region a negative strain perpendicular to the line of pull, i.e. compression. This suggests that the widths of aponeuroses are reduced primarily in a region further from the central region. Extrapolating these observations to the active condition is rather speculative, nevertheless this study indicates that compression of tendinous tissue is possible.

Muscle integrity is also disturbed effectively by surgical interventions. These interventions performed on muscle are aimed at improving or altering muscle force. Due to the complex cooperation of structures in muscle, it is difficult to predict the result of such interventions. Though, clinicians know how to perform an operation effectively, there is a lack of detailed knowledge about the mechanism responsible for the success. and in future to increase clinical knowledge regarding success. The FEM-model is valuable tool to study the effects of a variety of surgical interventions (e.g. chapter 6). Knowing the effects of the presently modeled interventions on muscle performance, and a detailed clinical goal of an operation is aimed for, the next stage in research is to optimize interventions in dialogue with clinicians.

7.3. Prediction of muscle performance

The preceding paragraphs indicate which role the various structures play in muscle force exertion. Insight is gained in how force generated by the sarcomeres is finally exerted a origin and insertion of the muscle. Besides the heuristic purpose of this study, it is also of interest if muscle force under specific conditions can be predicted well (Huijing, 1998b). The revised planimetric model is rather simple and good in predicting muscle force over a large active muscle length range. These are ingredients for such a model to be applied in large-scale multi-segment models for the predictions of movement. A large number of parameters necessary for this model are experimentally determined for humans and documented (e.g., Winters and Woo,

1990). However, information about the aponeurosis active slack length is lacking. The aponeurosis slack length under passive and active condition is different (by 5 - 10%) as results of compression due to shortening of fibers at low muscle length (chapter 6). The length differences are expected to depend on the angle of pennation, in such a way that a small angle of pennation result in large differences between aponeurosis slack length under passive and active conditions. Further research is necessary to reveal the relation between properties of aponeurosis in active and passive muscle to make the revised planimetric model applicable in large-scale segment models. However, this model has the ability to predict the functional characteristics well, which are expressed in muscle force and linearized muscle geometry, of uni-pennate muscle (chapter 3). It is therefore concluded that the revised planimetric model is a valuable tool in its present form. It is a useful heuristic tool for showing understanding the effects of pennation on muscle force-length characteristics and the importance of an elastic aponeurosis in combination with the preservation of the longitudinal area, for the prediction of muscle geometry.

7.4. Reconsideration isolated muscle research

The way of modeling muscle performance of single muscle based on the results of the present study leads to the following consideration regarding muscle performance *in vivo*. For simplicity reasons is in studies, experimentally *in situ* and in modeling, generally focused on one muscle. Nonetheless, based on this study one should consider the following effects of doing so. Muscle shape is expected to be changed in isolated condition, compared to *in vivo* conditions and consequently performance will be altered. This is in contrast with what is suggested by experiments on isolated muscle *in situ* condition. Nevertheless, comparison of results from *in situ* experiments and model results seems acceptable. However, the extrapolation of observations from model as well as from experiments to *in vivo* muscles with complex three-dimensional geometries, which interact with surrounding muscles, organs and bony structures is highly speculative. Due to the existence of adhesive connections between adjacent muscles, which are experienced by every one that has dissected muscle, the mechanical interactions between adjacent muscle can be more pronounced.

Very illustrative is a study of Riewald and Delp (1997), where in human subjects is tried to convert a knee extensor into a knee flexor. The result was that when the newly attached flexor was activated an extension moment was found, which suggests that a mechanism exist that transmits force form the activated flexor to adjacent passive extensors. This is an indication that interaction between fibers also occur between adjacent muscle, due to force transmission between adjacent muscle (Huijing, 1998a). It is possible that the influence of mutual muscle is not so large as that of fibers within a muscle, but a small connection allows force transmission. Within a muscle, these lateral connections are strong either, as is observed by Huijing *et al.* (1998), and strong enough to transmit force in sideward direction. Finite element models are based on mechanical equilibrium of continua, whether a model is build for one muscle or a muscle group. Properties of interfaces between muscle should be defined, but based on experimental observations, these properties can be estimated. When a model is build of a group

of adjacent muscles, contributions of individual muscle or combinations of muscles in the group, to the muscle performance can be studied. This could be studied with the existing two-dimensional model, but it is recommended to use a three-dimensional version of the present model.

7.5. Recommendations

For heuristic purposes, the FEM-model has proved to be powerful. Though, many parameters need to be identified, this model revealed contribution to muscle performance of several properties. Nevertheless, validation of parameters is difficult, due to the limited amount of information that can be obtained experimentally of internal deformations. An indirect way of determining internal deformations can be obtained from intramuscular pressure. Commercial available pressure sensors are so small that penetration of the muscle belly occurs without damaging muscle fibers. It is therefore assumed that pressure can be measured of an intact muscle. The experimentally determined intramuscular pressures can be compared to the hydrostatic pressure calculated by the model. In the model pressures can be determined based on the calculated stresses. In this way, model validation can be realized under various conditions.

7.5.1. Muscle element

Muscles as complex three-dimensional structures are treated in this thesis in two dimensions. Consequently, the mechanism of force exertion of muscle is simplified, but insights in these mechanism have been increased. However, a two dimensional model has its limitations as mentioned in this thesis. An obvious step is to convert the present FEM-model in a three dimensional version. It should be noted that has to be dealt with a number of aspects: the number of additional unknown parameters, three-dimensional geometries have to be defined, a distinction should be made in tendon and aponeurosis elements, due to the different morphology, and an other type of aponeurosis element should be used (see next paragraph). However, this conversion should only be done when predictions of the three-dimensional model are improved or for specific three-dimensional problems, such as: What is the effect of a constant muscle volume compared to a constant mid-longitudinal area of muscle? How do fibers not located in the central region of the line of pull contribute to the total muscle performance? What effects have interactions of fibers and aponeurosis further away from the mid-longitudinal area of muscle and to the line of pull on muscle force exerted?

7.5.2. Aponeurosis element

In this thesis a considerable amount of attention is paid to muscle tissue, which is modeled by a specially designed element for a FEM-model of a muscle-tendon complex. However, chapter 6 indicated that the role of the aponeurosis is underestimated and is more than a transmitter of force produced by the fibers to origin and insertion. Muscle integrity is to some extent preserved by the aponeuroses for optimal exertion of muscle force. Furthermore, it is revealed that, at low muscle lengths, the aponeurosis is compressed by shortening of fibers attached at

an angle to the aponeurosis. Due to the linear character of the aponeurosis element, compression results in negative force. This negative force, which counteracts the muscle force, which is not expected to exist *in vivo*, due to the fact that a passive elastic structure can not resist compression below slack length. Without this counteracting force, muscle force will be higher and consequently ℓ_{mas} will shift to lower muscle lengths. In future studies it is recommended to use an element to represent aponeuroses with non-linear stiffness, with a zero stress for negative strains, in accordance with experimental evidence (Ettema and Huijing, 1989; Zuurbier *et al.*, 1994). Consequently, compression of such a modeled aponeuroses is then only allowed without compression forces. This thesis showed mechanisms, interactions and pathways of force transmission and those are expected not to be altered by a revised aponeurosis element.

7.5.3. Adaptation

If interest of muscle performance lies in long term processes, muscle adaptation should be implemented in the muscle element. Muscle adaptation, as is expected to happen during growth, after immobilization or after surgical interventions, is assumed to change muscle performance. The hypothesis tested by Herring *et al.* (1984) indicated that the number of sarcomeres in series would be altered. In the muscle-element such an adaptation at sarcomere level yields altering the constants of the active fiber stress-strain relationship during for example sustained and cyclic contractions (chapter 4, eq. 5).

REFERENCES

Abbott BC and XM Aubert (1952) The force exerted by active striated muscle during and after change of length, *J Physiol* 117: 77-86.

Atteveldt, H van and A Crowe (1980) Active tension changes in frog skeletal muscle during and after mechanical extention, *J Biomech*, 13: 323-331.

Ballice-Gordon, RJ and WJ Thompson (1988) The organization and development of compartmentalized innervation in rat extensor digitorum longus muscle, *J Physiol*, 398: 211-231.

Barnes, MJ and JA Herring (1991) Combined split anterior tibial-tendon transfer and intramuscular lengthening of the posterior tibial tendon. Results in patients who have a varus deformity of the foot due to spastic cerebral palsy, *J Bone Joint Surg (am*), 73(5) 734-738.

Bavel, H van, MR Drost, JDL Wielders, JM Huyghe, A Huson and JD Jansen (1996) Strain distribution on rat medialgastrocnemius (MG) during passive stretch, *J Biomech*, 29(8): 1069-1074.

Baumann, JU and HG Koch (1989) Ventrale aponeurotische Verlängerung des Musculus gastrocnemius, *Operat Orthop Traum*, 4: 254-258.

Benninghoff, A and H Rollhäuser (1952) Zur inneren Mechanik des gefiederte muskels, *Pfüg Arch Gesammte Physiol*, 254:527-548.

Bodine, SC, A Garfinkel, RR Roy and VR Edgerton (1988) Spatial distribution of motor unit fibers in cat soleus and tibialis anterior muscles: local interactions, *J Neurosc*, 8: 2142-2152.

Borelli, GA (1681-1682): 'De motu animalum', On the movement of animals. Translated into English by Paul Mayet, Springer Berlin, 1989.

Brand, RA, DR Pedersen and JA Friederich, The sensitivity of muscle force predictions to changes in physiologic cross-sectional area, *J Biomech*, 19: 589, 1986

Brenner, B and LC Yu (1991) Characterization of radial force and radial stiffness in Ca^{2+}-activated skinned fibers of the rabbit psoas muscle, *J Physiol*, 441: 703-718.

Brunner, R, (1995) A change in the muscle force after lengthening the tendon and tendon transfer, *Orthopäde*, 24: 246:251.

Brunner, R, PA Huijing, R Jaspers and J Pel (1997) Effects of intramuscular aponeurotomy and recovery on pennate skeletal muscle, *Rehab R&D Prog Rep*. 34: 181.

Brunner, R, RT Jaspers, JJM Pel and PA Huijing (1998) Muscle force after intramuscular aponeurotomy: Acute and long term effects on the gastrocnemius medialis muscle of the normal rat, submitted

Buchthal, F, E Kaiser and P Rosenfalck (1952) The rheology of the cross striated muscle fiber, with particular reference to isotonic conditions, *Daniske Biolog Meddelerser*, 21 (7): 121.

Colomo, F, V Lombardi and G Piazzesi (1986) A velocity-dependent shortening depression in the development of the force-velocity relation in frog muscle fibers, *J Physiol*, 380: 227-238.

Cook CS and MJN McDonagh (1995) Force responses to controlled stretches of electrically stimulated human muscle-tendon complex, *Exp Physiol*, 80: 477-490.

Edman KAP and T Tsuchiya (1996) Strain of passive elements during force enhancement by stretch in frog muscle fibers, *J Physiol*, 490: 191-205.

Edman, KAP (1975) Mechanical deactivation induced by active shortening of isolated muscle fibers of the frog, *J Physiol*, 246: 255-275.

Edman, KAP (1980) The role of non-uniform sarcomere behavior during relaxation of striated muscle, *Eur Heart J*, 1 suppl A 49-57.

Edman, KAP and F Lou (1990) Changes in force and stiffness induced by fatigue and intracellular acidification in frog muscle fibres, *J Physiol*, 424: 133-149.

Edman, KAP, C Caputo and F Lou (1993) Depression of tetanic force induced by shortening of frog muscle fibres, *J Physiol*, 466: 535-552.

Edman, KAP, G Elzinga and MIM Noble (1978) Enhancement of mechanical performance by stretch during tetanic contraction of vertebrate skeletal muscle fibers, *J Physiol*, 281: 139-155.

Eisenberg, E, TL Hill and Y Chen (1980) Cross-bridge model of contraction, quantitative analysis, *Biophys J*, 29: 195-227.

Eldred, E, M Ounjian, RR Roy and VR Edgerton (1993) Tapering of the intrafascicular endings of muscle fibers and its implications to relay of force, *Anat Rec*, 236: 390-398.

Ettema, GJC and PA Huijing (1989) Properties of tendious structures and series elastic components in EDL muscle-tendon complex of the rat, *J Biomech*, 22: 1209-1215.

Ettema, GJC and PA Huijing (1993) Series elastic properties of rat skeletal muscle: distinction of series elastic components and some implications, *Neth J Zool*, 43(3-4): 306-325.

Ettema, GJC, PA Huijing, GJ van Ingen Schenau and A de Haan (1990) Effects of pre-stretch at the onset of stimulation on mechanical work output of rat medial gastrocnemius muscle-tendon complex, *J Exp Biol*, 152: 333-351.

Fitts, RH (1994) Cellular mechanism of muscle fatigue, *Physiol Rev*, 74 (1): 49-94.

Flory, PJ (1956) Role of crystallization in polymers and proteins, *Science*, 124: 53-60.

Friden, J and RL Lieber, (1994) Physiologic consequences of surgical lengthening of extensor carpi radialis brevis muscle-tendon junction for tenis elbow, *J Hand Surg*, 19A: 269-274.

Fung, YC (1981) Biomechanics : mechanical properties of living tissues, Springer-Verlag, New York, ISBN 0-387-90472-7.

Gans, C and CW Bock (1965) The functional significance of muscle architecture: a theoretical analysis, *Ergebn Anat Entw Gesch*, 38: 115-142.

Gordon AM, AF Huxley and FJ Julian (1966) The variation in isometric tension with sarcomere length in vertebrate muscle fibers, *J Physiol*, 184: 170-192.

Granzier, HLM and GH Pollack (1989) Effect of active pre-shortening on isometric and isotonic performance of single frog muscle fibres, *J Physiol*, 415: 299-327.

Granzier, HLM and GH Pollack (1990) The descending limb of the force-sarcomere length relation revisited, *J Physiol*, 421: 595-615.

Häkkinen, K, KL Keskinen and PV Komi (Eds.) (1995) Proceedings XVth Congress of Int Soc of Biomechanics, University of Jyväskylä, Finland.

Hatze, H (1981) Myocybernetic control models of skeletal muscle, University of South Africa, Pretoria.

Herring, SW and AF Grimm and BR Grimm (1984) Regulation of sarcomere number in skeletal muscle: a comparison of hypotheses, *Muscle Nerve*, 7(2): 161-173.

Heslinga, JW and PA Huijing (1990) Effects of growth on architecture and functional characteristics of adult rat gastrocnemius muscle, *J Morphol*, 206: 119-132.

Heslinga, JW and PA Huijing (1992) Effects of short length immobilization of medial gastrocnemius muscle of growing young adult rats, *Eur J Morphol*, 30: 257-273.

Heslinga, JW and PA Huijing (1993) Muscle length force characteristics in relation to muscle architecture: a bilateral study of gastrocnemius medialus muscles of unilaterally immobilized rats. *Eur J Appl Physiol* 66: 289-298.

Herzog, W (1996) Force-sharing among synergistic muscle: theoretical considerations and experimental approaches, *Exerc Sport Sci Rev*, 24: 173-202.

Hill, AV (1938) The heat of shortening and the dynamic constants of muscle, *Proc R Soc Lond B*, 126: 136-195.

Hill, TL, E Eisenberg and Y Chen (1975) Some self-consistent two-state sliding filament models of muscle contractions, *Biophys J*, 15: 335-372.

Horowitz, A, I Sheinman and Y Lanir (1988b), Nonlinear Incompressible Finite Element for Simulating Loading of Cardiac Tissue - Part II: Three Dimensional Formulation for Thick Ventricular Wall Segments, *J Biomech Eng*, 110: 63-68.

Horowitz, A, I Sheinman, Y Lanir, M Perl and S Sideman (1988a), Nonlinear Incompressible Finite Element for Simulating Loading of Cardiac Tissue - Part I: Two dimensional Formulation for Thin Myocardial Strips, *J Biomech Eng*, 110: 57-61.

Huijing PA, AAH Van Lookeren Campagne and JF Koper (1989) Muscle architecture and fiber characteristics of rat gastrocnemius and semimembranosus muscle during isometric contractions. *Acta Anat* 135: 46-52.

Huijing, PA (1995) Parameter interdependence and success of skeletal muscle modeling, Hum Mov Sci, 14(4-5) 443-486

Huijing, PA (1996) Algemene myologie, Inleiding in de kinesiologie van de mens (in Dutch; Edited by RH Rozendal and PAJBM Huijing) pp. 199-281, 6th edition, Robijns, Houten.

Huijing, PA (1998a) Muscle as a collagen fiber reinforced composite material: Force transmission in muscle and whole limbs, *J Biomech*, in press,

Huijing, PA (1998b) Muscle the motor of movement: Properties in function, experiment and modeling *J Electrom Kinesiol*, in press.

Huijing, PA and RD Woittiez (1984) The effect of architecture on skeletal muscle performance: A simple planimetric model, *Neth J Zool*, 34: 21-32.

Huijing, PA and RD Woittiez (1985) Notes on planimetric and three-dimensional muscle models, *Neth J Zoology* 35: 521-525.

Huijing, PA, GC Baan and GT Rebel (1998) Non-myotendious force transmission in rat extensor digitorum longus muscle, *J Exp Biol*, in press.

Hunter, PJ and AD McCulloch (1988) A finite element model of passive ventricular mechanics, in Computational Methods in Bioengineering, Spilker, RL and BR Simons Eds, vol. BED-9, ASME Chicago, pp 387-397.

Huxley AF (1957) Muscle contraction and theories of contraction, *Prog Biophys Biophys Biochem*, 7: 225-318.

Huxley AF and R Niedergerke (1954) Interference microscopy of living muscle fibers, *Nature*, 173: 971-973.

Huxley AF and RM Simmons (1971) Proposed mechanism of force generation in striated muscle, *Nature*, 233: 533-538.

Huxley, HE and J Hanson (1954) Changes in the cross-striations of muscle during contraction and stretch and their structural interpretation, *Nature*, 173: 973-976.

Huyghe, JM, DH van Campen, T Arts and RM Heethaar (1991) A Two-phase Finite Element Model of the Diastolic Left Ventricle, *J Biomech*, 24 (7): 527-538.

Huyghe, JMRJ (1986) Non-linear Finite Element Models of the Beating Left Ventricle and the Intramyocardial Coronary Circulation, PhD Thesis.

Jaspers, RT, R Brunner, JJM Pel and PA Huijing (1998) Acute effects of intramuscular aponeurotomy on rat GM: Force transmission, muscle force and sarcomere length, in prep.

Julian, FJ and DL Morgan (1979a) Intersarcomere dynamics during fixed-end tetanic contractions of frog muscle fibers. *J Physiol* 293: 365-378.

Julian, FJ and DL Morgan (1979b) The effects on tension of non-uniform distribution of length changes applied to frog muscle fibers, *J Physiol*, 293: 379-392.

Julian, FJ and MR Sollins (1975) Variations of muscle stiffness with force at increasing speeds of shortening, *J Gen Physiol*, 66: 287-302.

Kardel, T (1990) Niels Stensens geometrical theory of muscle contractions (1667): A reappraisal *J Biomech* 23, pp 953-965.

Kaufman, KR, KN An and EYS Chao (1989) Incorporation of muscle architecture into the muscle length-tension relationship, *J Biomech*, 22: 943-948.

Latash M and VM Zatsiorsky (1993) Joint stiffness: Myth or reality? *Hum Mov Sciences* 12: 653-692.

Leeuwen, JL van and CW Spoor (1992) Modelling mechanically stable muscle architecture, *Phil Trans R Soc London B*, 336 (1277): 275-292.

Leeuwen, JL van and CW Spoor (1993) Modelling the pressure and force equilibrium in unipennate muscle with in-line tendons, *Phil Trans R Soc London B*, 342: 321-333.

Leeuwen, JL van and CW Spoor (1996) A two dimensional model for the prediction of muscle shape and intramuscular pressure. *Eur J Morphol* 34: 25-30.

Linden, BJJJ van der, PA Huijing, HFJM Koopman, K Meijer, M Kuiper and HJ Grootenboer (1995) Finite element model of anisotropic muscle: effects of curvature on fiber-length distribution, pp. 956-957, Cited from Häkkinen *et al.* (1995).

Linden BJJJ van der, PA Huijing, HFJM Koopman and HJ Grootenboer (1996) Is High-frequency stiffness a measure for the number of attached cross-bridges? Proc. 18th IEEE EMBS congress in Amsterdam, eds. Rutten and Neuman, 2.8.1-7 (2 pages).

Linden BJJJ van der, PA Huijing, HFJM Koopman and HJ Grootenboer (1997) Mechanical explanation of muscle fiber slack-length, proc. ISB Tokyo, Japan, 39.

Linden BJJJ van der, HFJM Koopman, HJ Grootenboer and PA Huijing (1998a) Modeling functional effects of muscle geometry, *J Electromyog Kinesiol*, in press.

Linden BJJJ van der, HFJM Koopman, HJ Grootenboer and PA Huijing (1998b) Revised Planimetric Model of Unipennate Skeletal Muscle: A Mechanical Approach, *Clinic Biomech*, in press.

Linden, BJJJ van der, PA Huijing, HFJM Koopman, K Meijer and HJ Grootenboer (1998c) A finite element skeletal muscle model for simulation of isometric and concentric contractions, *Comp Meth Biomech Biomed Eng*, conditional accepted.

Linden, BJJJ van der, K Meijer, PA Huijing, HFJM Koopman and HJ Grootenboer (1998d) A Reducing Cross-Bridge Model Explains Experimentally Observed Contraction History Effects, *Biol Cybern*, submitted.

Loeb GE, CA Pratt, CM Channaud and FJR Richmond (1987) Distribution and innervation of short interdigitated muscle fibers in parallel-fibered muscle of the cat hindlimb, *J Morphol*, 191: 1-15.

Ma SP and GI Zahalak (1987) A simple self-consistent distribution-moment model for muscle: chemical energy and heat rates, *Math Bioscienc*, 84: 211-230.

Margulies, SS, GT Lei, GA Farkas, JR Rodarte (1994) Finite-element analysis of stress in the canine diaphragm, *J Appl Physiol*, 76(5): 2070-2075

Maughan, DW and RE Godt (1979) Strech and radial compression studies on relaxed skinned muscle fibers of the frog, *Biophys J*, 28: 391-402.

McCulloch AD, L Waldman, J Rogers and Julius Guccione (1992) Large-scale finite element analysis of the beating heart" *Crit Rev Biomed Eng*, 20(5, 6): 427-449.

McDonald, KA, M Lakonishok and AF Horwitz (1995) α_v and α_3 integrin subunits are associated with myofibrils during myofibrillogenesis, *J Cell Sci*, 108: 2573-2481.

McLester jr, JR (1997) Muscle contraction and fatigue, *Sports Med*, 23(5): 287:305.

Meijer, K, HJ Grootenboer, HFJM Koopman and PA Huijing (1997) Isometric length-force curves during and after concentric contractions differ from the initial isometric length-force curve in rat muscle, *J Appl Biomech*, 2: 135-152.

Meijer, K (1998) Effects of stretch and shortening on skeletal muscle force, PhD-thesis, in preparation.

Meijer, K, HJ Grootenboer, HFJM Koopman, BJJJ van der Linden, and PA Huijing (1998a) Hill-type model of rat medial gastrocnemius muscle that accounts for shortening history effects, *J Biomech*, in press.

Meijer, K, HJ Grootenboer, HFJM Koopman and PA Huijing (1998b) Shortening history effects at sub-maximal and maximal stimulation frequencies in rat medial gastrocnemius muscle, *Exp physiol*, submitted

Meijer, K, HJ Grootenboer, HFJM Koopman and PA Huijing (1998c) Stretch induced force enhancement in maximal and submaximal soleus and medial gastrocnemius muscles of rat, *J Exp Biol*, submitted

Meijer, K, HJ Grootenboer, HFJM Koopman and PA Huijing (1998d) A model of inter sarcomere dynamics that accounts for shortening history induced force depression, in preparation.

Mijailovich, SM, JJ Fredberg and JP Butler (1996) On the theory of muscle contraction: filament extensibility and the development of isometric force and stiffness, *Biophys J*, 71: 1475-1484.

Morgan DL, and U Proske (1984) Mechanical properties of toad slow muscle attributed to non-uniform sarcomere lengths, *J Physiol*, 349: 107-117.

Morgan, DL (1990) New insights in the behavior of muscle during active lengthening, *Biophys J*, 57: 209-221.

Otten, E (1988), Concepts and models of functional architecture in skeletal muscle, *Exerc Sport Sci Rev*, 16: 89-137.

Ounjian M, RR Roy, E Eldred, A Garfinkel, J Payne, J Amstrong, A Toga, VR Edgerton (1991) Physiological and developmental implications of motor unit anatomy, *J Neurbiol*, 22:547-549.

Pardo, JV, JD Siliciano and SW Craig (1983) A vinculin-containing cortical lattice in skeletal muscle: transverse lattice elements ("costameres") mark sites of attachment between myofibrils and sarcolemma, *Proc Natl Acad Sci USA*, 80: 1008-1012.

Patel TJ and RL Lieber (1997) Force transmission in skeletal muscle: from actomyosin to external tendons, *Exec Sports Sci Rev*, 25:321-363.

Pollack GH, (1990) Muscle and molecules, helix-coil transition in myosin rod, Chapter 6, WA: Ebner and Sons, Seattle.

Press, WH, SA Teukolsky, WT Vetterling and BP Flannery (1992) Numerical Recipes in C: The art of scientific computing, eds Press, Teukolsky, Vetterling and Flannery, Cambridge University Press, New York.

Riewald, SA and SL Delp (1997) Rectus femoris knee moment after transfer, *Dev Med Child Neurol*, 39: 99-105.

Roszek, B, GC Baan, PA Huijing (1994) Decreasing stimulation frequency-dependent length-force characteristics of rat muscle, *J Appl Physiol*, 77: 2115-2124.

Savelberg, HHCM and H.C. Schamhardt (1995) The influence of inhomogeneity in architecture on the modelled force-length relationship of muscles, *J Biomech*, 28(2): 187-198.

Schippel, K and D Reissig, (1968) Zur Feinstruktur des Muskel-Sehnenuberganges, *Z Mikrosk Anat Forsch*, 789: 235-255.

Scott, SH and DA Winter (1991) A comparison of three muscle pennation assumptions and their effect on isometric and isotonic force, *J Biomech* 24(2): 163-167.

Spector, GA, PF Gardiner, RF Zernicke and VR Edgerton (1980) Muscle architecture and force velocity characteristics of cat soleus and medial gastrocnemius: Implications for motor control. *J Neurophysiol* 44: 951-960.

Stensen, N (1667) Elementorum myologiae specimen, cited from Kardel (1990).

Street, SF (1983) Lateral transmission of tension in frog myofibres: a myofibrillar network and transverse cytoskeletal connections are possible transmitters, *J Cell Physiol*, 114: 346-364.

Street, SF and RW Ramsey (1965) Sarcolemma: transmitter of active tension in frog skeletal muscle, *Science*, 149, 1379-1380.

Strumpf, RK, JD Humphrey and FCP Yin (1993) Biaxial mechanical properties of passive and tetanized canine diaphragm, *Am J Physiol*, 265: H469-475.

Sugi, H (1972) Tension changes during and after stretch in frog muscle fibers, *J Physiol*, 225: 237-252.

Sugi, H and T Tsuchiya (1988) Stiffness changes during enhancement and deficit of isometric force by slow length changes in frog skeletal muscle fibres, *J Physiol*, 407: 215-229.

Swammerdam J, 1737, Bilia Naturae, cited from Kardel (1990).

Trotter, JA (1990) Interfibre tension transmission in series-fibred muscles of cat hindlimb, *J Morphol*, 206: 351-361.

Trotter, JA (1993) Functional morphology of force transmission in skeletal muscle, *Acta Anat*, 146: 205-222.

Vries, YWR de (1998) Spieranalyse met behulp van het aangepaste eindige elementen spiermodel, Doctoral thesis, BW-109, (in Dutch).

Warwic, R and PL Willems (editors) (1973) Gray's Anatomy, 35th Edition, Longman Group Ltd, Edinburgh, ISBN 0-443-01011-0.

Willems, MET and PA Huijing (1992) Effects of growth on architecture of rat semimembranosus lateralis muscle, *Anat Rec* 233: 25-31.

Willems, MET and PA Huijing (1994) Mechanical and geometrical properties of rat semimembranosus lateralis muscle during isometric contractions. *J Biomech* 27: 1109-1118.

Winters, JM and L Stark (1987) Muscle models: what is gained and what is lost by varying model complexity, *Biol Cybern*, 55: 403.

Winters, JM and SL-Y Woo (Editors) (1990) Multiple Muscle Systems, Biomechanics and Movement Orgainsation,Springer Verlag, NewYork, ISBN 0-387-97307-9.

Woittiez, RD, PA Huijing, HBK Boom and RH Rozendal (1984) A three-dimensional muscle model: A quantified relation between form and function of skeletal muscles, *J Morphol*, 182: 95-113.

Xu, S, B Brenner and LC Yu (1993) State-dependent radial elasticity of attached cross-bridges in single skinned fibres of rabbit psoas muscle, *J Physiol*, 461: 283-300

Yin, FCP, RK Strumpf, PH Chew and SL Zeger (1987) "Quantification of the Mechanical Properties of Noncontracting Canine Myocardium under simultaneous Biaxial Loading", *J Biomech*, Vol. 20 (6), pp. 577-589.

Zahalak, GI (1981) A distribution-moment approximation for kinetic theories of muscular contraction, *Math Bioscienc*, 55: 89-114.

Zahalak, GI and SP Ma (1987) Muscle Activation and Contraction: Constitutive Relations Based Directly on Cross-Bridge Kinetics, *J Biomech Eng*, 112: 52-62.

Zajac, FE (1989) Muscle and tendon: properties, models, scaling and applications to biomechanics and motor control, *CRC Crit Rev Biomed Eng*, 17(4): 359-411.

Zienkiewicz, OC and RL Taylor (1991) "The finite element method, Vol 2", McGraw-Hill Book Company, London.

Zienkiewicz, OC and RL Taylor (1994) "The finite element method, Vol 1", McGraw-Hill Book Company, London.

Zuurbier, CJ and PA Huijing (1992) Influence of muscle geometry on shortening speed of fiber, aponeurosis and muscle, *J Biomech*, 25: 1017-1026.

Zuurbier, CJ and PA Huijing (1993) Changes in geometry of actively shortening unipennate rat gastrocnemius muscle, *J Morphol*, 218(2): 167-180.

Zuurbier, CJ, AJ Everard, P van der Wees and PA Huijing (1994) Length-force characteristics of the aponeurosis in passive and active muscle conditions and in the isolated condition, *J Biomech*, 27 (4): 445-454.

Zuurbier, CJ, JW Heslinga, MBE Lee-de Groot and WJ van de Laarse (1995) Mean sarcomere length-force relationship of rat muscle fibre bundles, *J Biomech*, 28: 83-88.

Summary

For movement of body or body segments is combined effort needed of the central nervous system and the muscular-skeletal system. This thesis deals with the mechanical functioning of skeletal muscle. That muscles come in a large variety of geometries, suggest the existence of a relation between muscle morphology and the ability to exert force. Models are utilized to gather detailed knowledge about the way muscle work, i.e. the heuristic approach and to some extent to predict muscle force under specific conditions. Several types of models are used to study different aspects of muscle performance. These aspects are of material and structural nature. The material properties addressed are active and passive elasticity and incompressibility. Structural properties studied are pennation, anisotropy, in series and in parallel arrangement of functional units. A great deal of muscle force under a specific condition can be attributed to interactions of these aspects. During modeled isometric and isokinetic contractions muscle geometry, force, fiber lengths and velocities are monitored. A great deal of the results is compared to uni-pennate gastrocnemius medialis muscle (GM) and some to extensor digitorum longus (EDL) of the rat.

In chapter 2, model results of simple geometric models such as a planimetric model and three-dimensional versions of this model are compared to the experimental results of the rat GM. The capabilities of such models to adequately calculate geometry of muscle and force-length characteristics were investigated. The planimetric model with elastic aponeurosis (tendon-sheet) predicted GM muscle geometry well: maximal differences are 6%, 1%, 4% and 6% for fiber length, aponeurosis length, fiber angle and aponeurosis angle respectively. A slanted cylinder model with circular fiber cross section did not predict muscle geometry as well as the planimetric model, whereas the geometry results of a second slanted cylinder model was identical to the planimetric model. It is concluded that the planimetric model is capable of adequately calculating the muscle geometry over the muscle length range studied. Modeled force-length characteristics showed an over-estimation of muscle optimum length by 2 mm with respect to experimental data and in addition, force at the ascending limb of the length force curve was underestimated.

An improvement of the predicted force-length characteristic is found when mechanical equilibrium of whole muscle is guaranteed of the linearized geometry (chapter 3). A volume-related force is introduced to keep muscle volume constant. Mechanical equilibrium of whole muscle yields a different relation between fiber and muscle force as fiber and muscle length changes as a result of pennation, compared to relations derived when only equilibrium of aponeurosis is considered (chapter 2). The newly derived relation improved prediction of the rat GM muscle force-length characteristics. It is concluded that prediction of muscle geometry as well as prediction of force-length characteristics is very good with a simple model such as a planimetric model. This conclusion suggests that the influence of properties neglected in such a simple model are either small or are internally compensated for in the net effects.

In chapter 4 a mechanical muscle model based on the Finite Element Method (FEM) is presented, to study the effects of muscle tissue properties and their mechanical interactions on

muscle force exerted. The strength of this method is the capability to combine non-linear material properties of fibers as well as incompressibility and anisotropic behavior of muscle within solutions of mechanically stable muscle geometries for various lengths and loads. Simulations of static and dynamic muscle contractions are performed and compared to experimental data of rat GM. The model indicates the functional importance of combining properties such as passive stiffness (in fiber longitudinal direction, perpendicular to it and shear) as well as incompressibility. That the FEM-model allows fibers and aponeurosis to curve, introduces secondary fiber length distributions in active muscle, even if the muscle tissue was initially modeled homogeneous. Under isokinetic conditions, the fibers develop a different shortening velocity. The observed differences in length and velocity of fibers depend on the position of a fiber in the muscle belly and are based on two independent passive properties, stiffness perpendicular to the fibers and shear stiffness. It is concluded that these properties are of significant influence on force exerted by a whole muscle.

The generation of force in a sarcomere is addressed in chapter 5. A model based on the sliding-filament and cross-bridge theory is used in to describe effects of contraction history during sustained contractions with phases where shortening or lengthening are imposed. The model presented has some modifications with respect to the general Huxley-model, such as: a force-length relationship, a Kelvin element arranged in series with the contractile filaments and a cross-bridge detachment function for cross-bridges, stretched over their maximal binding length, that detach without consuming energy. The main extension of the model is the assumption that the number of available cross-bridges is reduced each cycle, thus introducing effects of fatigue. The obtained model is referred to as the reducing cross-bridge (RCB) model. The RCB-model is compared to the general Huxley model and to experimental observations under isometric and isokinetic conditions.

In accordance with experiments, the RCB-model is able to describe post-shortening force deficit in the entire sarcomere length range and post-lengthening force enhancement in the length range below sarcomere optimum length. Over optimum sarcomere length, two RCB-models arranged in series are able to predict an enhanced force after lengthening. Furthermore, it is shown that exerted sarcomere force changes, due to superimposed high-frequency vibrations, compared to conditions without vibrations, because of changed cross-bridge distributions. A dissociation of force and number of attached cross-bridges is found, which implies that experimentally obtained stiffness, based on contractions with superimposed vibrations, does not relate to the number of attached cross-bridges.

Chapter 6 deals with force transmission in a FEM-model of uni-pennate rat EDL. In addition, the role of the aponeurosis and shear stiffness is addressed. A distinction is made between myotendinous and myofascial force transmission, where force is transmitted from fibers to aponeurosis and from fibers in sideward direction, respectively. Surgical interventions such as tenotomy, aponeurotomy and myotomy are performed to study the effects on the force-length characteristic, fiber length, active fiber stress, shear stress and fiber strain. Aponeurotomy implicates removal of direct myotendinous connection to insertion of a considerable amount of

muscle fibers at several locations. In addition is in two stages myofascial connection removed of sideward connected fibers, i.e. myotomy.

After surgical intervention, a considerable amount of the fibers had no direct myofascial connection to insertion but force decrease found, was only minor. The shortening of these fibers was small and not enough to explain the reduction in muscle force. The force reduction is cause by a decrease in active fiber stress just distally of the invention in the intact part of the muscle as a result of high local fiber strain. The results indicated that up to 48% of the force exerted, is transmitted through myofascial pathways under specific conditions. Due to myofascial force transmission, fibers without direct myotendinous connection to insertion are prevented to shorten much, and generate a substantial amount of active fiber stress. The force decrease found after interventions performed is strongly related to the amount of deformations. If muscle integrity is thoroughly disturbed by myotomy or by removal of a large part of the aponeurosis, the force reduction is significant. The results indicated that the role of the aponeurosis is besides transmitting force from fibers to origin and insertion, extended with the maintenance of muscle integrity, to allow the muscle to produce optimal force. Based on the results an explanation for the success of intramuscular aponeurotomy performed on spastic muscle is suggested.

In the final chapter the results of this thesis are discussed in general, model improvements are suggested and some recommendation for future research are indicated.

Samenvatting

Voor de beweging van het lichaam of lichaamsdelen is een gekombineerde inspanning nodig van het centrale zenuwstelsel en het spierskelet systeem. Dit proefschrift heeft betrekking op het functioneren van de skelet spier. Het feit dat spieren voorkomen in een grote variëteit aan vormen, suggereert het bestaan van een relatie tussen de morfologie van de spier en de mogelijkheid tot het leveren van kracht. Modellen zijn gebruikt om gedetailleerde kennis te verzamelen over de manier waarop een spier werkt, met andere woorden de heuristische benadering. Tot op zekere hoogte worden de modellen ook gebruikt voor het doen van de voorspellingen van de spierkracht onder bepaalde omstandigheden. Verschillende typen modellen zijn gebruikt om verschillende aspecten van spierente bestuderen. Deze aspecten zijn onderverdeeld in materiaal eigenschappen en structurele eigenschappen. Bij materiaal eigenschappen is onderscheid gemaakt in actieve en passieve elasticiteit de constantheid van spiervolume. Structurele eigenschappen zijn pennatie, anisotropie en serie en parallelle rangschikking van functionele eenheden. Een groot deel van de spierkracht onder een bepaalde conditie is te wijten aan wisselwerking van deze eigenschappen. Tijdens de gemodelleerde isometrische en isokinetische contracties zijn de spiergeometrie, spierkracht, vezel lengten en snelheden bestudeerd. Veel van model resultaten zijn vergeleken met de uni-pennate mediale gastrocnemius (GM) van de rat en enkele resultaten met de extensor digitorum longus (EDL) van de rat.

In hoofdstuk 2 zijn model resultaten van simpele geometrische models, zoals een planimetrisch model en driedimensionale varianten daarop, vergeleken met experimentele resultaten van de rat GM. In de twee dimensionale modellen wordt het spiervolume beschreven door een constant mid-longitudinaal oppervlak. De mogelijkheden van dergelijke modellen om de spiergeometrie alsmede de spierkracht-lengte karakteristiek adequate te voorspellen zijn onderzocht. Het planimetrisch model met een elastische aponeurose (pees-plaat) voorspelt de spiergeometrie goed: de maximale verschillen zijn 6%, 1%, 4% en 6% voor respectievelijk de vezellengte, aponeuroses lengte en de vezelhoek en aponeuroses hoek. Een model gebaseerd op een scheve cilinder met een circulaire dwarsdoorsnede van de vezels is niet in staat de spier geometrie zo goed te voorspellen als het planimetrisch model. Desalniettemin, de resultaten van een tweede cilinder model met een variabele elliptische dwarsdoorsnede, zijn identiek aan die van het planimetrisch model. Hieruit is geconcludeerd dat het planimetrisch model met een constant mid-longitudinaal oppervlak beter in staat is om de spiergeometrie te berekenen dan een 3D-model met een circulaire dwarsdoorsnede. Daarentegen laat de gemodelleerde kracht-lengte karakteristiek een overschatting zien van de spier optimum lengte van 2 mm in vergelijking met experimentele data. Bovendien is de spierkracht op de stijgende flank van de kracht-lengte curve onderschat.

Als mechanisch evenwicht van de hele gelineairiseerde spiergeometrie is gegarandeerd, wordt een verbetering van de voorspelling van de kracht-lengte karakteristiek gevonden (hoofdstuk 3). Een volume gerelateerde kracht is geïntroduceerd om een konstant volume te waarborgen. Mechanisch evenwicht van de hele spier resulteert in een andere relatie tussen de vezel- en de

spierkracht, in vergelijking met de relaties verkregen wanneer alleen evenwicht is beschouwd van de aponeurosis (hoofdstuk 2). Deze nieuw afgeleide relatie verbetert de voorspelling van de kracht-lengte karakteristiek van de rat GM. Hieruit is geconcludeerd dat het mogelijk is om een goede voorspelling te doen van zowel de spiergeometrie als de kracht-lengte karakteristiek, met een simpel model als het planimetrisch model.

In hoofdstuk 4 is een spiermodel gepresenteerd dat is gebaseerd op de Eindige Elementen Methode (EEM), om de effecten van spierweefseleigenschappen en de mechanische interacties op de spierkracht te bestuderen. De kracht van deze methode is dat het de mogelijkheid biedt niet lineaire materiaal eigenschappen van spieren, het constante volume van spieren en het anisotrope karakter van spieren binnen mechanisch stabiele spiergeometrieën te combineren op verschillende lengten en onder verschillende belastingen. Simulaties van statische en dynamische spiercontracties zijn uitgevoerd en vergeleken met experimentele data van de GM van de rat. Model resultaten wijzen op het functionele belang van het combineren van eigenschappen als passieve stijfheid (in zowel vezelrichting, loodrecht daarop en afschuiving) en onsamendrukbare karakter van spieren. Deze combinatie van eigenschappen in het EEM-model resulteert het krommen van de vezels en de aponeuroses. Dit introduceert een secondaire vezellengte distributie in een actieve spier, zelfs als de spier initieel homogeen in materiaal en vezellengten is gemodelleerd. Onder isokinetische condities ontwikkelen de vezels verschillende verkorting snelheden. De geobserveerde verschillen in lengte en snelheid van de vezels is afhankelijk van de positie in de spierbuik. Hiervoor zijn twee onafhankelijke passieve eigenschappen verantwoordelijk: de stijfheid loodrecht op de vezels en de weerstand tegen afschuiving. Er is geconcludeerd dat deze eigenschappen significante invloed hebben op de geleverde spierkracht.

De ontwikkeling van kracht in een sarcomeer is bestudeerd in hoofdstuk 5. Een model gebaseerd op de sliding-filament en cross-bridge theorie is gebruikt om effecten te beschrijven van contractie geschiedenis tijdens een volgehouden contractie met fases waarin verkortingen en verlengingen zijn uitgevoerd. Het gepresenteerde model heeft enkele modificaties ten opzichte van het orginele Huxley-model: een kracht-lengte karakteristiek, een Kelvin element gerangschikt in serie met de contractiele filamenten zijn toegevoegd, een crossbridge ontbindfunctie voor crossbridges die verder zijn gerekt dan de maximale bindlengte. Bovendien worden deze crossbridges losgemaakt zonder dat het energie kost. De belangrijkste aanpassing in het model is de aanname dat het aantal beschikbare cross-bridge afneemt per cross-bridge cyclus, van binding en ontbinding. Hiermee zijn effecten van vermoeidheid tijdens een contractie geïntroduceerd. Het aldus verkregen model is aangeduid als het “reducing cross-bridge” (RCB) model. Het RCB-model is vergeleken met het originele Huxley-model en experimentele observaties onder isometrische en isokinetische condities.

In overeenstemming met experimenten is het RCB-model in staat de post-verkortings krachtsdaling te beschrijven over de gehele sarcomeer lengte range and de post-verlengings krachtstoename voor sarcomeerlengten onder de sarcomeer optimum lengte. Boven sarcomeer

optimum lengte zijn twee in serie geschakelde RCB-modellen in staat een krachtstoename te voorspellen na een fase met een verlenging. Daarnaast, heeft met dit model laten zien dat de geleverde kracht veranderd, door het opleggen van hoog-frequente trillingen om de spierstijfheid te bepalen. Dit wijst op een ontkoppeling van kracht en het aantal gebonden cross-bridges, wat impliceert dat experimenteel bepaalde stijfheid, gebaseerd op contracties met additionele trillingen, niet is gerelateerd aan het aantal gebonden cross-bridges.

In hoofdstuk 6 wordt aandacht besteed aan de krachtsoverdracht in een EEM-model van de unipennate (EDL) van de rat. Bovendien is de rol van de aponeurose en de bijdrage van afschuiving nader belicht. Een onderscheid is gemaakt tussen myotendineuse en myofasciale krachtsoverdracht, waarbij respectievelijk kracht is overgedragen van vezels naar de aponeuroses en tussen vezels onderling in zijdelingse richting. Chirurgische ingrepen zoals tenotomie, aponeurotomie en myotomie zijn gesimuleerd om de effecten op de kracht-lengte karakteristiek, vezel lengten, actieve vezel spanning, afschuifspanning en vezelrek te bestuderen. Aponeurotomie houdt in dat van een aanzienlijke hoeveelheid spiervezels de directe myotendineuse verbinding met insertie van de spier wordt verwijderd. Vervolgens zijn in twee stadia myofasciale verbindingen van zijdelings verbonden vezels verwijderd, wat is aangeduid met myotomie. Na deze chirurgische ingrepen, hebben een aanzienlijke hoeveelheid vezels geen directe myotendineuse verbinding met de insertie van de spier, daarentegen is de krachtsafname minimaal. De verkorting van deze vezels is klein en bovendien niet genoeg om de gevonden krachtreductie te verklaren. De krachtsreductie wordt veroorzaakt door een afname van de actieve vezel spanning net distaal van de locatie waar de ingreep heeft plaatsgevonden, dus in het intacte gedeelte van de spierbuik. De sterke afname van de actieve vezelspanning wordt veroorzaakt door een sterkte toename van de lokale vezel rek. De resultaten suggereren dat onder deze specifieke condities 48% van de geleverde spierkracht wordt overgedragen via myofasciale verbindingen. Tengevolge van de myofasciale krachtsoverdracht wordt voorkomen dat de vezels zonder directe myotendineuse verbinding met de insertie van de spier, veel verkorten, dientengevolge leveren ze nog steeds een substantiële hoeveelheid actieve spanning. De krachtsreductie is sterk gerelateerd aan de grootte van de vervorming van de spier tengevolge van een chirurgische ingreep. Indien de spier integriteit grondig is verstoord door bijvoorbeeld myotomie of het gedeeltelijk verwijderen van een aponeurose is de krachtsreductie significant. Deze resultaten geven aan dat de rol van de aponeuroses meer is dan alleen het doorgeleiden van vezelkracht naar origo en insertie van de spier, maar ook belangrijk is voor het bewaken van de spierintegriteit, zodat de spier optimaal kan presteren. Op basis van de resultaten gepresenteerd in dit hoofdstuk zijn suggesties gedaan die het succes van intramusculaire aponeurotomie die zijn uitgevoerd op spastische spieren.

In het laatste hoofdstuk zijn de resultaten van deze dissertatie bediscussieerd, model verbeteringen voorgesteld en aanbevelingen voor toekomstig onderzoek gedaan.

Dankwoord

Hoewel er maar één naam op de voorkant van dit boekje staat, is het tot stand gekomen dankzij medewerking van verschillende personen. Allereerst ben ik dank verschuldigd aan mijn begeleiders gedurende het onderzoek.

Mijn promotor, Henk Grootenboer, wil ik bedanken voor het vertrouwen, zijn goede impulsen.

Mijn co-promotor, Peter Huijing ben ik dank verschuldigd voor zijn onophoudelijke stimulans en enthousiasme en zijn onvermoeibare geduld om de goede boodschap op de juiste manier op papier te zetten.

Bart Koopman, assistent-promotor, bedank ik voor de bereidheid als klankbord te dienen en zijn bijdrage in de discussies.

Degene met wie ik het hele proces vanaf het begin heb doorlopen is Kenneth Meijer. Meteen was de samenwerking goed, gezellig en vooral productief. We hebben elkaar in vele opzichten prima kunnen aanvullen, maar jouw kennis van de literatuur kan ik niet evenaren.. Ik kan met veel plezier en genoegen terugkijken op deze tijd die we samen tot een goed einde hebben gebracht. We waren een goed team,

Daarnaast wil ik graag de studenten bedanken die tijdens hun afstuderen hun tanden hebben gezet in de weerbarstige programmatuur en de complexe eigenschappen van spieren: Madelon Kuiper, Johan Pel, Robert Schaart, Guido Rebel en Ydo de Vries. Verder, wil ik Tom Mattaar bedanken voor zijn programmeer bijdrage.

Een belangrijke randvoorwaarden voor het succes van het onderzoek is geschapen door Ray Klumpert. Dankzij zijn goede verzorging van de hard- en software binnen de vakgroep konden de computers optimaal worden benut.

Voor de sfeer tijdens de noodzakelijk afleiding gedurende koffiepauzes en ‘dagjes-uit’ en andere gelegenheden om de gedachten te verzetten, zijn verantwoordelijk geweest: Arthur, Anjenet, Bart, Dorien, Eddy, Edsko, Herman, Johan, Ron, Paul, Peter, Ray, Roel en Laurens: Bedankt allemaal!

Groningen, mei 1998

Bart van der Linden